AD NUMBER

AD909365

NEW LIMITATION CHANGE

TO

Approved for public release, distribution unlimited

FROM

Distribution authorized to U.S. Gov't. agencies only; Test and Evaluation; MAR 1972. Other requests shall be referred to Air Force Avionics Laboratory, Attn: TEL, Wright-Patterson AFB, OH 45433.

AUTHORITY

AFWAL ltr, 3 Feb 1976

SPACE LASER DESIGN

J. E. Peterson, E. C. Yates

Lockheed Missiles & Space Company, Inc.
Research and Development Division

TECHNICAL REPORT AFAL-TR-73-28

March 1973

Air Force Avionics Laboratory
Air Force Systems Command
Wright-Patterson Air Force Base, Ohio

NOTICE

When government drawings, specifications, or other data are used for any purpose other than in connection with a definitely related Government procurement operation, the United States Government thereby incurs no responsibility nor any obligation whatsoever; and the fact that the government may have formulated, furnished, or in any way supplied the said drawings, specifications, or other data, is not to be regarded by implication or otherwise as in any manner licensing the holder or any other person or corporation, or conveying any rights or permission to manufacture, use, or sell any patented invention that may in any way be related thereto.

Copies of this report should not be returned unless return is required by security considerations, contractual obligations, or notice on a specific document.

SPACE LASER DESIGN

J. E. Peterson, E. C. Yates

FOREWORD

This final technical report on Space Laser Design summarizes the work performed on Air Force Contract F33615-72-C-1960. This study was conducted for the Air Force Avionics Laboratory, Wright-Patterson Air Force Base, Ohio, by Lockheed Missiles & Space Company, Inc. (LMSC), Palo Alto Research Laboratory, Palo Alto, California, during the period from March 1972 to December 1972. Dr. Walter L. Knecht (AFAL/TEL) was the project monitor for the Air Force. The work was supported by Advanced Development Program 405B.

The work was performed in the LMSC Palo Alto Communications Sciences Laboratory, headed by Dr. R. C. Ohlmann. Mr. J. E. Peterson was the project leader, and Mr. E. C. Yates, Dr. H. W. Lavendel, Mr. R. R. Emery and Mr. W. F. Ekern were the other principal contributors to the project. Technical assistance was provided by Mr. R. M. Zeller and Mr. B. L. Fowles.

The report, LMSC-D315647, was submitted in January 1973 and has been reviewed and is approved for publication.

Paul Freedman

PAUL M. FREEDMAN, MAJ, USAF
Program Manager
405B Advanced Development Program

ABSTRACT

This report describes the results of a program to design and develop a high-efficiency CW Nd:YAG laser which has space-applicable thermal properties. Means were found for efficiently cooling the laser rod and pump lamp without using direct liquid cooling, and for removing the lamp envelope infrared radiation from the pump cavity. A laser was constructed that incorporated radiation cooling of the CW potassium-rubidium-arc pump lamp and direct-conduction cooling of the laser rod. The rod was soldered to a slotted composite metal wedge heat sink for minimum residual stress and greatest uniformity of thermal gradients in the rod. An optical pumping cavity was developed, using a Pyrex sphere coated with a multilayer dielectric cold mirror which transmits or absorbs unwanted lamp radiation while efficiently imaging pump band radiation in the laser rod. To date, the laser has produced 0.7 W of multimode output at 1.06 μm without correction of the astigmatism thermally induced in the rod.

CONTENTS

ILLUSTRATIONS

TABLES

SECTION I

INTRODUCTION

The work reported in this document is one step in a continuing effort to develop a laser suitable for the Air Force 405B Program, Laser Communication – Space Data Relay Subsystem. This effort was specifically concerned with designing, constructing, and operating a K-Rb lamp pumped Nd:YAG laser. The objective was to develop a laser capable of delivering 1 W of quiet, stable, TEM_{oo} power with an input power of 300 W to the lamp.

The design problems in making a laser of this type center around preventing the absorption in the laser rod of unwanted infrared radiation from the K-Rb lamp, and preventing the reabsorption in the lamp of this same radiation after reflection from the surface of the pump cavity. The absorption has serious deleterious effects on both the laser rod and the K-Rb lamp.

Water has very desirable properties for filtering out this undesired radiation. Because of the problems associated with liquid cooling in a space environment, however, the use of water for such purposes is not practical. Another solution for removal of the IR radiation therefore is required.

The LMSC design approach is illustrated in Figure 1. The laser rod is attached along one side to the apex of a truncated metallic wedge for conduction cooling. The lamp is mounted parallel to and above the laser rod. A spherical glass pump cavity, with an inner selectively-reflecting, multilayer-dielectric coating, reflects the useful light from the lamp into the laser rod. The cavity also partially absorbs and transmits the unwanted infrared radiation, which is ultimately absorbed in the metallic cap surrounding the reflector. A quartz rod interposed between the lamp and laser rod filters the longer wavelength components of the direct radiation. The laser resonator consists of a flat mirror and a short-radius concave mirror. These mirrors, in conjunction with a positive lens either ground on one end of the laser rod or as a separate element, produce a narrow beam waist inside the cavity and a large TEM_{oo} mode volume inside the rod for high TEM_{oo} mode efficiciency.

A number of design problem areas for such a laser system have been treated during this contract period. Among these are the following:

- Design of a low-stress, conduction-cooled rod mount
- Development of a reliable method for bonding the rod to the mount
- Development of a method for uniform deposition of dielectric multilayers on glass hemispheres

TECHNIQUE: POTASSIUM-LAMP PUMPING, WITH SPHERICAL, COLD MIRROR, OF FOCUSING, CONDUCTION-COOLED, Nd:YAG LASERED.

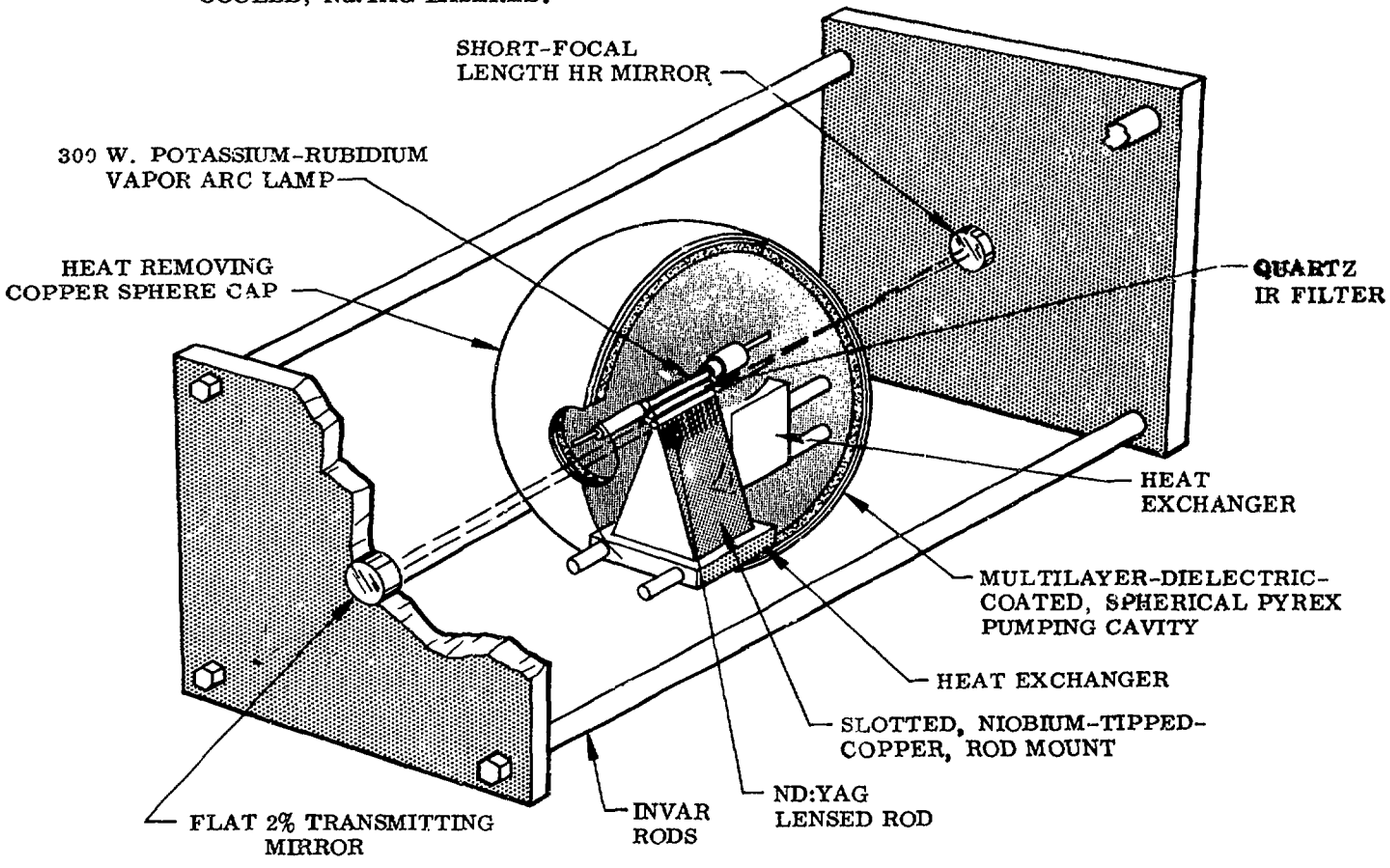

Figure 1 Space Laser Design – Schematic

- Optimization of the following elements:
  - Laser rod diameter
  - Mount attachment angle
  - Spherical reflector diameter
  - Laser resonator configuration

More accurate data regarding the spectral output of the K-Rb lamp were needed to determine the heat balance for cavity and rod mount design. Some spectral measurements were therefore made with the K-Rb lamp.

The selection of rod diameter involves a tradeoff between gain and saturation parameters. Measurements of the distribution of fluorescence intensity inside pumped laser rods were made to aid in optimizing the rod diameter. The attachment angle of the rod to the mount affects rod birefringence, rod cylindrical lensing (astigmatism), total temperature difference between the mounted side of the rod and the opposite side, and the temperature gradient in the rod mount. Isothermal patterns in the rod were calculated for various rod attachment angles so that this parameter could be optimized. The theoretical considerations and the measurements and calculations relating to the choice of values for these parameters as well as the lamp measurements are covered in Section II.

SECTION II

PRELIMINARY DESIGN CONSIDERATIONS

Certain calculations and measurements were needed to help establish suitable values for the laser rod diameter and angle of contact with the rod mount in order to complete the laser design.

1. SELECTION OF ROD DIAMETER

The laser output power at optimum output coupling can be shown to be:

$$P_o = (2S)^{-1} \left(\sqrt{2g_o} - \sqrt{L} \right)^2 \qquad (1)$$

where

S = saturation parameter (W^{-1})

g_o = single-pass unsaturated gain

L = round trip losses

The saturation parameter is inversely proportional to the mode area in the rod, while g_o is proportional to the power absorbed per unit volume, primarily at the rod center.

The relative gain at rod center for rods of various diameters has been estimated by first calculating the population-inversion density by numerical integration as a function of distance into a Nd:YAG slab. The excitation and absorption were computed, using the Nd:YAG absorption spectrum and assuming that the slab is illuminated normally with radiation from a K-Rb lamp (Figure 2). A first-order correction for the average path distance from the surface to center for isotropic illumination was made by considering that the maximum angle with respect to a rod surface normal which is expected for rays in the rod is determined by the critical angle (about 34° for YAG). Average optical path length in the isotropically illuminated slab is therefore about 5 percent greater than for normal incidence. Using Figure 2, with a distance 5 percent greater than the rod radius it is seen that gain should be reduced by roughly 17 percent when the rod diameter is increased from 3 to 5 mm, and reduced by roughly 7.5 percent when the rod diameter is increased from 5 to 6 mm. Because of the approximations made, it is necessary to consider these values as upper limits of the gain differences to be expected.

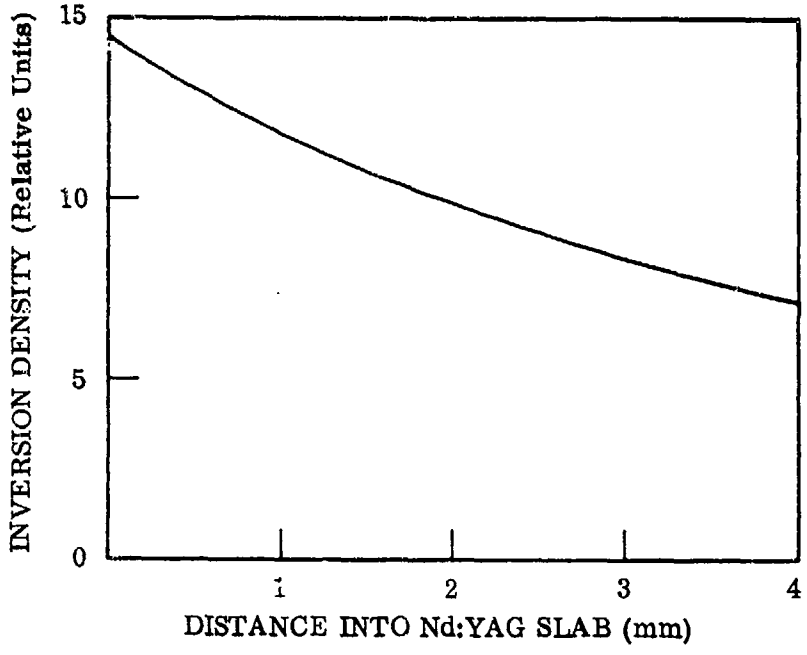

Figure 2 Calculated Population Inversion Produced in an Nd:YAG Slab by Normally Incident Radiation From a K-Rb Lamp

The geometrical efficiency for spherical pumping cavities has been calculated by Church & Liberman (Ref. 1). Extension of that calculation to relevant cases indicates an increase of geometrical coupling efficiency of greater than 25 percent in going from a 3-mm rod to a 5-mm rod. This increase would tend to offset the gain decrease due to attenuation in the Nd:YAG. The profile of the K-Rb arc, which was measured by scanning a detector with a narrow slit across the image of the lamp formed by a lens, is shown in Figure 3. These data indicate that about 20 percent of the useful lamp energy lies outside a 3-mm aperture with ideal imaging. If it is assumed that the resonator loss L is 1.5 percent, that g_o is 5 percent for a 5-mm-diam. rod and 6 percent for a 3-mm-diam. rod, and that the saturation parameter is inversely proportional to the rod diameter squared, then, on the basis of Eq. (1), the expected output for a 5-mm rod is twice that expected from a 3-mm rod.

To obtain a better understanding of the pumping process and the effect of rod diameter on gain, some measurements were made of the transverse distribution of fluorescence intensity in a pumped rod. These measurements were made on water-cooled rods pumped in spherical cavities with K-Rb and tungsten lamps.

The apparatus consisted of an 0.25-m spectrometer (Jarrell Ash), mounted with detector and input optics on an X - Z stage so that the system could "look" down the rod holder into the end of the Nd:YAG rod with a very narrow field of view and scan the fluorescence intensity as a function of position in the plane perpendicular to the rod axis (Figure 4).

The spatial resolution of the system is determined by the width and height of the spectrometer slit and the magnification of the input optics. This yields a spot size of 0.32 mm x 1 mm inside the rod. To preserve this spot size along the length of the rod,

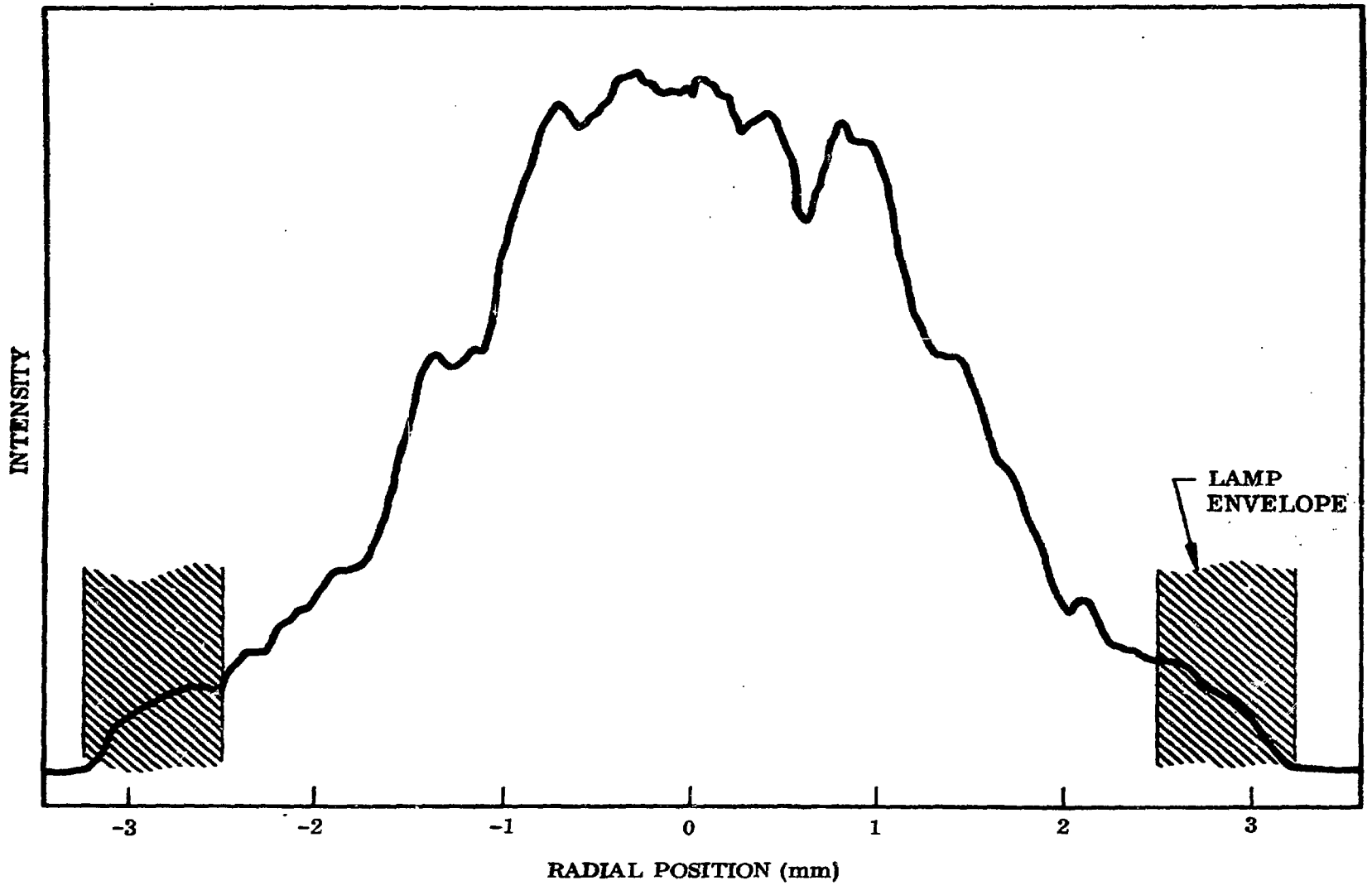

Figure 3 Intensity Distribution Across the Image of a K-Rb Lamp (5-mm Bore)

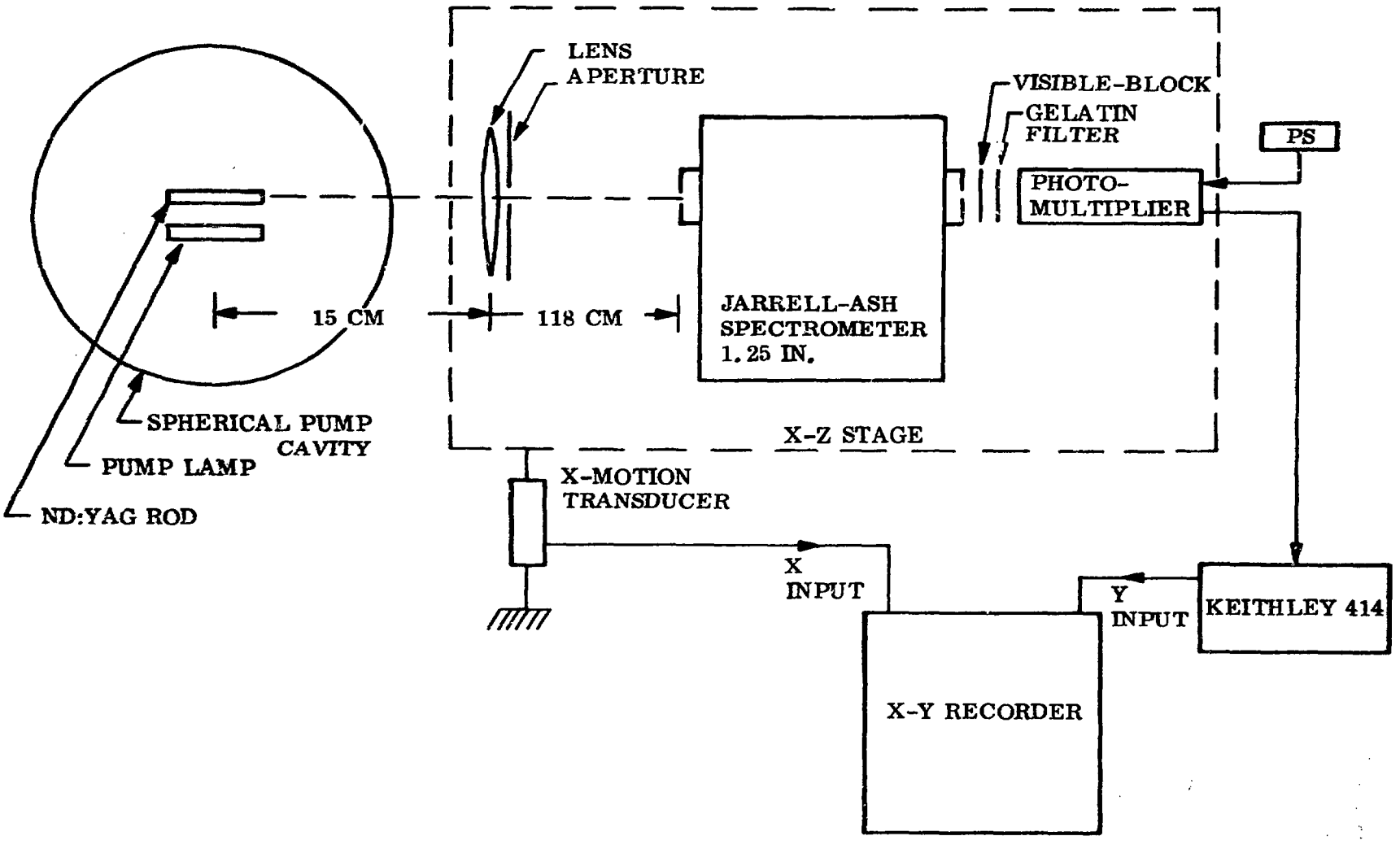

Figure 4 Apparatus for Measurement of Transverse Distribution of Fluorescent Intensity in Pumped Nd:YAG Laser Rods

the f number coming into the input lens was restricted to f/30. A two-dimensional scan was produced by manually setting the height of the scanner and the displacement of the zero for the y deflection on the recorder, and recording a series of horizontal scans.

The resolution of the system was verified by scanning a circular diffusing screen, one-half of which was covered with a piece of black tape, for three positions of the screen to correspond to the near-end, center, and far-end of the rod. Figure 5a shows a typical scan of this screen. The measured resolution agreed with the calculated value. Scattered light background was determined by setting the spectrometer slightly off the 1.064-μ line; it was found to be negligible.

Fluorescent intensity profiles were measured using the apparatus previously described. Two Nd:YAG rods with a nominal Nd^{3+} concentration of 1 atomic percent, 30-mm length, and diameters of 5 mm and 6 mm, respectively, were measured in a water-cooled mount An 8-in. i.d. dielectric mirror sphere was used to image either tungsten or K-Rb lamps onto the laser rods. A typical scan, showing the fluorescent emission profile of the 6-mm o.d. rod with 1 kW tungsten lamp pumping is shown in Figure 5b. The relative fluorescent intensities of the 5-mm and 6-mm rods were measured with optimized sphere focus and 500-W input to the tungsten lamp in both cases. The scans are shown in Figure 6a and b, respectively. In this case, the peak intensity is about 12 percent higher in the 5-mm rod.

A similar set of measurements was made with a K-Rb lamp which had a 5-mm bore and 23-mm arc length, and a 200-W input to the lamp. The scans for the 5-mm and 6-mm rod are shown in Figure 7a and b. To indicate the sensitivity of the results to the position of the sphere relative to the lamp and laser rod, the center of the sphere was moved 1 mm closer to the laser rod as shown in Figure 7c. The displacement of the fluorescent peak between the cases shown in Figures 7b and 7c is only 0.9 mm, rather than the 2-mm shift which would be predicted for focusing in air. This relative insensitivity to sphere position is due to refractive imaging by the laser rod and cooling jacket. In this case, the difference in peak fluorescence between the 5-mm diam. and 6-mm diam. rod is about 20 percent. The lower relative fluorescent intensity of the 6-mm rod compared to the 5-mm rod, when pumped by a K-Rb lamp rather than by a tungsten lamp, is consistent with the better matching of K-Rb lamp emission to the strongest Nd:YAG absorption bands.

The fluorescence measurements indicate a somewhat greater reduction in rod-center gain than expected from the inversion density calculation. These measurements are somewhat dependent on possible differences between rods in Nd^{3+} concentration. However, the greater mode area possible (2.7 x) when using the 5-mm-diam. rod rather than the 3-mm-diam. rod appears to more than compensate for the anticipated gain reduction. Consequently, the 5-mm dimension has been chosen for the rod diameter.

2. DETERMINATION OF THE LASER-ROD ATTACHMENT ANGLE

Water cooling of the laser rod was specifically excluded from the Space Laser Design contract. The need for maintaining the integrity of water seals, assuring the adequate lifetime of circulating pumps, and solving related corrosion problems was the primary reason for avoiding the water cooling approach. Alternative techniques are gas cooling and conduction cooling.

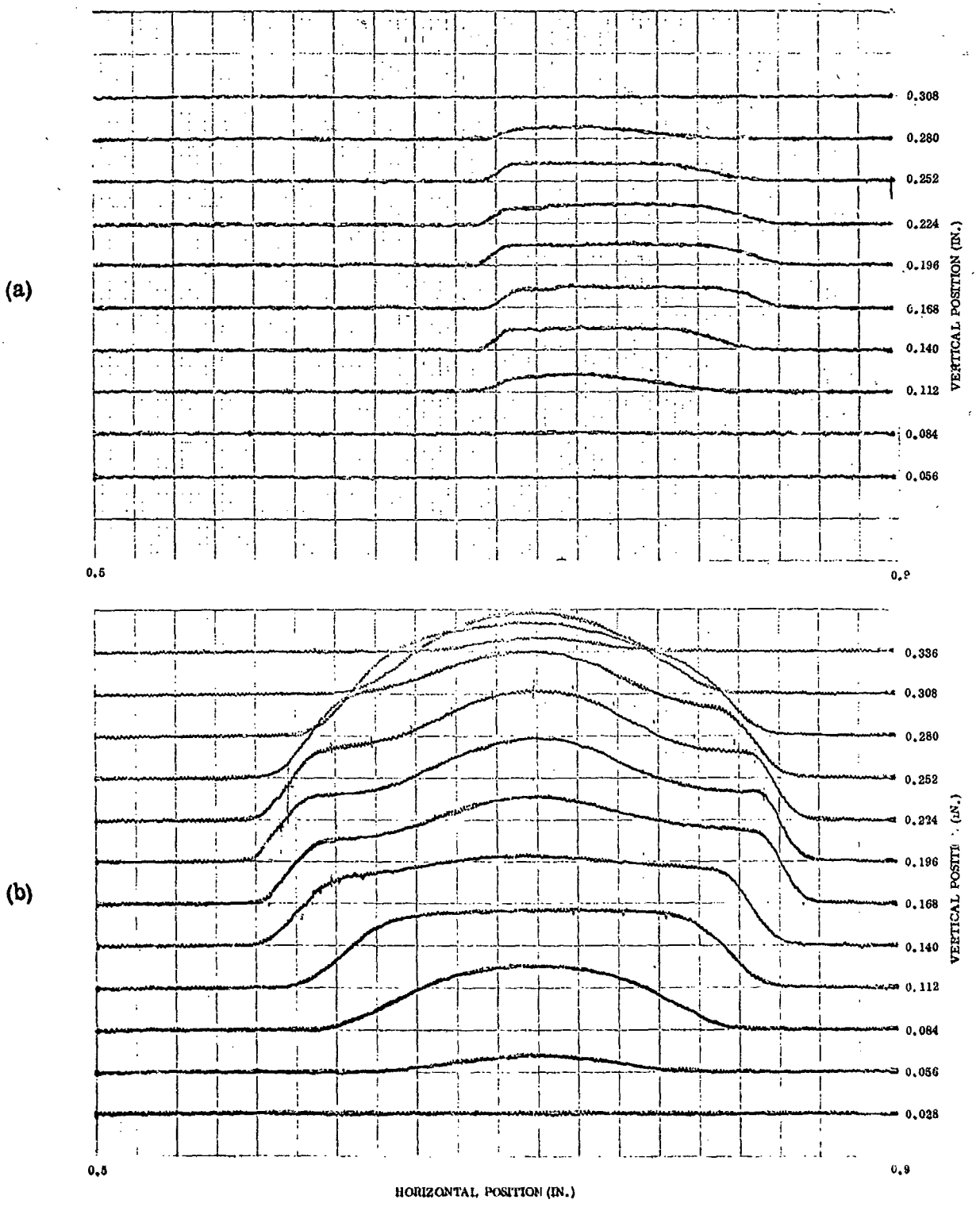

Figure 5 Measurement of System Resolution and Fluorescent Intensity Distribution – (a) Resolution Test Scan of One-Half-Circular Diffuse Scatterer, Using Apparatus Shown in Figure 4, (b) Transverse Distribution of Fluorescent Intensity – 6-mm OD Rod With 1-kW Tungsten Lamp Pumping

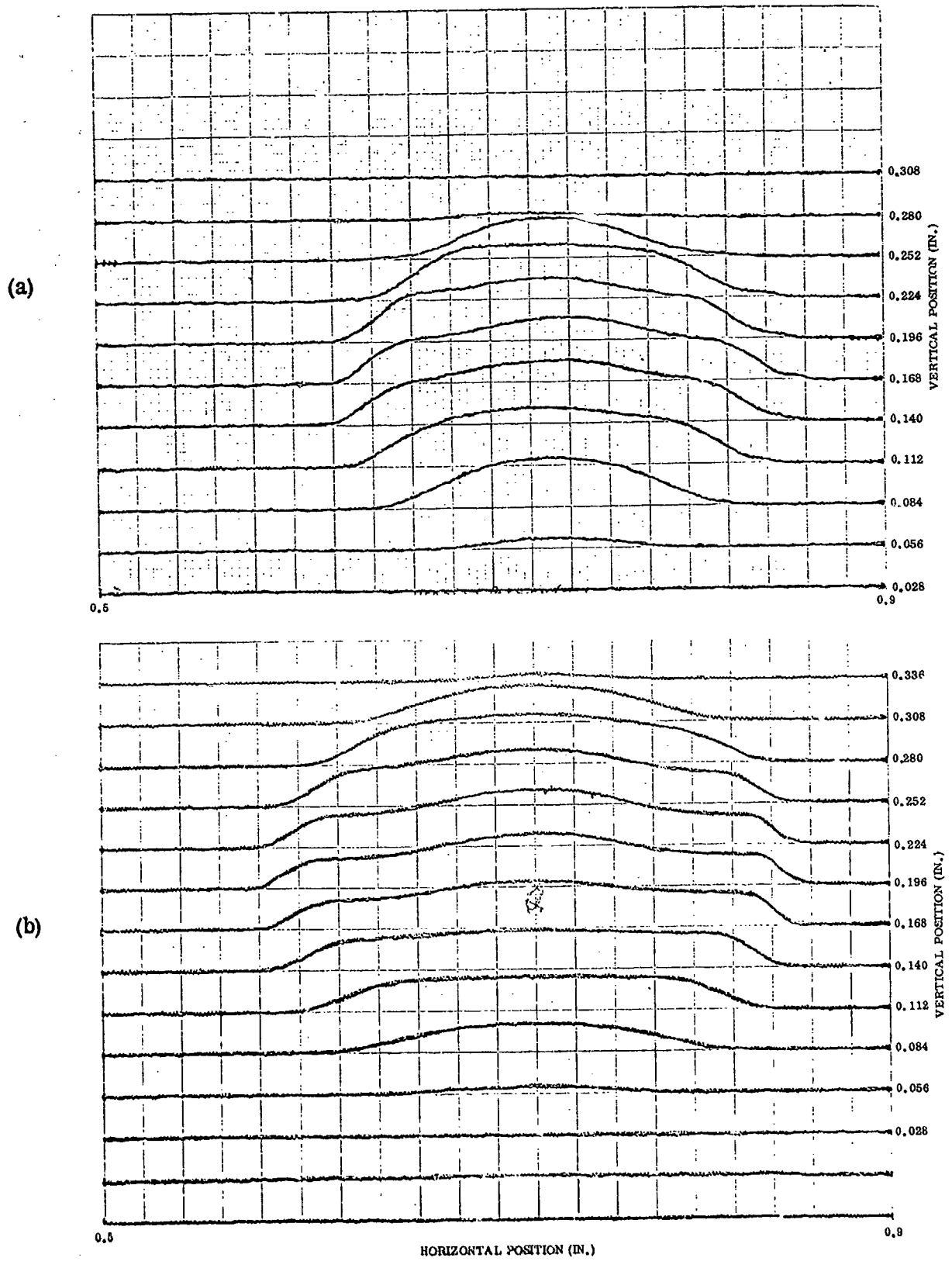

Figure 6 Fluorescent Intensity Distribution for 500-W, Input to Tungsten Lamp – (a) 5-mm-OD Rod, and (b) 6-mm-OD Rod

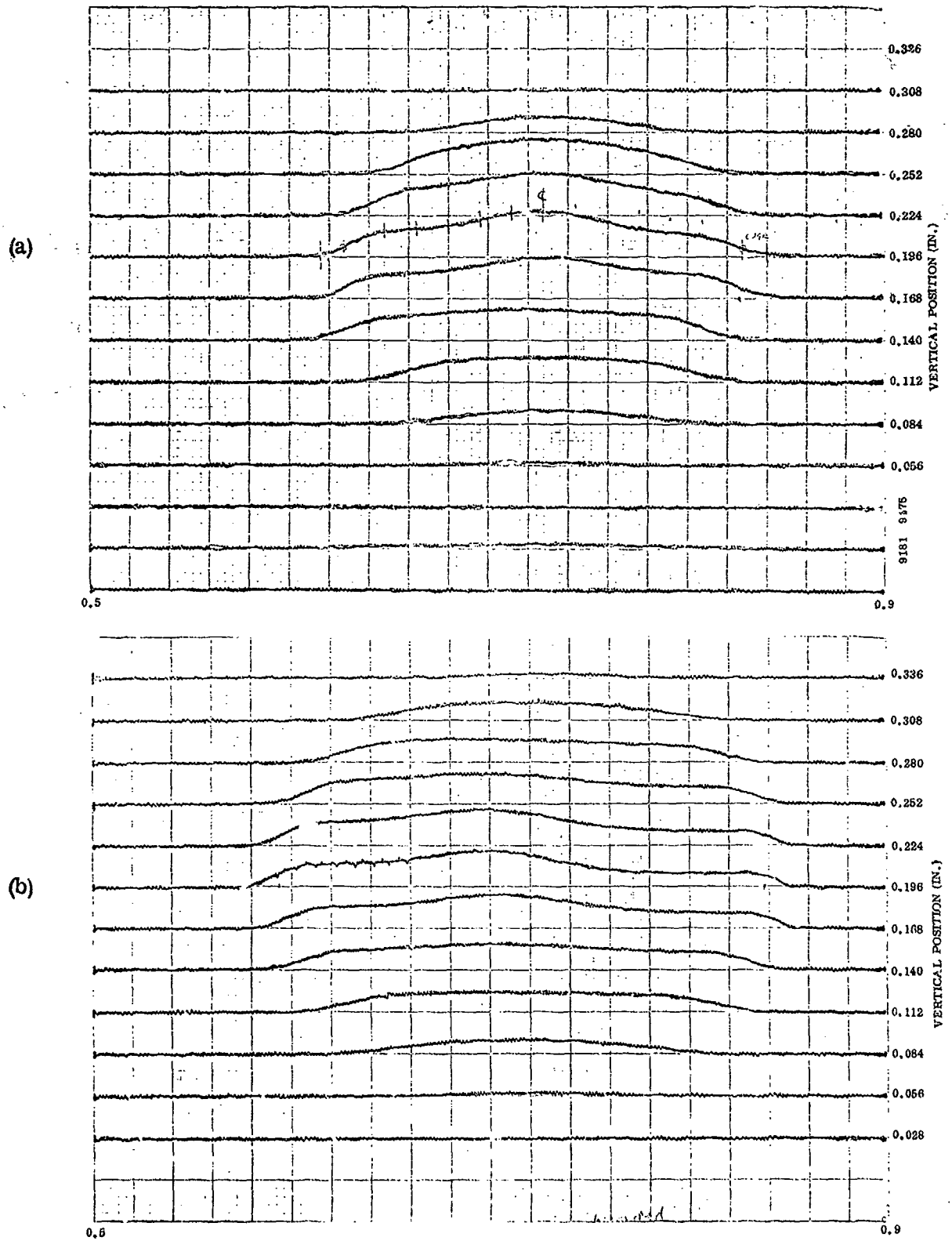

Figure 7 Fluorescent Intensity Distribution for 200-W Input to K-Rb Lamp – (a) 5-mm-OD Rod, (b) 6-mm-OD Rod, and (c) 6-mm-OD Rod With Center of Reflector Sphere Displaced 1-mm Distance Toward Rod From Position b

(c)

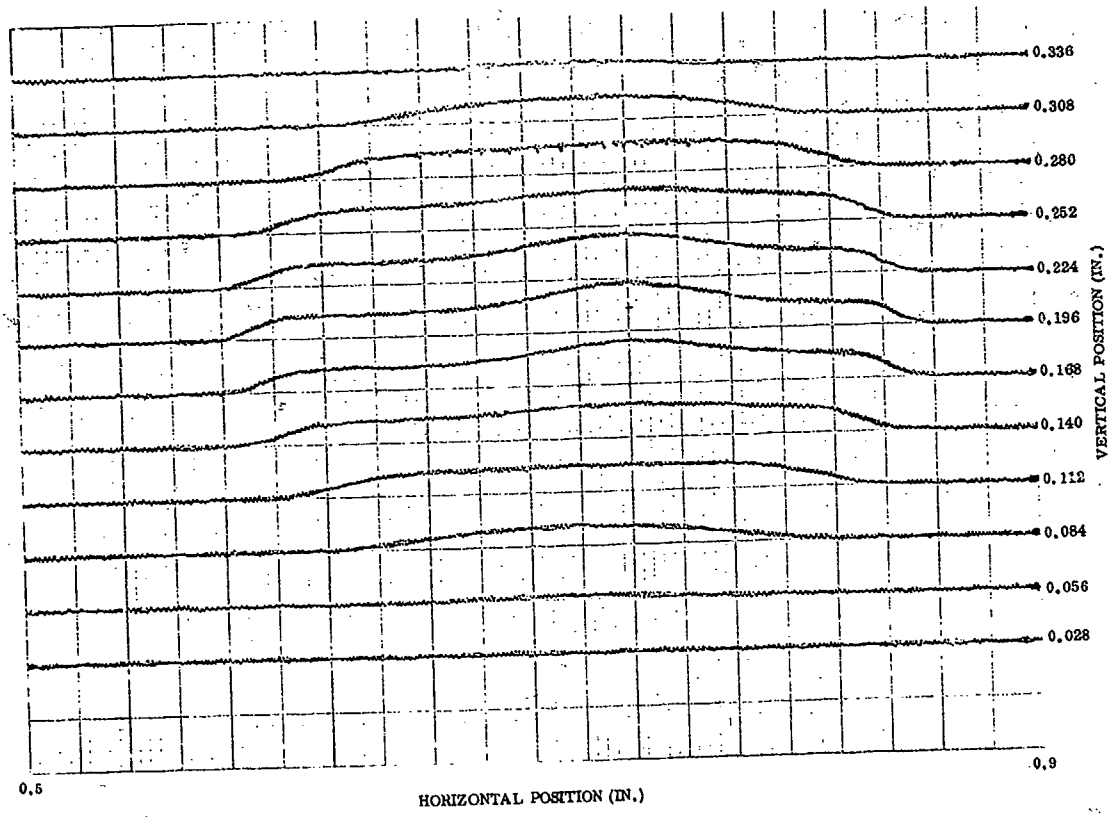

Figure 7 (Continued)

For a laser which must eventually operate at a single frequency and in a single polarization such as the subject laser, there are two distinct advantages to conduction cooling in addition to avoidance of the above-mentioned problems. The first is elimination of water turbulence, which causes mechanical vibrations and random temperature variations that interfere with single frequency operation of the laser.

The second advantage of conductive cooling is that, for a rod which is conduction-cooled by mounting one side of the rod on a heat sink, the temperature distribution inside the rod changes in a favorable way. In a pumped, water-cooled rod, the temperature is highest in the center of the rod and the isothermals are concentric cylinders. The rod tries to expand but since it is self-constrained, stresses are induced and birefringence results from the stress. This effect has been studied in detail (Refs. 2 and 3). The axes of the birefringence are radial and tangential to the isotherms, and it is therefore not possible to adjust the polarization angle so that the beam is polarized along one of the birefringence axes over the entire cross section of the rod. As a result, parts of the beam are rotated in polarization and effectively lost. The distribution of the isothermals in a rod which is conduction-cooled from one side tends to be rectilinear rather than cylindrical. Consequently, the beam can be polarized along one of the birefringence axes over a substantial fraction of the rod cross-section with the expectation of large circumventing the birefringence problem.

The degree to which the pattern of isothermals can be made rectilinear depends on the distribution of heat generation in the rod and the distribution and temperature profile of the heat-removal surfaces contacting the rod. In order to optimize the isothermal pattern, the pattern was computed using various angles of attachment to the rod surface. Since the distribution of heat generation in the rod was not known with certainty, the isothermal pattern was also computed for several possible distributions.

The analytical model used for this computation consisted of 144 nodes formed by the intersections of 12 equally spaced cylindrical rings and radial lines spaced 15 deg apart. One-half the cross-sectional area was used. The nodes which lie at the surface of the laser rod within the bonding apex angle were assumed to be constant temperature heat sinks since the metal at the bond was assumed to be isothermal. Nodal volumes and thermal resistance between nodes were calculated, and the LMSC THERM computer program was used to establish the steady-state temperature of each node. Isotherms were then drawn on the basis of the temperature distribution thus obtained.

Isotherms were computed for a cross section perpendicular to the long axis of a 5-mm-diam. x 50-mm long YAG rod, assuming uniform volumetric heat generation within the rod. Results are shown in Figures 8a, b, and c for conductive heat removal apex angles of 90, 60, and 30 deg, respectively. A total heat generation of 10 W was used. Longitudinal heat flow in the rod was neglected, and the rod surface area not used for heat removal was assumed to be adiabatic.

The appearance of the calculated isotherms is very similar to the interference pattern observed from pumped, conductively cooled rods, as shown in Figure 9b. In this figure, the rod is conductively cooled on one side, using an apex angle of 80 deg. Some misalignment of the rod caused a greater temperature gradient at the top than at the bottom of the rod. The interference pattern observed from a pumped, water-cooled rod is shown in Figure 9a for reference.

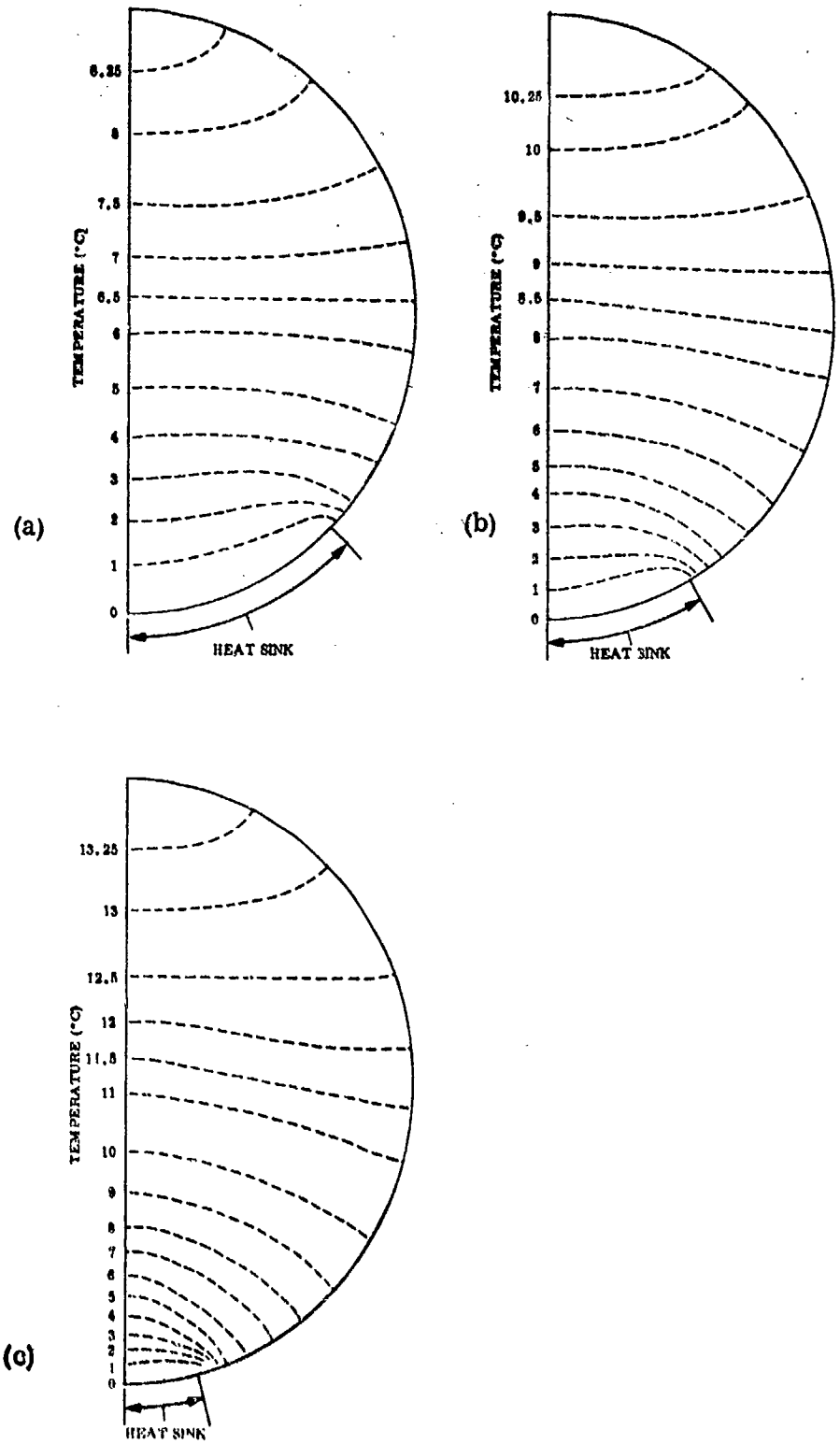

Figure 8 Computed Isotherms for Conductively Cooled 5-mm × 50-mm Laser Rods With Low Total Heat Input Uniformly Distributed Over the Volume, Using Attachment Angles of (a) 90-deg, (b) 60-deg, and (c) 30-deg

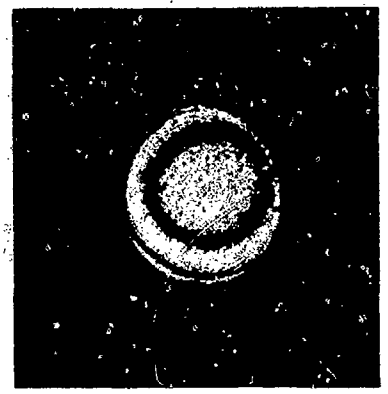

(a) Water-cooled rod, tungsten-lamp pumped at 250 W; pattern shown due to interference between the reflections from the two ends of the rod when HeNe laser beam reflected from the rod

(b) Conduction-cooled rod, tungsten-lamp pumped at 200 W, with 80-deg angle of attachment; water filter used around the lamp for IR absorption

Figure 9 Fizeau Interference in 5-mm-OD Nd:YAG Rods With Flat End Faces, Using 0,633-μm Illumination With (a) Water-Cooling Rod, and (b) Conductive Cooling of Rod With an 80-deg Attachment Angle

These results led to a decision to use a 90-deg apex angle for a baseline test since the greater linearity of the isothermals and lower temperature rise is indicated for 90-deg attachment than for the more acute attachment angles.

In additional runs, isotherms were computed for nonuniform heat input. The case of a gaussian distribution of heat generation in the rod, corresponding roughly to the case of precise focusing of the lamp in the rod, is shown in Figure 10. The case of 5-W additional heat generation on the surface of the rods, corresponding to surface absorption of infrared radiation, is shown in Figure 10b. Results such as these indicate that the linearity of the isotherms is not critically dependent upon the details of the heat-input distribution.

It is desirable, of course, from the point of view of efficiency in coupling the lamp light to the laser rod, to minimize the angle of attachment to the rod. To increase pumping efficiency the rod is coated at the point where it is soldered to the heat sink to provide a highly reflecting surface from inside the rod. This mirror surface reflects some light which would otherwise be transmitted out of the rod. This is expected to compensate partially for the pumping loss due to obscuration of the pump light by the rod mount.

The spacing of the isothermals is not uniform for any of the cases studied. This nonuniformity is due to the generation of heat within the volume of the rod. The effect of the nonuniformity is to cause the rod to act like a cylindrical lens, or equivalently, to introduce astigmatism into the cavity. This effect is discussed in Section II, 3.

The temperature gradient in the rod causes the center of the rod to tend to bow away from the rod mount. The lower temperature rise from the attached side of the pumped rod to the opposite side, for the case of 90-deg attachment angle, causes this bowing to be less than in the case of more acute attachment angles. The stresses thermally induced in the mounted rod are discussed in Section II, 4.

3. ASTIGMATISM OF THE PUMPED ROD

Because there is heat generation in the laser rod, the thermal gradient over the cross section of the rod does not have a constant value even in regions where the isothermals are relatively flat. This gives rise to a cylindrical lensing or astigmatic effect.

A picture of the Fizeau interference pattern of a 5-mm-diam. rod, tungsten-lamp pumped at 200 W, was analyzed to estimate the magnitude of this effect. The position of each fringe along the plane of symmetry of the rod mount was measured, and the variation in the optical length (fringe number x $0.6328\mu m/2$) was plotted as a function of this position. A linear correction was then applied to remove the optical wedge effect and leave the cylindrical lensing effect. This correction yielded a roughly symmetrical curve from which a value was determined for the radius of curvature of a cylindrical lens which could be ground on the rod to compensate for the cylindrical lensing induced by pumping. The value obtained was 13.2 m for 200 W tungsten pumping.

This procedure was later repeated for a 5-mm-diam. rod pumped at 150 W with a K-Rb lamp. The central 3-mm portion of the rod diameter was analyzed to give a value of 9.4 m for 150 W. This implies that a 4.7-m radius at 300 W would be necessary to correct the cylindrical lensing.

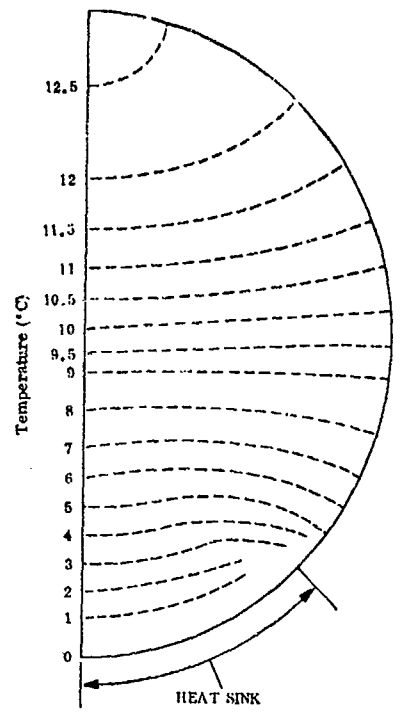

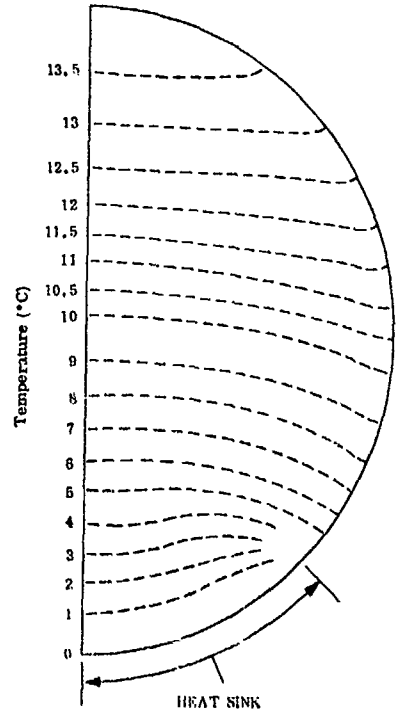

Figure 10 Computed Isotherms for Conductively Cooled 5-mm × 50-mm Laser Rods Assuming Nonuniform Heat Input – (a) 15-W Total Heat Input With Gaussian Distribution in Rod, and (b) 5-W Surface Heating in Addition to 10-W Uniform Input

These data were obtained from Fizeau interferograms in which the rod acts as a Fabry-Perot etalon. The effects of physical distortion of the rod which changes the length $l(x)$ of the rod as a function of the distance x across the rod diameter results in fringes whenever $n(x)\, l(x)$ is a integral number of half wavelengths. However, the beam wavefront distortion caused by the rod in a laser cavity is proportional to $\Delta(n\, l) - \Delta l$, i.e., the difference in optical path for rays in two positions in the rod less the difference in the length. The Fizeau interferogram can only give $\Delta(n\, l)$. It is therefore necessary to determine the distortion from a Twyman-Green interferogram, which will properly include the effect of physical distortion of the rod ends, or determine from the stress calculations that the magnitude of bowing of the rod ends is not significant.

Once the correction is properly determined, a cylindrical curvature can be ground on one end of the rod to compensate the thermally-induced astigmatism. The amount of astigmatism depends on the pumping level so the correction can only be made in this manner for one power level. For experimental purposes, the astigmatism was corrected by a tilted lens internal to the laser resonator. Optimization of operating conditions will lead to the selection at a later time of optimum rod face curvature for maximum laser output.

4. STRESSES THERMALLY INDUCED IN THE PUMPED LASER ROD

When a temperature gradient is impressed on the laser rod so that one side is at a higher temperature than the other, the rod tends to bend due to unequal thermal expansion. If the temperature gradient in the rod were uniform (without heat generation inside the rod), the rod then could bend and remain free of stress. However, because of the nonuniform temperature gradient, stresses are set up in the rod even when it is free to bend. When the rod is constrained not to bend (e.g., by the rod mount), tensile stresses in the axial z direction are produced in the pumped rod on the side near the mount, and axial compressive stresses are produced in the opposite side. Additional axial stresses can be produced in the rod by differential thermal expansion when the mounted rod is cooled from the soldering temperature. The stresses resulting from these effects were calculated to aid in the design of the rod mount.

The following types of rod-mounting structures were considered:

(1) Copper mount tipped with solid niobium

(2) Niobium-tipped copper mount with slots to give high compliance in the longitudinal direction

(3) Laminated mounts for high compliance to bending of the rod as well as high longitudinal compliance

To aid in evaluating these candidate structures, the stresses were calculated for the following simplified models:

- Unconstrained YAG slab,
- YAG slab constrained to avoid bending along one side
- Composite slab consisting of YAG and Nb without constraint on bending

- Composite slab consisting of YAG and Nb constrained to avoid bending along the side of the Nb opposite the YAG
- Composite slab with a finite offset temperature to simulate a rod soldered at a higher temperature.

The calculations were performed using a two-dimensional, finite-element, structural analysis program and are further described in the Appendix.

Computations were carried out for a 5-mm-thick infinitely wide slab of YAG, 50 mm in length. The temperature distribution in the slab was chosen to be the same as the distribution along the diameter containing the symmetry axis of the rod, as shown in Figure 8a. Longitudinal stresses in an infinitely wide slab would be similar to, but slightly higher than, equivalent stresses in a circular cross-section rod with the same transverse temperature distribution, so the model is expected to be fairly accurate in predicting upper limits on stress.

For the cases most relevant to the conduction-cooled laser rod, the maximum stress for a rod free to expand or contract longitudinally but constrained not to bend is 1,650 psi. This would be equivalent to the niobium-tipped slotted copper mount configuration. For a solid niobium heat sink with a solder-hardening temperature of 200°C, and an operating temperature of 0°C, the residual tensile stress at the bond would be about 7,000 psi. None of the stresses computed came close to the 25,000-psi tensile strength of YAG, so the criterion for low stress mounting must be based more on reducing optical distortion due to stress birefringence and minimizing the danger of rupture at the solder bond. Since the stress in slotted mounts is relatively low, the laminated mount was eliminated from further consideration because of complexity of fabrication and its high thermal resistance. The mount finally selected was a niobium-tipped copper wedge with 0.5-mm-wide slots at 3-mm intervals along the mount, cutting through the niobium into the copper to a depth of 25 mm from the rod surface.

5. TEMPERATURE DISTRIBUTION IN THE ROD MOUNT

The temperature distribution in a wedge-shaped rod mount was calculated for wedges having apex angles of 30, 60, and 90 deg, respectively, and with respective compositions of solid niobium, solid copper, and a niobium-copper composite. The distributions were calculated from the following expression for cylindrical heat flow:

$$\Delta T = \frac{q}{K l \theta} \ln \frac{r_2}{r_o}$$

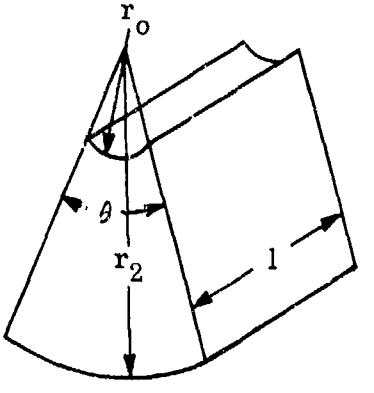

where

ΔT = temperature difference (°C)
q = heat flow (W)
l = rod length (cm)
K = thermal conductivity (W/cm/cm^2°C)
θ = apex angle (rad)
r_o = rod radius (cm)
r_2 = radius of base of mount (cm)

In these calculations the angle of attachment to the rod is the same as the wedge angle of the mount. The assumed heat input is 10 W.

Figure 11a shows the temperature distributions for a solid niobium mount for wedge angles of 30, 60, and 90 deg. Figure 11b shows the distributions for slotted copper wedges with void factors of 0, 25, and 50 percent.

Considering a 30-deg wedge, tipped with 0.2 in. (5 mm) of niobium and with an attachment angle of 90 deg, the calculated temperature drop across the niobium is approximately 0.6°C for 10 W dissipated in the rod, and the drop across the copper is 2°C for a total expected drop of 2.6°C.

6. K-Rb LAMP SPECTRUM AND HEAT BALANCE

A spectrum of the radiant output of the K-Rb lamp was needed for heat-balance studies on the pumping cavity design. In its proposal for the work covered by this report, LMSC had included a measured potassium lamp spectrum. It soon became apparent that this spectrum indicated too much intensity in the infrared, and this situation was corrected by measuring the radiant power from the lamp transmitted by each of a series of optical filters of known transmission characteristics. The spectral intensity in each band isolated by the filters was adjusted to match the measured transmission factors.

The filters were interposed between a K-Rb arc lamp and a thermopile detector with a response that was independent of wavelength over the spectral region of interest. The arc lamp was operated at 150 W input power, not including power for lamp thermal control. Shields were placed near the lamp so that radiation from the end caps and electrodes could not reach the detector. The detector was a No. 7105 Eppley Thermopile. The detector output was monitored with an HP425A Microvoltmeter. The distance between the lamp and detector was 25 cm and the filters were placed directly in front of and adjacent to the detector. The transmission fractions thus obtained are given in Table I.

Table I. Bandpass Filter Characteristics

Filter Material	Filter Thickness (mm)	Approx. Cutoff (μm)	K-Rb Light Transmitted (%)	Calculated Transmission Using ILC Spectrum (%)
Sapphire	2.2	5.7	80	86
Quartz	1	4.3	69	81
Pyrex	1	3	67	69
Water	7	1.3	48	44
Corning 3-69		2.8	62	61

A new spectrum from ILC (Figure 12) became available which was derived in part from LMSC data. The ILC spectrum includes contributions from end caps and electrodes so a direct comparison with the earlier spectrum was not possible. However, it was decided to calculate transmission fractions for the filters, using this spectrum, and to compare the values obtained with the observed transmission fractions. The results,

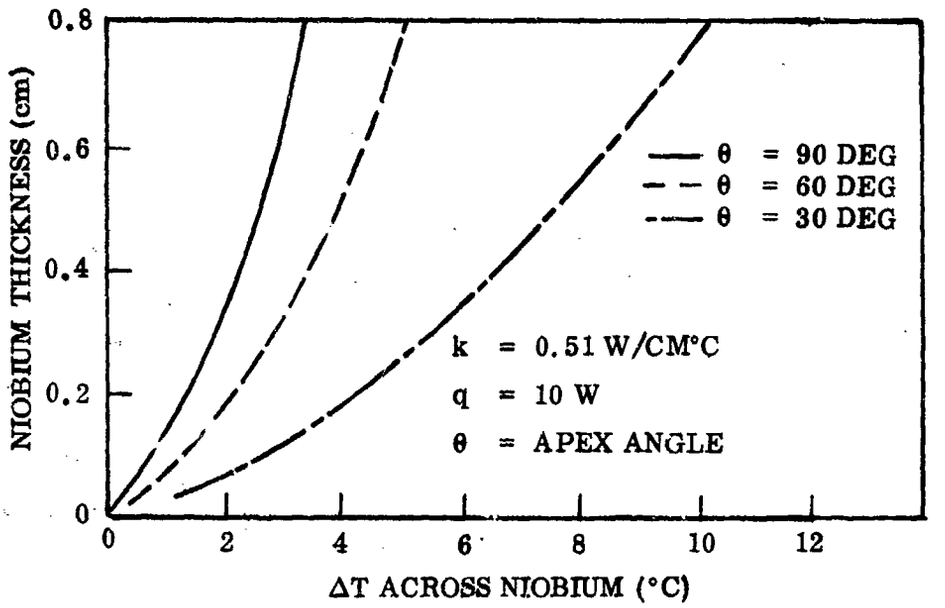

(a) TEMPERATURE DROP IN SOLID NIOBIUM MOUNT FOR THREE DIFFERENT WEDGE ANGLES

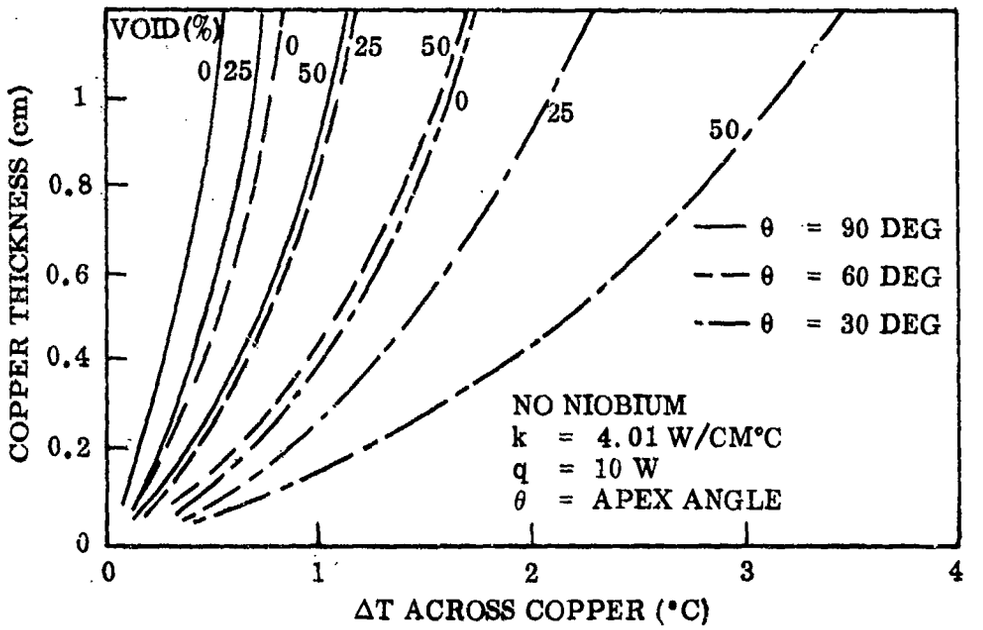

(b) TEMPERATURE DROP IN SLOTTED COPPER MOUNT FOR THREE WEDGE ANGLES – VOID FACTOR REPRESENTING FRACTION OF MATERIAL REMOVED DURING MOUNT SLOTTING PROCESS (VOID FACTOR IN FINAL DESIGN = 0.17)

Figure 11 Temperature Distribution in Rod Mounts

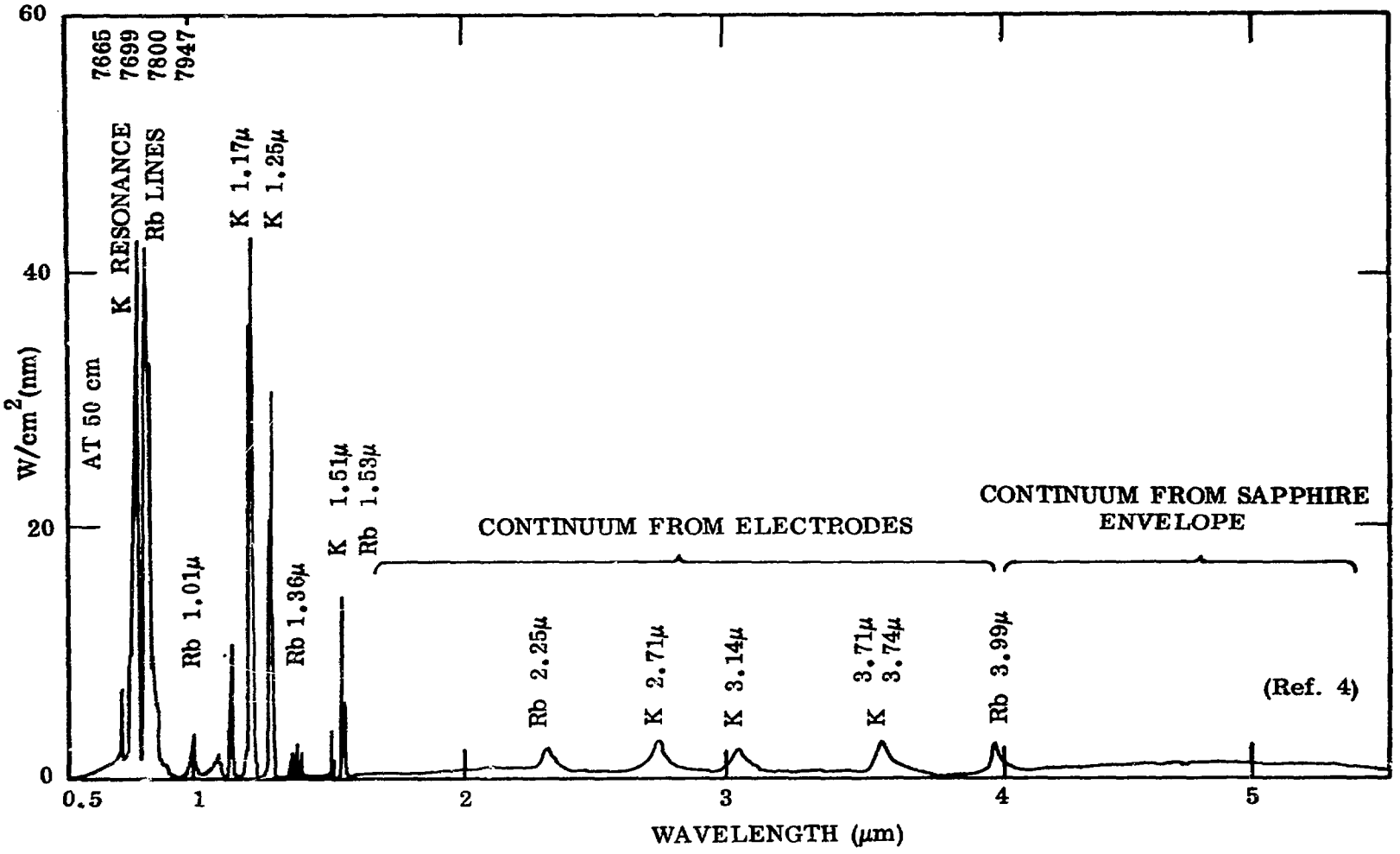

Figure 12 Spectrum of K-Rb Lamp With Protected End Seals

also given in Table I, indicate reasonably good agreement with the observed values. Therefore, it was concluded that the ILC spectrum, even though it includes radiation from end caps and electrodes, is still a good approximation to the spectrum with end cap and electrode radiation blocked.

For purposes of heat balance estimates, the lamp power was divided into conducted heat, electrode radiation, and arc radiation. The arc radiation was subdivided into three spectral regions, as shown in Table II. A heat-balance diagram (Figure 13) was then constructed. The division of arc power into spectral regions was later re-estimated on the basis of the ILC lamp spectrum; the results were also included in Table II for comparison.

Table II. Estimated Division of Radiated Power Into Spectral Bands for a K-Rb Lamp Operating at 300 W-Input

Power Category	Preliminary Power Estimate [a] (W)	Power Estimate, New ILC Spectrum (W)
End Caps and Electrode Radiation	35	35
0.5 to 1 μm	100	90
1 to 4 μm	80	116
4 to 10 μm	70	44
Conducted	15	15

[a] Estimate used for Heat Balance Diagram (Figure 13)

7. PUMP CAVITY DESIGN

The cold mirror design calls for a multilayer dielectric coating on the precision-ground inner surface of a Pyrex sphere. The mirror should have maximum reflectivity over the strong Nd:YAG absorption bands from 0.72 to 0.9 μm and maximum transmission for infrared radiation of wavelength longer than 1 μm. Part of the radiant energy transmitted by the coating will also be transmitted by the Pyrex substrate and part ($\lambda > 3$ μm) will be absorbed by the Pyrex. A means for intercepting and absorbing the transmitted radiation and for cooling the Pyrex sphere is therefore required. An outer metallic sphere is used to satisfy these requirements.

In order to determine whether radiative heat transfer across a narrow gap between the Pyrex sphere and the outer sphere would be adequate to cool the Pyrex sphere, a calculation was made of the temperature the Pyrex would reach if it had only radiative cooling. Radiation cooling is desirable because it eliminates the problem of differential thermal expansion stresses, inherent in physically bonding the inner and outer spheres together. The calculation was performed for two values of the outer jacket temperature. The Pyrex infrared emissivity was assumed to be 0.9. The results of the calculation, as a function of heat transferred, are shown in Figure 14. With 400 W radiating from the Pyrex sphere, the sphere temperature is less than 260°C. Since the coated spheres can tolerate at least 300°C and probably much more, a design using radiative cooling

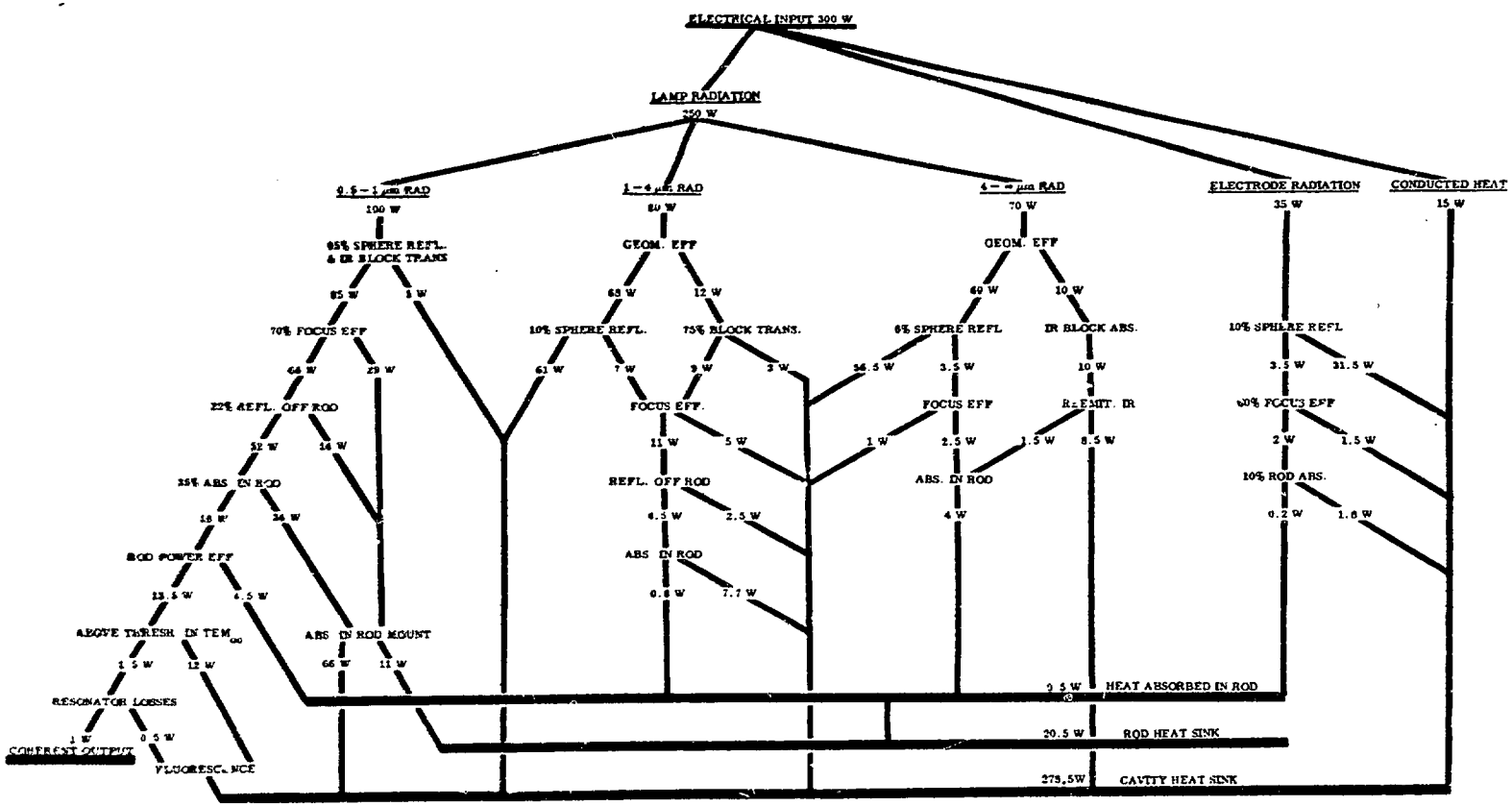

Figure 13 Laser Pumping Heat Balance Diagram

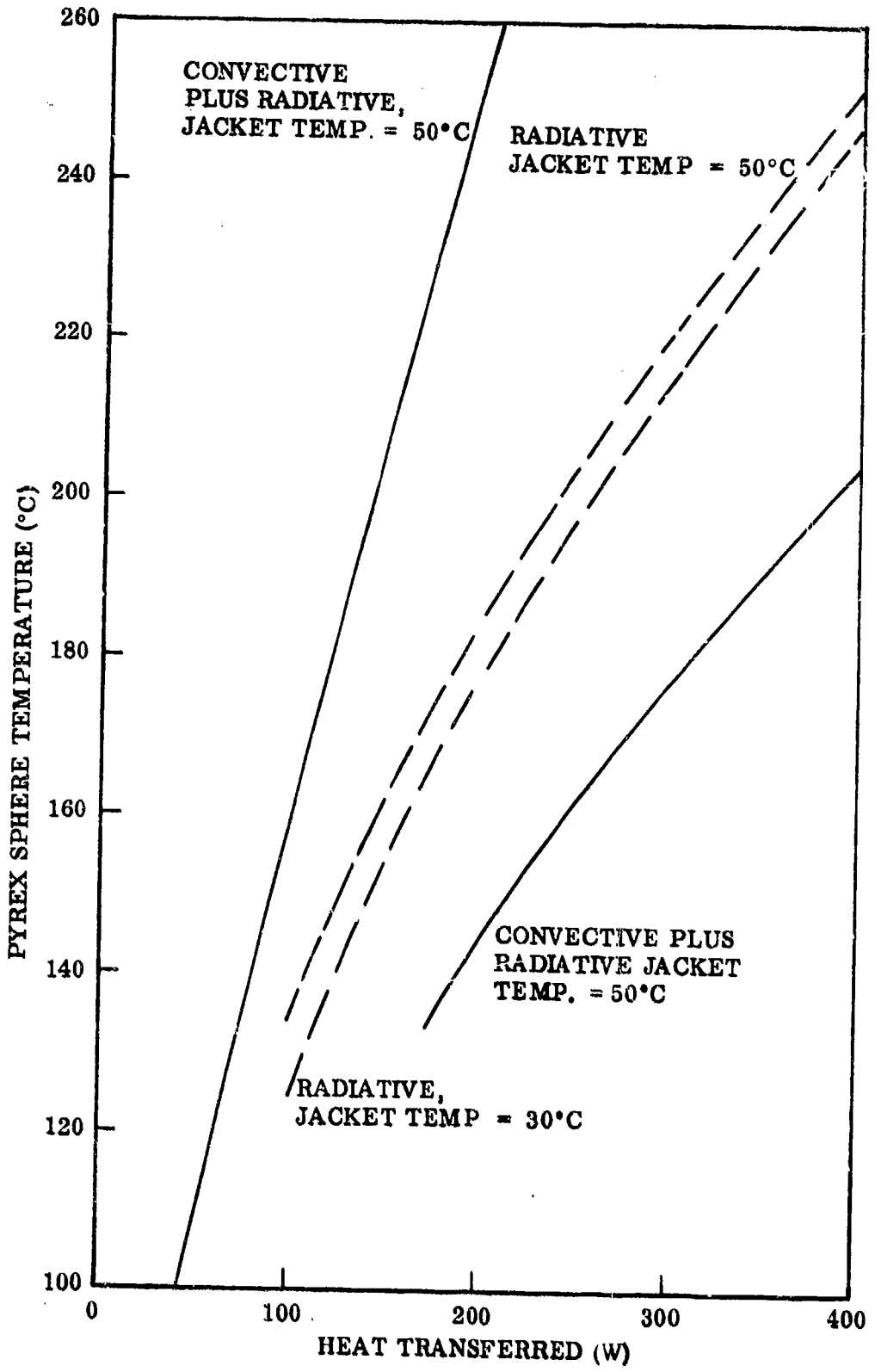

Figure 14 Radiative and Convective Heat Transfer Between Pyrex Sphere and Cooling Jacket

alone was considered to be adequate and the sphere was spring-mounted in the cooling jacket. The cooling jacket was coated on the inside with a black coating to obtain high broadband emissivity.

The outer jacket consisted of two hemispherical caps with a 3-in.-diam.cold plate for heat removal at the center of each cap. The temperature difference from the edge to the center of the hemisphere was calculated, assuming 300 W absorbed uniformly over the sphere surface. A copper cap 0.1-in.-thick at the edge and 0.3-in.-thick at the center is expected to have a 13°C drop from edge to center. A similar cap, fabricated from aluminum, would have a 26°C drop.

The performance of the cold plate on the sphere cap was also estimated. The assumptions were that each cold plate would measure 3 in. x 3 in. x 0.5 in., remove 250 W, provide a cooling-water passageway with an inside diameter of 5/16 in. and a length of 18 in. The cooling water temperature rise would be 5°F for a flow rate of 0.3 gal/min. For an input water temperature of 60°F, the cold plate temperature would be 77°F. The pressure drop would be less than 0.5 psi.

Since this cavity would be filled during laboratory tests with 1 atm of dry argon gas, the effects of heat convection were estimated. The convective heat transfer between concentric spheres (Ref. 5) is

$$q = \frac{4\pi \; k_e \; r_i \; r_o \; \Delta T}{r_o - r_i}$$

where

$$\frac{k_e}{k} = 0.106 \; Gr_\delta^{0.276}$$

$$\delta = r_o - r_i$$

$$Gr_\delta = g \; \beta \; \frac{(T_i - T_o)}{\nu^2} \; (\delta)^3$$

Assuming the gap δ between the two spheres to be 0.125 in. and the jacket temperature to be 50°C, the convective heat transfer was calculated for various temperatures of the Pyrex sphere. This result and the combined radiative plus convective heat transfer, are also shown in Figure 13.

The convective heat transfer to the rod was calculated, assuming the rod to be a horizontal cylinder 0.5 cm in diameter x 5 cm in length, with a temperature of 0°C, and suspended in 1 atm of argon at various temperatures.

Convective heat transfer to the rod support was estimated, assuming the support to be a vertical plate 5 cm long by 10 cm high and 0.6 cm thick, at a temperature of 0°C. In the first case, a bare mount was assumed and, in the second case, a layer of insulation

1/16 in. thick covering the mount was assumed. These results are given in Table III.

Table III. Convective Heat Transfer to Laser Rod and Rod Mount Inside Pumping Cavity

Argon Temp. (°C)	Heat Transfer To Rod (W)	Heat Transfer To Mount, No Insulation (W)	Heat Transfer To Mount, 1/16-in. Insulation (W)
50		11	
100	1	25	6.7
150		41	
200	2.3		
250			
300	3.9		

Convective heating of the argon by the hot potassium lamp was calculated, assuming the lamp to be a horizontal cylinder with an outside diameter of 0.65 cm and a length of 5 cm, at a temperature of 1,000°C to 1,200°C, and immersed in argon gas of 100° to 300°C temperature. Values for the convected heat are given in Table IV. Clearly, the gas fill will have only a small effect on cooling of a 300-W lamp.

Table IV. Convective Heat Transfer From Hot K-Rb Lamp Envelope to Argon Gas

Lamp Temperature (°C)	Argon Temperature (°C)	Heat Transfer (W)
1200	100	22
1200	200	20
1200	300	18
1000	100	17
1000	200	15
1000	300	13

To assure that the thermal gradient induced in the Pyrex sphere by heat flowing through it conductively was not excessive, the temperature difference that a 400-W radial flow would create in a 0.2-in.-thick Pyrex sphere of 8-in. diam. was calculated to be 15°C. This heat load is higher than expected to be encountered in the test program but should serve as an upper bound. The calculated temperature difference was then compared to the temperature gradient that would give the maximum design tensile stress in Pyrex when heated on one side and cooled on the other side. A substantial safety factor of greater than three is obtained even in this extreme case.

SECTION III

CONDUCTION – COOLED ROD MOUNT DEVELOPMENT

1. METALLURGICAL BONDING

The aim of this task was to develop materials and processes for mounting the Nd:YAG laser rod to its metallic heat sink. The following requirements had to be fulfilled in accomplishing this task: (1) provide a second-surface mirror of high reflectivity for the laser's pumping bands as the first layer in the joint, directly adjacent to the laser rod, and (2) avoid a buildup of thermal stresses in the finished assembly, since they are likely to cause a damaging distortion in the rod.

For maximum efficiency in conductive cooling, metallic materials with the highest possible thermal conductivity are required, and interfaces or intermediate layers with high thermal impedance have to be avoided. In particular, the bond between the second-surface mirrors and the laser must be chemical in nature to ensure an efficient transmission of heat across the interface and to withstand mechanical and thermal stresses associated with handling and service. Materials and processes adaptable for producing chemically bonded second-surface mirrors on ceramic surfaces such as YAG were developed at the LMSC Palo Alto Research Laboratory before the starting date of the subject contract. Both gold and silver mirrors were prepared by a two-step process involving, first, a deposition by physical vapor deposition of the mirror layer (1 to 2 μ thick), and then followed by a bonding heat treatment. The bond is formed by reaction between the oxygen ions at the YAG surface and a reactive metal, such as titanium or manganese, present in the system. The formation of the bond requires an elevated temperature, ranging from about 400° to 800° C, applied in a vacuum of about 10^{-5}mm Hg for about 2 hr. The bond withstands standard adhesion tests, such as Scotch-Tape tearing, and severe heat shocks where the failure is produced within the body of the ceramic rather than at the mirror-to-ceramic interface. The reflectivity of the bonded mirrors in the Nd:YAG pumping bands is higher than 90 percent.

Silver-mirrored Nd:YAG rods were prepared in this task for joining to a heat sink made of copper. However, copper has a thermal expansion coefficient more than twice that of the laser garnet. To avoid the buildup of damaging thermal stresses, a niobium metal insert was used as an intermediary between the laser crystal and the copper mounting block, with the niobium closely matching the Nd:YAG in thermal expansion. The insert was joined on one surface (with a cylindrical curvature) to the Nd:YAG rod, and on the other surface (flat) to a copper heat conductor. The copper and niobium were slotted to relieve further the strain resulting from the differential expansion between the mount and the niobium. Residual strain should be primarily resisted by the niobium and not transferred to the Nd:YAG rod. Figure 15 shows the design of the bonded combination.

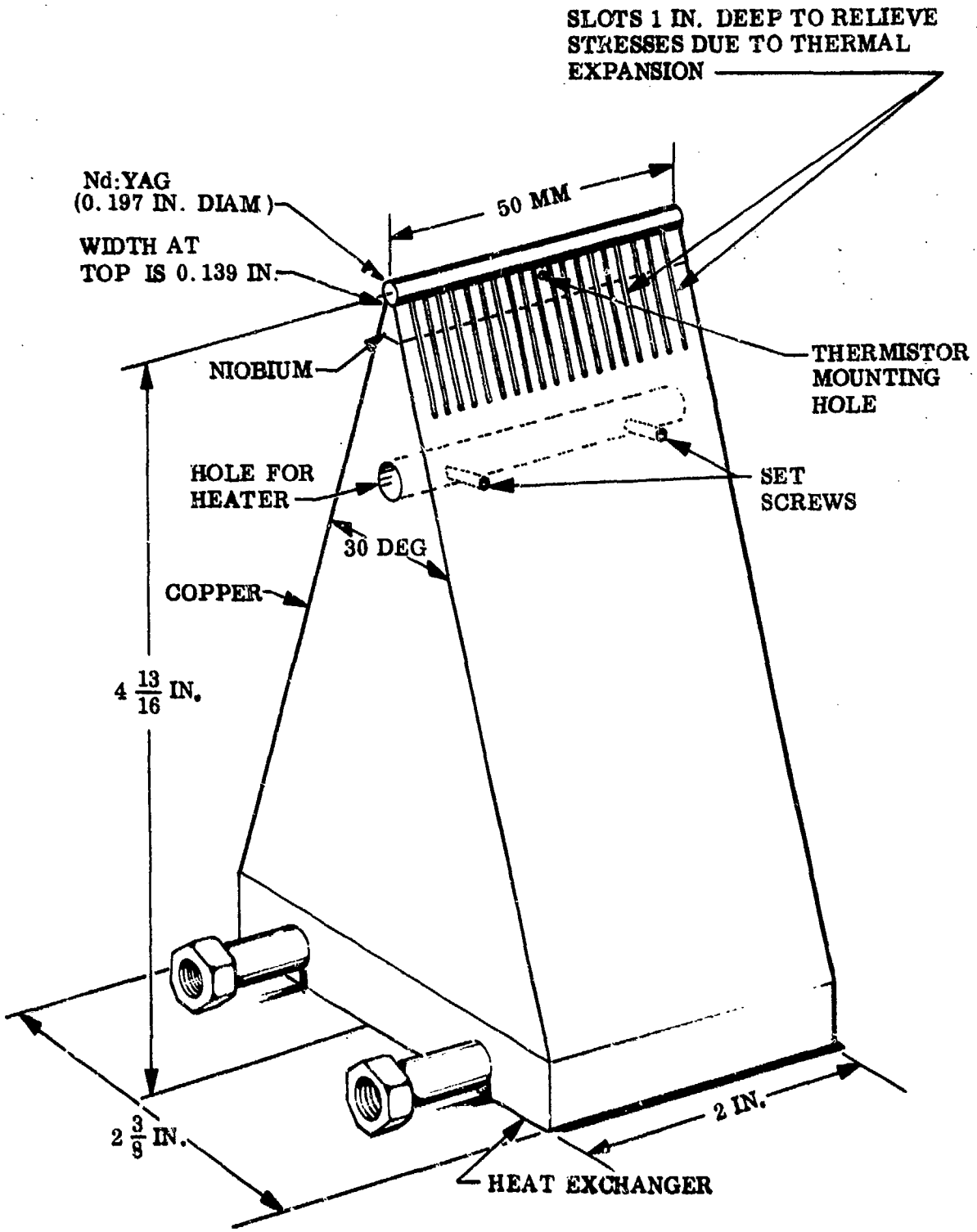

Figure 15 Conductive-Cooling Rod Mount Design

During this contract period, the effort was mainly concerned with sealing the second-surface mirror on the YAG to the niobium and joining the niobium and copper members of the heat sink. In the actual assembly process which was developed under the contract, a niobium strip was first joined to a copper block; the composite was then machined to the final configuration; and the slots were cut by electric discharge machining (EDM), after completion of the other machining processes. Finally, the laser rod was mounted to the matching niobium curvature.

a. Niobium-to-Copper Joining

The major considerations in the development of the niobium-to-copper joint were to ensure enough strength and ductility within the bond area to prevent a disruption under the thermal stress because of the considerable difference in thermal expansion coefficients of the two metals (exceeding a 2 to 1 ratio), and to provide the least impedance to the heat flow across the interface. A joint free from intermetallic compounds is the type most likely to fulfill these requirements.

From this last point of view, a direct diffusion bond between niobium and copper had to be excluded, considering the tendency of these two metals to form intermetallic compounds. Rather, a braze had to be found that was likely to dissolve in both the copper and the niobium lattices. Two promising candidates for such a braze – gold and titanium – were found. The former is completely soluble in all proportions in copper; the latter is soluble in niobium (Ref. 6). Metallurgically sound bonds were obtained with both metals, but titanium was chosen for the final assembly because of its tendency to flux (reduce) any oxides interfering with the bond formation.

Before the assembly in the treatment furnace, both the niobium and the copper metal surface are etched by 2-min immersion in a $2HNO_3$:$2H_2SO_4$:1HF mixture. Part of the hydrogen generated in the etch reaction remains adsorbed on the metal surface and also dissolved in it. In order to avoid gas cavities in the joint, the heating of the assembly to the bonding temperature has to be conducted at a slow rate to permit the chemisorbed gas to leave the system.

The titanium hydride powder, suspended in isopropyl alcohol, is applied to the surface of the niobium. First, a film of the alcohol is deposited on the metal surface, and -325 mesh TiH_2 powder is then added to the film; the liquid wets the particles and spreads them uniformly. A single layer of particles covering the surface is sufficient for producing a satisfactory bond.

The processes leading to the formation of the bond begin with decomposition of the titanium hydride into free metal and hydrogen gas at about 400°C, followed by generation of a liquid Cu-Ti alloy when the temperature of the assembly passes that of the $TiCu_3/Ti_2Cu_3$ eutetic, i.e., about 880°C (Figure 16). As the temperature continues to rise above 1,000°C, more and more liquid is formed until, at the treatment temperature at any point between 1,000°C and somewhat below the melting point of copper (1,083°C), the system is composed of niobium and copper separated by a homogeneous ti-Cu liquid. The system is held at this temperature long enough to permit a complete disappearance of the liquid by diffusion into the solid copper and niobium. By maintaining the treatment temperature above 1,000°C, formation of the Cu/Ti intermetallics and the consequent embrittlement of the joint are prevented.

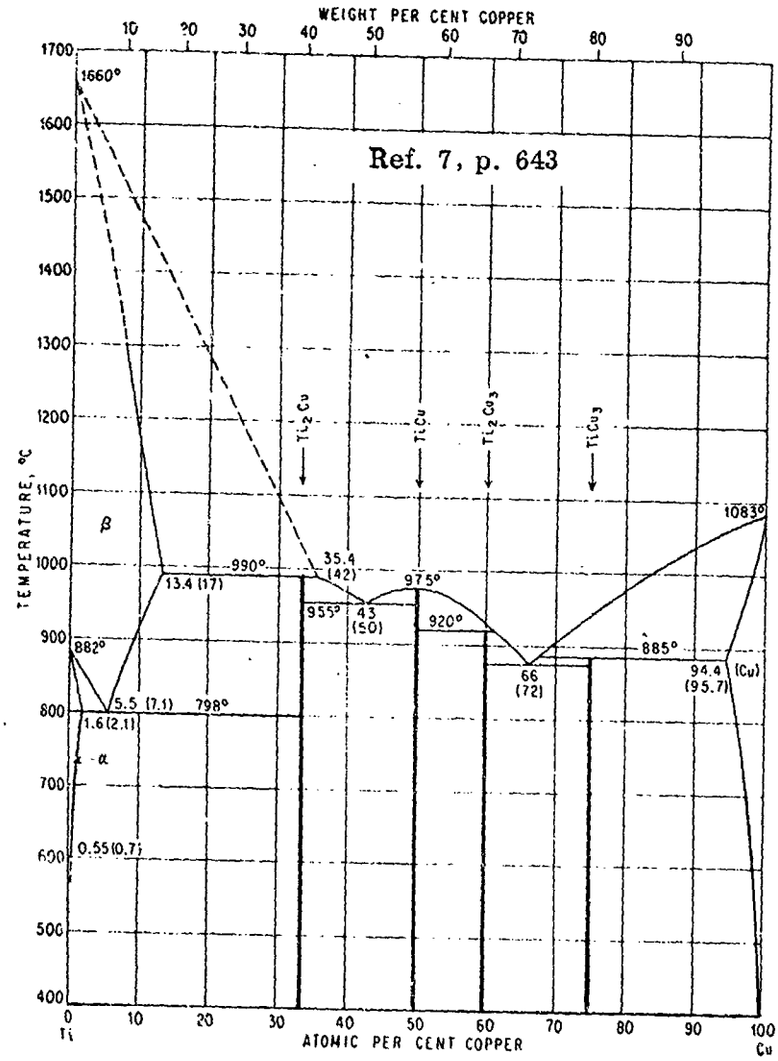

Figure 16 Titanium-Copper Phase Diagram

Figure 17 shows the microstructure of the niobium-copper bond developed in this process. The bond is made of large crystals of a solid solution epitaxially grown from the copper, showing a wide dark band through their structure. This band most likely denotes the area of high concentration of titanium in the alloy composition. A large number of fine black particles are found mostly at the interface between the band and the niobium metal. This impurity most probably is titanium oxide generated by reduction of the surface oxidation film (usually present on niobium)by the molten Cu/Ti alloy. The bond successfully withstands without fracture an immersion of the joint metals into liquid nitrogen.

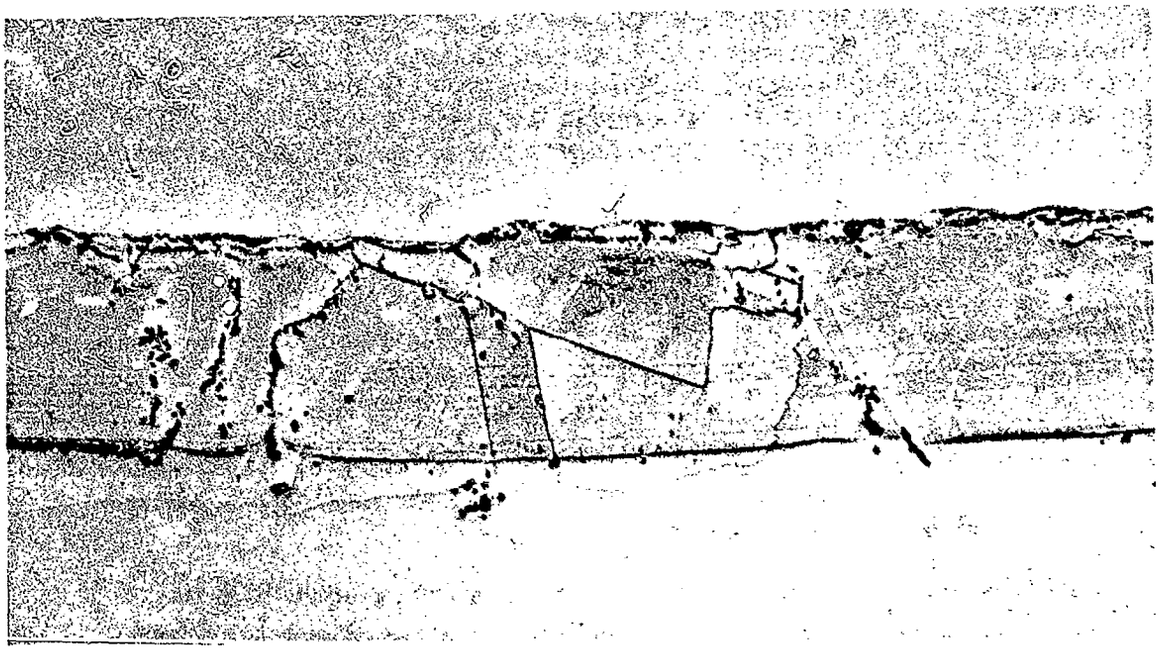

B1337 500×

Figure 17. Metallic Photomicrograph of Niobium-Copper Joint, Using a Titanium Bond (Cross Section)

b. Nd:YAG-to-Niobium Seal

Tin has been chosen as the sealant between the silver-mirrored laser rod and the heat sink. The following considerations dictated this choice:

- Room-temperature ductility of tin is extremely high, permitting an easy relief of stress by plastic deformation
- Tin layers are readily deposited in controlled thicknesses by physical vapor deposition.

In fact, a series of exploratory experiments, in which quartz rods bearing a silver mirror were joined to copper supports using tin-based solders, indicated an excellent adaptability of these sealants to the thermal expansion coefficient mismatch between the joint members. The assembly could be disrupted only by subjecting it to a severe heat shock resulting from immersion into liquid nitrogen. Again, the failure occurred within the ceramic.

When tin is used as the sealant, however, the joining operation requires temperatures on the order of 250° C, i.e., within 20° C above the melting point of the metal. At this temperature, silver reacts with tin to form solid-solution alloys and intermetallic compounds. Consequently, the mirror has to be protected by an appropriate diffusion barrier against attack by the liquid tin. Copper was initially chosen as a candidate for this function because it reacts with both silver and tin only to a very slight extent at the considered joining temperature, and also is readily wetted by molten tin. In fact, in the abovementioned experiments with joining the silver-mirrored quartz rods to copper supports, copper was used successfully to protect the mirrors from attack by the molten tin solder.

In the same fashion, a vapor-deposited copper layer was considered for application also to the niobium, in order to eliminate interference of any niobium oxide with the wetting by the molten tin. However, the adherence of copper layers, formed by physical vapor deposition on the silver and the niobium, lacked the strength of a true metallurgical bond and could be stripped off by simple mechanical means.

Attention was then directed towards reactive metals (titanium and manganese) as the tin-to-substrate binders and diffusion barriers for the mirror protection. Examination of reactive-metal/tin, reactive-metal/silver, and reactive-metal/niobium phase diagrams (Ref. 8) indicates the following:

- Both the manganese and the titanium are practically insoluble in tin
- Manganese (but not titanium) is slightly soluble in silver at the considered sealing temperature between 200° and 300° C, and
- Titanium (but not manganese) is soluble in niobium at the same temperature.

Both manganese and titanium would therefore protect the silver mirror against attack by molten tin, but only manganese is likely to form a metallurgical bond with it. On the other hand, only titanium would form a good bond with niobium.

On the basis of these considerations, a satisfactory seal has been developed between the silver-mirrored Nd:YAG and its niobium-copper support. The assembly procedure entails the following steps:

(1) A 300-Å-thick, manganese layer is applied by physical vapor deposition to the laser-rod bonded-silver-mirror back surface. The laser rod is held in a precision-machined, stainless-steel mask exactly defining the area for the metal deposition so as to overlap the mirror edges by a small amount.

(2) Directly after deposition of the manganese, a 2-μ layer of tin is applied on the top of the manganese. The rod is not removed from the deposition chamber between the two depositions in order to avoid oxidation of the reactive manganese.

(3) A 300-Å-thick titanium layer is deposited on the surface of the niobium member of the support assembly. The surface of the niobium is for 2 min in a $2HNO_3$:$2H_2SO_4$:1HF mixture prior to the deposition.

(4) A 2-μ layer of tin is deposited directly on the titanium layer, as in the case of the laser rod (see Step 2).

(5) The coated rod and mount are assembled with a 0.0015-in.-thick Sn-01.% Bialloy foil between the rod and mount (the addition of bismuth to the tin sealant is necessary to stabilize the tin against transformation to grey tin). A weight of about 200 g is applied to the assembly in order to maintain the alignment and reciprocal contact during the subsequent heat treatment.

(6) The assembly is heated to a temperature between 250° and 300° C; the heating rate is slow to allow for a thorough degassing; and the temperature is held at its maximum for 5 min.

(7) The assembly is furnace-cooled to room temperature.

Fizeau interferograms of the rod, taken during processing and mounting, are shown in Figure 18. It appears that no noticeable distortion is introduced when the mirror is bonded, and only three fringes are introduced during the soldering process, thus indicating that the stresses are very small. The interferogram of the solder-bonded rod was repeated 3 days later to see whether stress relief would occur, but no change was observed.

2. ROD MOUNT COOLING

It was estimated that it would be necessary to remove 35 W at -15° C from the base of the rod mount in order to maintain the rod at 0° C with K-Rb pumping at 300 W. To determine the rod mount cooling characteristics, a chiller unit on hand in the laboratory was filled with glycol solution, set for minimum temperature, and allowed to run to establish its lower temperature limit. This limit turned out to be 9.5° C. Subsequently, the hot gas bypass on the chiller unit compressor was closed. This move improved the performance of the unit, but was still unsatisfactory for rod pumping tests.

A convenient method for cooling the rod mount utilizes dry nitrogen gas from a cylinder as the coolant. The gas passes through a large dewar of liquid nitrogen and then through the base of the rod mount. In this manner, it is relatively easy to remove the required amount of heat simply by adjusting the nitrogen flow rate manually. It is possible, using this technique, to attain a desired temperature, ranging from room temperature down to -40° C at the base of the conductive cooling mount.

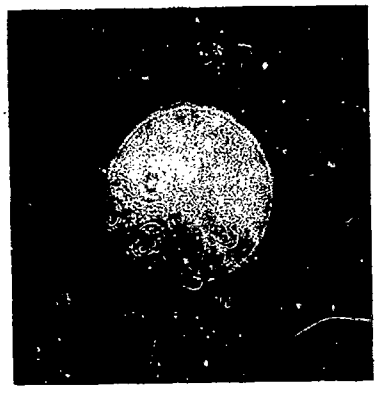

(a) After Vacuum Deposition of Metallic Mirror Coating

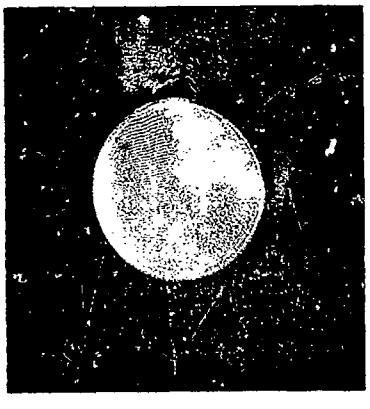

(b) After High Temperature Bonding of Mirror to YAG

(c) After Tin-Solder Bonding of YAG Rod to Niobium- Copper Mount

Figure 18 Fizeau Interferograms Using 0.633-μm Laser Light Reflected From Flat Faces on Nd:YAG Rod (Airtron No. 956) (5-mm-OD × 50-mm Length)

3. PUMPING THE CONDUCTION-COOLED Nd:YAG ROD

The conduction-cooled Airtron rod (No. 956) was mounted in the dielectric sphere and potassium-lamp pumped up to 300 W. Figure 19 is a photograph of the Fizeau fringe pattern of this rod for 300-W pumping with the rod held at 0°F. The pattern contains about 55 fringes. Lasing tests with this rod are reported in Section IV.

4. FLUORESCENCE COMPARISON BETWEEN TWO TYPES OF 50-mm RODS

The fluorescence output from the Linde No. E-28 rod (5-mm diam. x 50-mm length) and the Airtron No. 956 rod (5-mm-diam. x 50-mm-length) was compared, using the apparatus described in Section II. The rods were pumped at 1,000 W input power, using quartz iodide lamps and dielectric-coated spheres. The rods were then pumped with a K-Rb lamp having a 1-in. arc length. The image of the 1-in. arc was centered lengthwise in the 50-mm rod. In both cases, the Airtron rod gave a result 2 to 4 percent higher than the Linde rod. In a following test, however, in which the 50-mm rods were pumped with 2-in. arc-length K-Rb lamps, the Linde rod gave a slightly higher output. Therefore, the Nd concentration must be the same within experimental error in the two types of rods. Another rod had been ordered from Allied Chemical Corporation but, unfortunately, was not received in time to be included in this comparison.

5. LASING TESTS OF 5-mm-OD × 50-mm WATER-COOLED RODS

The Airtron No. 956 rod, in a water jacket cooling mount, was pumped in the dielectric-coated spherical cavity with a 2-in. K-Rb lamp. The lowest threshold achieved was 122 W with two HR mirrors. With 300-W pumping, the maximum multimode power of 3.5 W was obtained with a flat HR mirror and a 4-m radius, 2.1% transmitting output mirror and an intracavity iris aperture. A convex mirror would have been required to optimize TEM_{00} power output.

The Airtron Rod No. 952 with one flat end face and one 25-cm radius convex end face was mounted in an identical water-cooling jacket, and pumped in the dielectric-coated spherical cavity. At 300-W input to a 2-in. K-Rb lamp, the maximum multimode power of 3.0 W was achieved with a flat HR mirror and a 10-cm radius, 2% transmitting output mirror. The best TEM_{00} output was 1.8 W with a 5-cm radius mirror and 2.1% transmission.

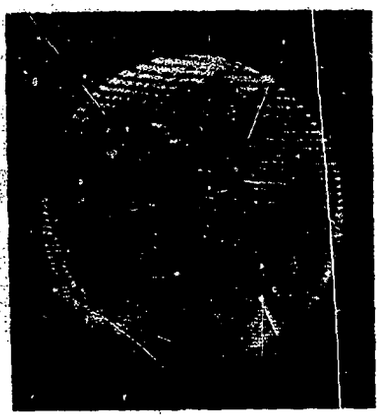

Figure 19. Fizeau Fringe Pattern of Conductively Cooled Airtron 5 × 50 mm Rod No. 956 at 300 W Potassium Rubidium Lamp Pumping

SECTION IV

PUMP CAVITY DEVELOPMENT

1. DIELECTRIC COATING OF THE SPHERE

A conveniently located coating company[1] was contacted to assist in the development of a multilayer dielectric coating for the inside of the 8-in.-diam. Pyrex hemisphere. Specification for the requested coating provided for a coating with maximum reflectivity for wavelengths between 0.72 to 0.90 μm and maximum transmission between 1.1 and 5.0 μm. The coating consisted of two overlapping, 21-layer Herpin stacks which produce a reflection band over a wavelength region 0.2 μm or greater in width. The coating was designed to minimize extraneous reflection peaks in the long wavelength region at the expense of producing rather large reflection peaks in the spectral region below 0.72 μm.

The company's coating chamber contains a large planetary gear arrangement which simultaneously moves the hemisphere around in an orbit and rotates the hemisphere on its own axis during the coating process. Specially shaped blades, counter-rotating in front of the surface being coated, served to make the coating thickness almost uniform over the hemispherical surface. A dummy hemisphere containing at least one witness flat was run on the same planetary gear during all coating runs. A typical transmission measurement of one of the witness flats is shown in Figure 20.

In the development of the technique, a coated sample hemisphere was sectioned and a direct measurement of the reflectivity in the wavelength region from 0.3 to 1.8 μm and from 2.5 to 10 μm was made of each section relative to the reflectivity of a similar section onto which a layer of gold had been evaporated. The gold-coated section served as a reflectivity reference in the infrared spectral region. A spectrophotometer with reflectivity attachment (Beckman IR-20A) was used for the 2.5 to 10 μm region. The samples were mounted from the front on a three-point jig so that the position of the center curvature of a sample would be identical for each sample tested. A NaCl lens was inserted in the beam to compensate partially for the defocusing caused by the concave sample and to improve the light-gathering efficiency. The raw data and the calculated reflectivity (the latter being the ratio of the intensity from the dielectric-coated sample to the intensity from the gold-coated sample, whose reflectivity in this spectral region is approximately unity) are shown in Figure 21. The reflectivity is about 6 percent on the average from 2.5 to 9 μm, has a 20 percent reststrahlen peak centered at 9.3 μm, and is about 0.9 μm wide.

---

[1] Scientific Coating Laboratories, 360 Martin Ave., Santa Clara, Calif. 95050

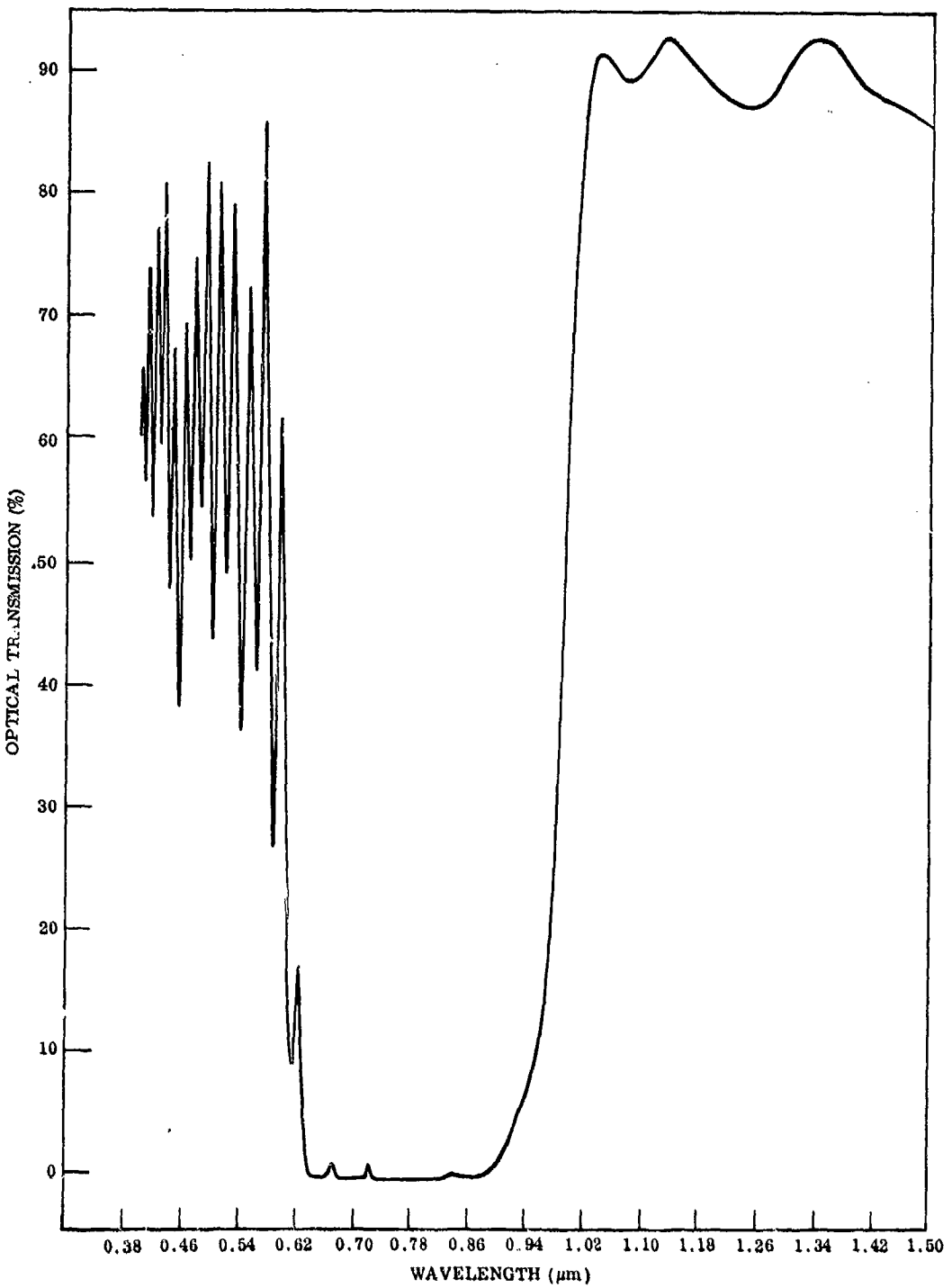

Figure 20 Spectral Transmittance of a Typical Witness Flat, Coated During Deposition of the Cold Mirror on a Hemispherical Pyrex Substrate

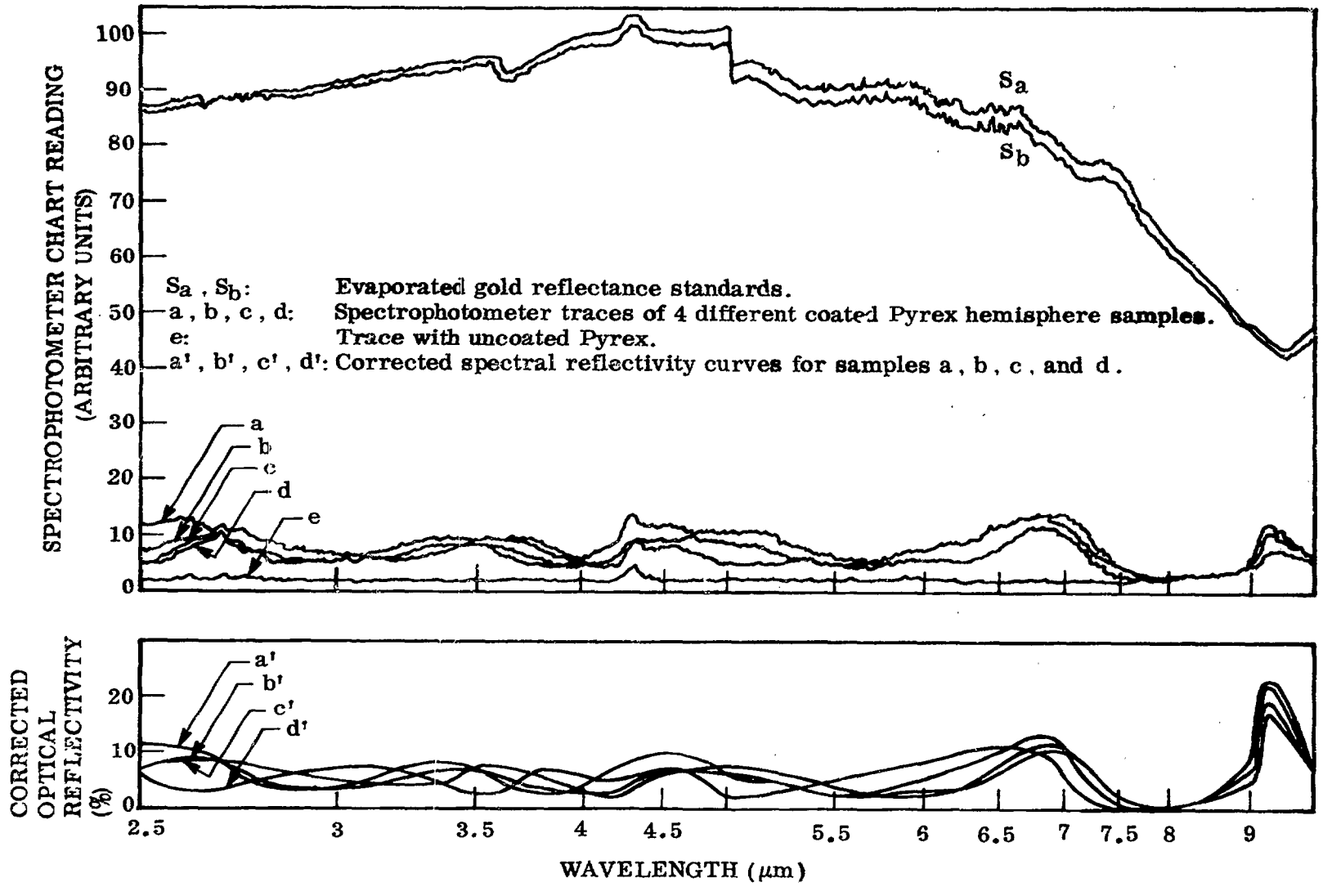

Figure 21 Infrared Reflectivity of the Dielectric-Coated Sphere

The reflectivity in the 0.3 to 1.8 μm region was measured on a spectrophotometer equipped with an integrating sphere (Cary 14). The samples were mounted on the same three-point mounting jig. The instrument was calibrated by assuming the reflectivity of the Au-coated sample to be unity above 0.7 μm. Figure 22 shows a typical trace. The reflectivity from 0.7 to 0.9 μm is greater than 95 percent, and the reflectivity between 1.2 and 1.8 μm averages about 8 percent. The large peaks below 0.7 μm are side effects of optimizing the coating for minimum reflectance above 1.2 μm. Problems due to these peaks have not been observed because there is little emission from the lamp in this spectral region.

2. PHYSICAL CONFIGURATION OF THE SPHERES

A sketch of the Pyrex hemispherical blank, which has the multilayer-dielectric cold mirror deposited on the inner surface, is shown in Figure 23. The rectangular hole is for accommodation of the conduction-cooled rod mount. The two diametrically opposed holes are ports for the laser beam and allow room for mounting of the pump lamp. The diameter of these ports was increased in this design, in comparison with previous designs, in order to facilitate possible close mounting of some resonator components for a shorter overall cavity length. The effect on pumping efficiency of increasing the port size was measured with gold-coated spheres (with 2-in.-diam. ports) by masking the ports with baffles to increase effectively their diameter. These measurements indicated that a 5-in.-diam. port on each end was equivalent to a 10-percent loss in pump power, and that a 4-in.-diam. port would produce a 2.5 percent loss. A 3-in.-diam. hole was selected for the present design and should result in negligible loss.

3. PUMPING EFFICIENCY MEASUREMENTS

The pumping efficiency of the dielectric spheres was compared with that of the gold spheres using the apparatus for scanning fluorescence. In order to increase the signal, the slit size and aperture diameter were increased so that the cross section of the volume of rod sampled was enlarged to about 1.3 x 1.3 mm. Measurements were performed using a 5- x 30-mm rod and a 1-in.-long K-Rb lamp operating at 200-W input. The position of the gold-coated spheres was adjusted to provide a symmetrical distribution of fluorescence in the rod as measured with the wide slit, and the fluorescence intensity at the peak noted. Because of the asymmetric, direct-light pumping from the lamp, a somewhat higher value of the fluorescence intensity may be obtained by adjusting the spheres to give a distribution peaked on the lamp side of the rod rather than centered in the rod. This value may be higher by about 4 percent.

When the dielectric spheres were measured, the sphere was peaked for maximum output, and the value obtained was equal to the value obtained with the gold spheres under conditions giving symmetrical pumping. Thus, the raw data indicate that the pumping efficiency of the dielectric spheres may be about 4 percent less than that of the gold spheres.

In order to measure the effectiveness of the dielectric sphere in reducing the thermal load on the rod, thermocouples were inserted in the input and output water cooling lines from the rod. Measurement of the temperature difference and water flow rate indicated that, for a 5- x 30-mm water-cooled rod pumped by a 1-in. K-Rb lamp at

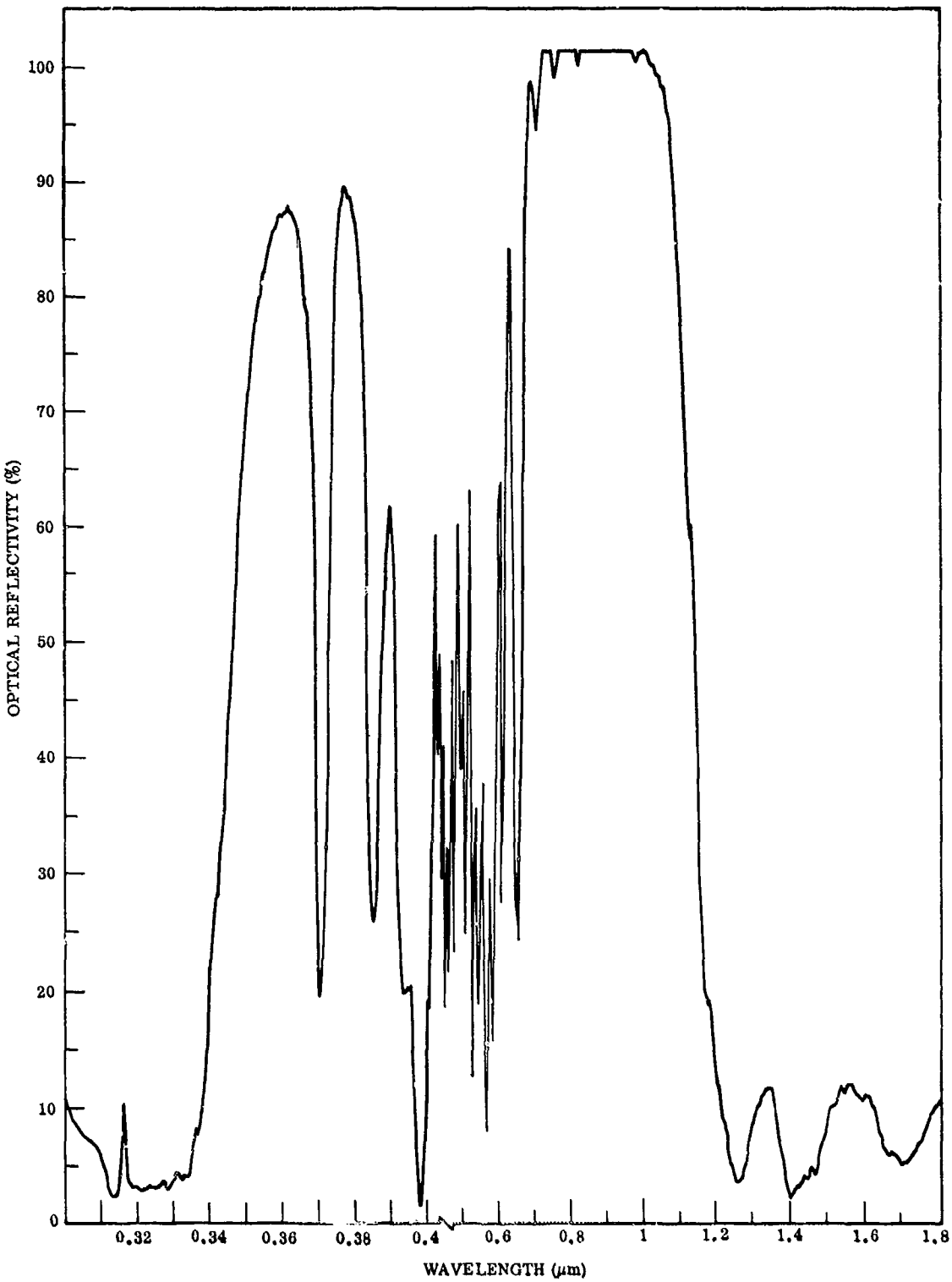

Figure 22 Visible and Near-Infrared Reflectivity of the Dielectric Sphere – Scale Change at 0.4 μm

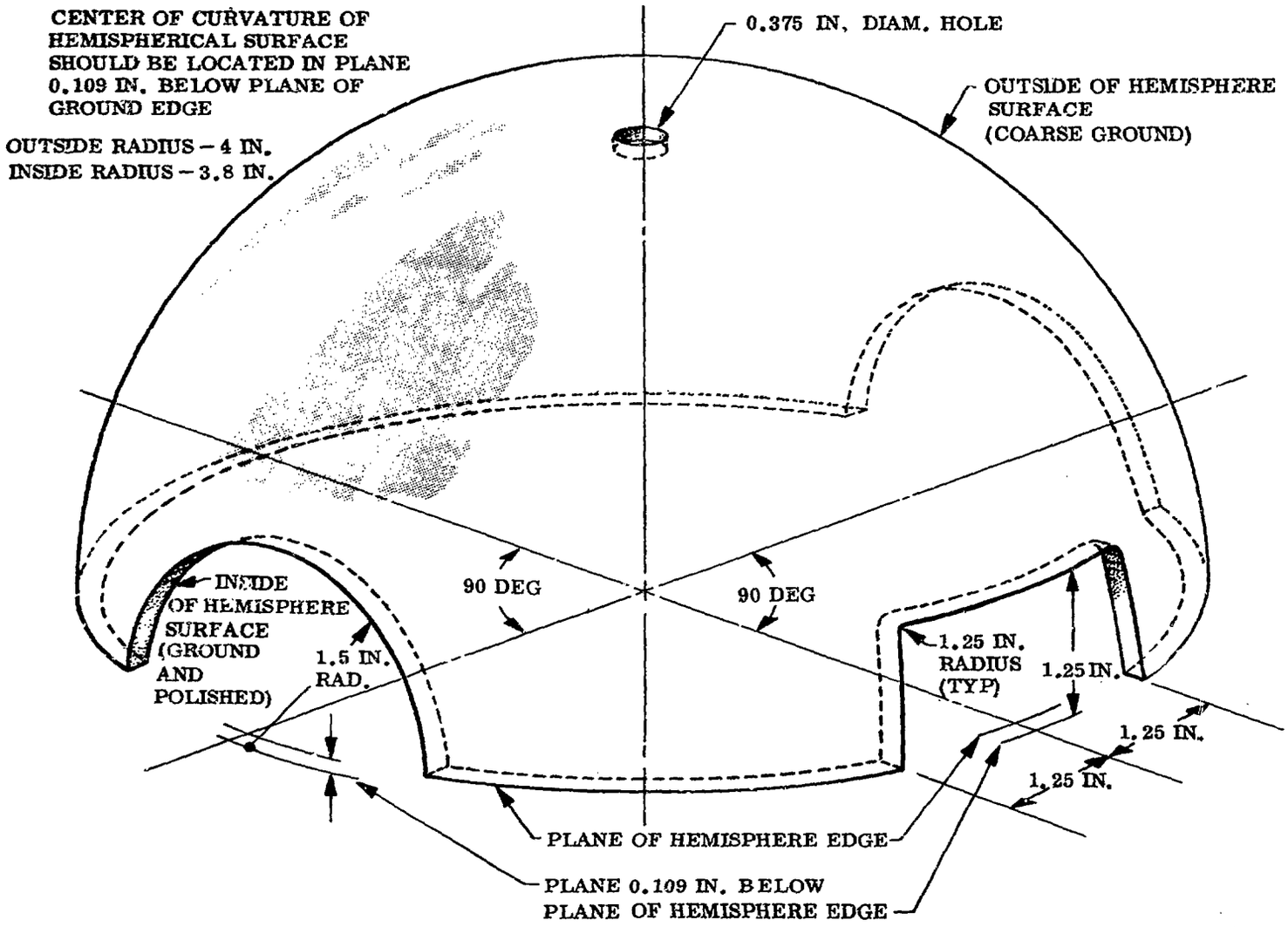

Figure 23 Geometry of Hemispherical Pyrex Blank for Cold-Mirror Pump Cavity

200-W input, 36 W are removed in the rod-cooling water when the dielectric sphere is used compared to 112 W when the gold sphere is used. When using the dielectric spheres and 200 W of input power to the lamp, the calculations predict that about 3 W is absorbed in the rod due to quantum efficiency, 7 W due to residual sphere reflectivity in the IR, and 13 W due to direct radiation and absorption in the water; the total is 23 W. The measured value is therefore somewhat higher than expected. With the gold spheres, it is estimated that there would be 3 W for quantum inefficiency, 86 W from reflected IR, and 1[illegible] W from direct absorption for a total of 102 W of heat, which is slightly lower than the measured value.

The quartz rod used as a filter for direct IR was also tested. The rod is interposed between the lamp and the laser rod to intercept that infrared radiation which would be incident directly on the laser rod. Useful pump light is focused into the laser rod by the quartz rod. Again, using the water-cooled rod, the effect of the quartz rod on pumping efficiency was measured by means of the fluorescence apparatus. No change in efficiency was observed with the addition of the quartz rod. The heat intake in the water changed from 36 W without the filter to 25 W with the filter, using K-Rb lamp pumping at 200-W input.

The apparatus for measuring the heat uptake with water-cooled rods was improved by adding insulation to the water lines and using a more sensitive detector for the thermocouple difference voltage. These tests, using a 2-in. K-Rb lamp operating at 300 W to pump a 2-in. water-cooled rod, gave the results listed in Table V.

Table V. Heat Removal by Laser Rod Cooling Water for 300-W K-Rb Lamp Pumping

Type of Sphere	Heat Uptake (W)
Dielectric-Coated Spheres (without quartz filter)	55
Spheres Removed	20
Gold-Coated Spheres	177
Dielectric Spheres (with quartz filter)	55

In contrast to the results of the 1-in. lamp tests, this test failed to confirm the utility of the quartz filter. These heat uptake values scale reasonably well with those values previously obtained for K-Rb lamp pumping at 200 W, using a 1-in. lamp and 1-in. rod.

SECTION V

MECHANICAL DESIGN

The mechanical structure was designed to provide versatility, stability, and compatibility with the single-frequency laser frame. Size and weight considerations were not emphasized. The frame incorporates four 1-in.-diam. invar rods for length stability, aluminum end plates, invar mirror mounts with x - y and tilt adjustments, a carriage for the rod and sphere mounted on two of the invar rods, a hermetic seal with plexiglass sides mounted inside the end plates, a movable plate inside the hermetic seal for mounting the lamp, and a movable plate outside the hermetic seal for mounting one end-mirror assembly. The other end mirror assembly is mounted on one of the end plates. An adjustable iris is mounted on one end plate with an x - y positioner. The mirrors are O-ring-sealed into tubes in the mirror mounts, and these tubes are connected to the iris and to the hermetic seal with flexible rubber bellows. The assembly is shown in Figure 24, and Figure 25 shows the completed assembly with one of the pump-cavity hemispheres removed.

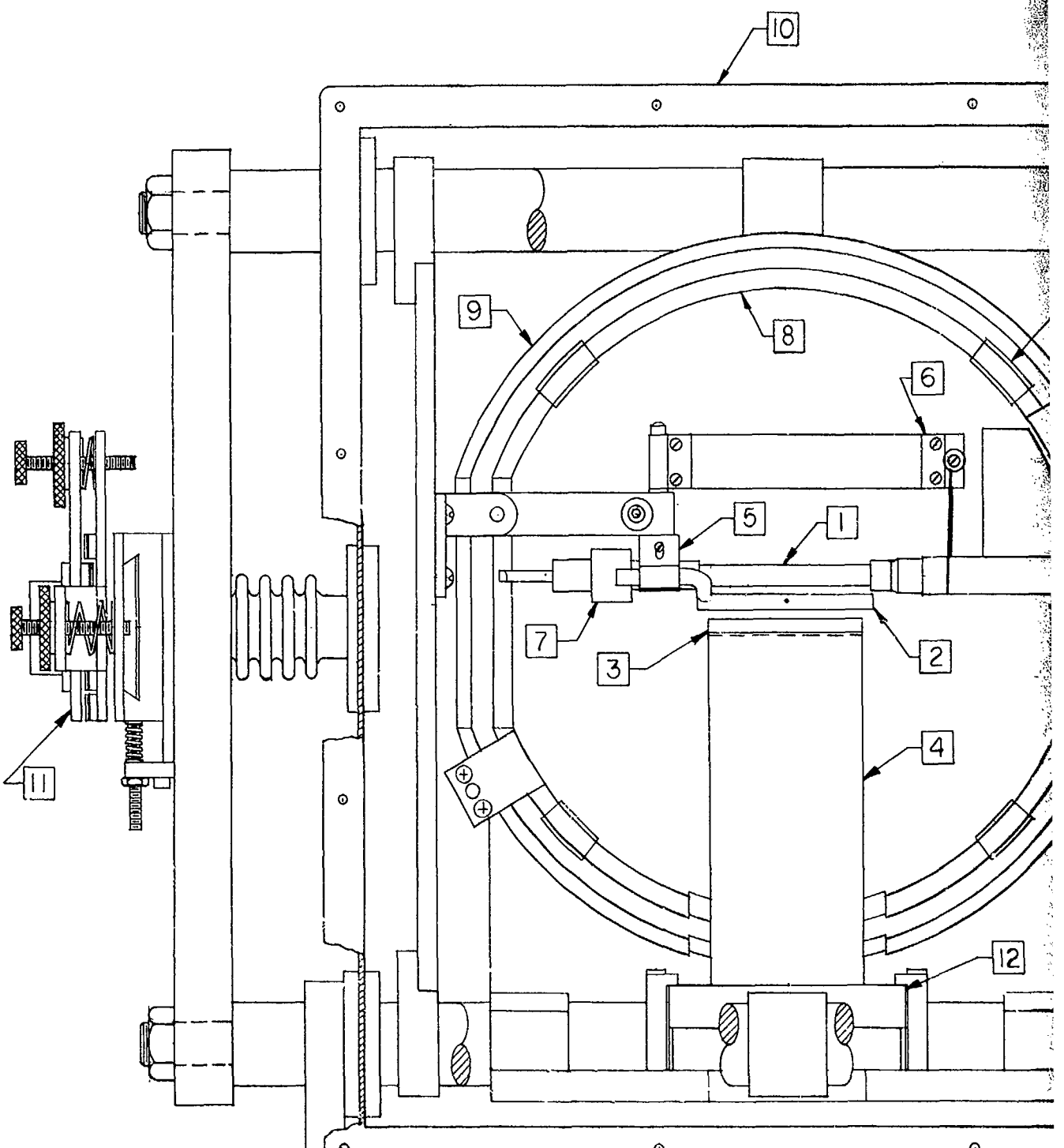
10
9
8
6
5
1
7
3
2
4
11
12

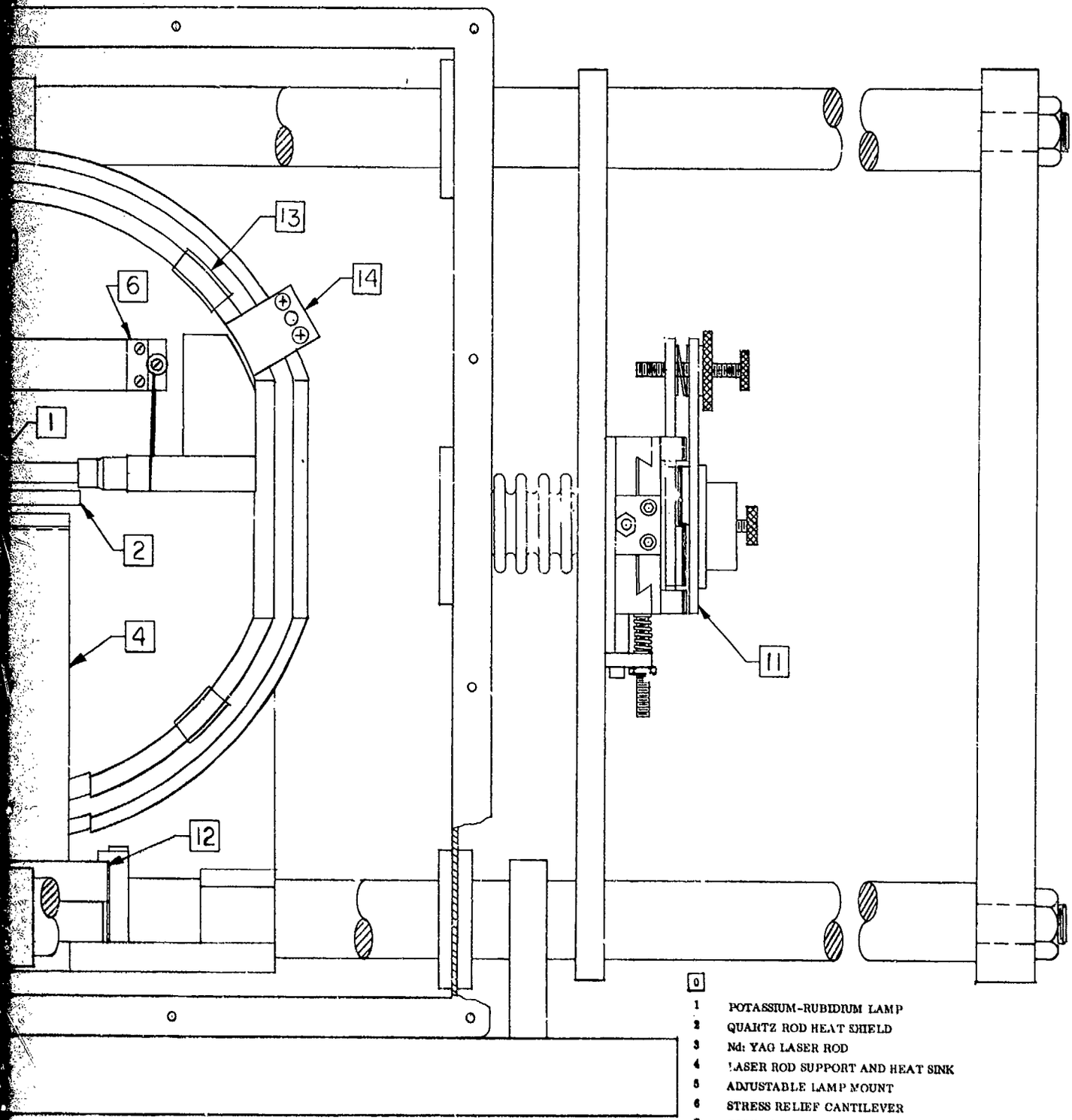

0

1 POTASSIUM-RUBIDIUM LAMP
2 QUARTZ ROD HEAT SHIELD
3 Nd: YAG LASER ROD
4 LASER ROD SUPPORT AND HEAT SINK
5 ADJUSTABLE LAMP MOUNT
6 STRESS RELIEF CANTILEVER
7 COLD SPOT HEATER FOR LAMP
8 DIELECTRIC COATED PYREX SPHERE
9 COPPER SPHERE
10 ATMOSPHERE CONTROL ENCLOSURE
11 MIRROR MOUNTS
12 COLD PLATE FOR HEAT SINK
13 SPACER BETWEEN HEMISPHERES
14 SPHERICAL REFLECTOR SUPPORT

Figure 24 Space Laser Assembly

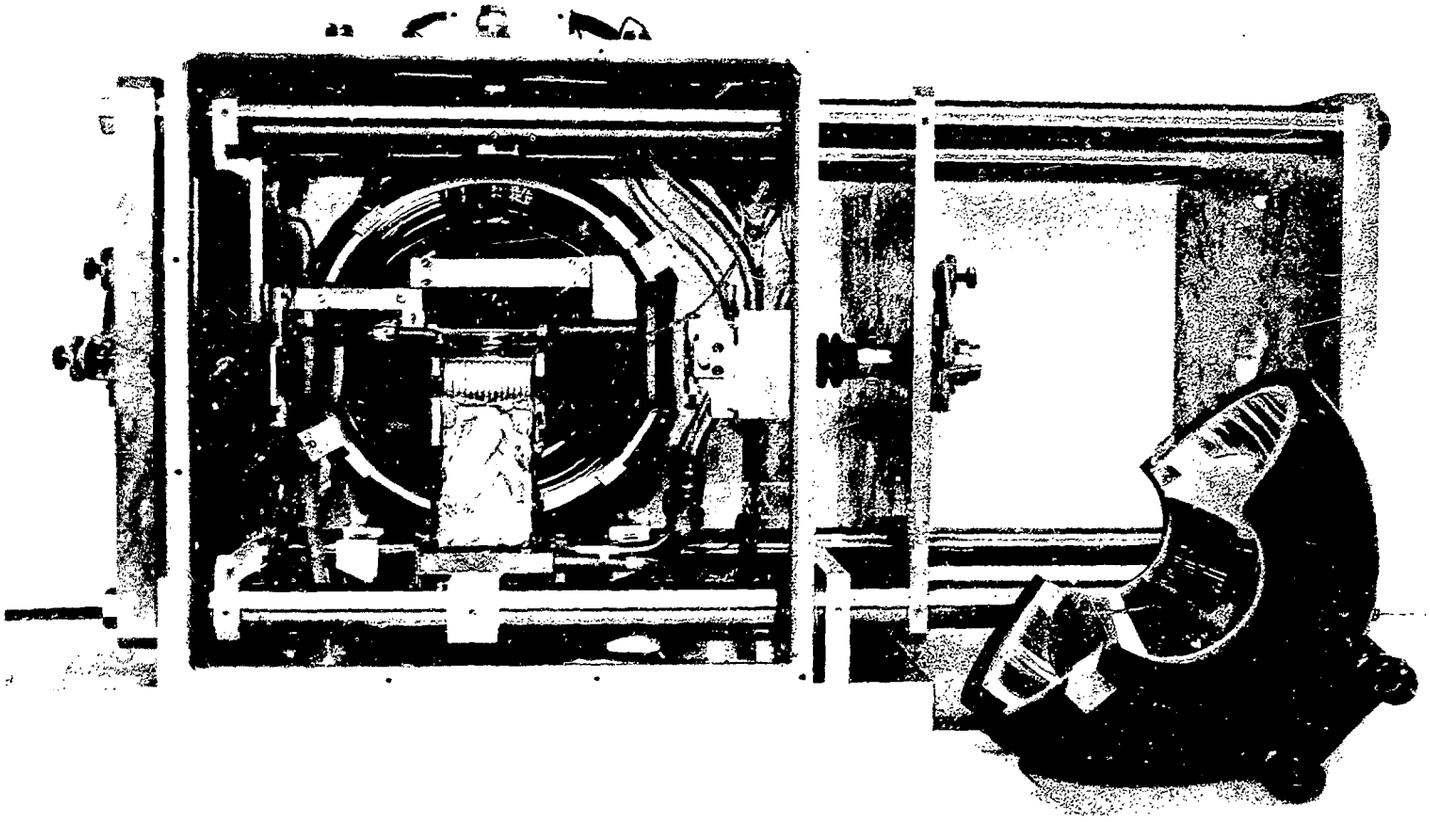

Figure 25 Space Laser Assembly – One Hemisphere of Pump Cavity Removed

SECTION VI
OPERATING TESTS AND RESULTS

1. OPERATION OF THE CONDUCTION-COOLED, FLAT-ENDED ROD

The flat-end-face 5-mm-OD × 50-mm-length rod (Airtron No. 956) was operated with a 2-in. arc-length K-Rb lamp in the hermetically sealed housing. The resonator consisted of a flat HR mirror and an HR mirror with a 1-m radius of curvature. Typical Fizeau interferograms of this rod taken during mounting and operation were shown in Figures 18 and 19.

The sphere was adjusted to focus light from the arc into the rod by monitoring rod excitation with the fluorescence apparatus. The sphere was mounted as a unit from underneath on three adjustment screws. It was found that the sphere position for optimum coupling could not be adjusted with certainty. Lasing was attempted with poor results. Although threshold was reached, the power output was 1 mW or less. It was not possible to adjust the sphere for lasing while the rod was cold because of the condensation problem. It was therefore decided to redesign the sphere-mounting mechanism. A side-mounting mechanism was built so that a single hemisphere could be mounted and adjusted to center visually the image of the arc inside the laser rod. This was a previous standard procedure. The second hemisphere was then attached to the first. Its alignment was fixed by the grooved spacer blocks separating the two hemispheres. A side plate containing a pair of rubber gloves was fabricated to make possible final adjustment of the sphere after flushing.

Although the new sphere mount greatly aided focusing adjustment of the spheres, lasing performance was still very poor. Disassembly of the laser and careful microscopic examination of the rod revealed that a very thin film of foreign substance had been deposited over the AR coatings on the rod ends. This material was removed with a few drops of distilled water, and the water was then evaporated for analysis of the residue by an electron microprobe. The analysis showed the presence of K, P, Mn, Ni, Cu, Sn, probably Sb, and perhaps a trace of Zn in addition to Ca, Cl, S and Fe which were also present in the control sample. Furthermore, examination of the K-Rb lamp revealed a crack in the sapphire envelope, thus accounting for the K presence. Also, the coating was very easily removed which was consistent with it being a potassium salt or hydroxide. The other elements were probably due to contamination during rod coating, bonding, and soldering.

Lasing was attempted again,using the same 2-in. K-Rb lamp with the cracked envelope. Two small tubes used to shield the beam from the turbulence of the cavity-filling gas were slid over the ends of the rods to shield them from K deposition. Typical Fizeau interferograms of this rod taken during mounting and operation were shown in Figures 18 and 19.

A 1-in. arc-length K-Rb lamp was then substituted for the cracked 2-in. lamp while delivery of another 2-in. lamp was awaited. It was found that, with this lamp operating at 250 W, and with careful purging of the cavity to avoid water condensation on the rod ends, a stable multimode output of 100 mW could be obtained. The rod was operated at about 0° F and an output mirror transmission of 0.8 percent was used.

A new 2-in. lamp was received and installed in place of the 1-in. lamp. A multimode output of 700 mW was then obtained with 300-W input to the 2-in. lamp. The decision was made to go directly to the curved-end rod rather than attempt to achieve and optimize TEM_{00} operation with the flat-end rod.

2. OPERATION OF THE CURVED-END ROD

The 2-in.-long Linde rod (No. E28) had been refabricated with a 25-cm radius of curvature on one end and mounted on a Nb-tipped copper wedge identical to the wedge on which the flat-ended rod was mounted. The 25-cm radius of curvature gives the rod a focal length of about 30 cm. This type of rod had been used previously in a water-cooled holder in conjunction with a resonator cavity consisting of a flat mirror and a 10-cm-radius mirror, and the region of stability had been established. This configuration was tried with the 2-in. conduction-cooled rod but lasing could not be achieved. Many variations of this configuration were tried but threshold could not be reached. Later, some cavities with small TEM_{00} mode volumes inside the rod were tried. Multimode lasing at the level of a few milliwatts was achieved with a cavity consisting of a 1-m radius mirror and a 60-cm radius mirror.

3. OPERATION OF THE FLAT-ENDED ROD WITH SEPARATE INTRACAVITY LENS

The reason for using a separate lens in the cavity as opposed to a curved end rod is that it enables the correction, by tilting the lens, of the beam distortion that is due to astigmatism (or cylindrical lensing) in the pumped rod resulting from the nonuniform temperature gradient. Tilting the lens about an axis in the plane of symmetry of the rod mount introduces an astigmatism which can be used to compensate the astigmatism introduced by the rod. The lens has not yet been thoroughly tested in the LMSC laser due to a rod contamination problem which will be subsequently discussed. However, Sylvania reports excellent results with a tilted lens in its conductively cooled laser (Ref. 9).

A 5-cm focal-length lens, antireflection-coated for 1.06 μm, was mounted adjacent to the pump cavity to form part of the resonator cavity. The resonator was completed with a 5-cm-radius mirror and a flat mirror. The region of stability was calculated for a gaussian beam with a waist at the flat mirror which is narrow in one case (0.11 mm) and wide in the other case (1 mm to fill rod). The radius of curvature of the beam is plotted versus distance from the lens in Figure 26. The desired radius is selected for the curved mirror on the ordinate scale, and the corresponding stability abscissa limits are read off the abscissa. The limits are seen to be rather narrow, only about 8 mm apart for the 5-cm focal-length lens.

This configuration was tried and lasing threshold was achieved, but the power level was very low, only about 1 mW. A possible reason for the low output power was the deposition of foreign material on the end of the rod. The source of the material is

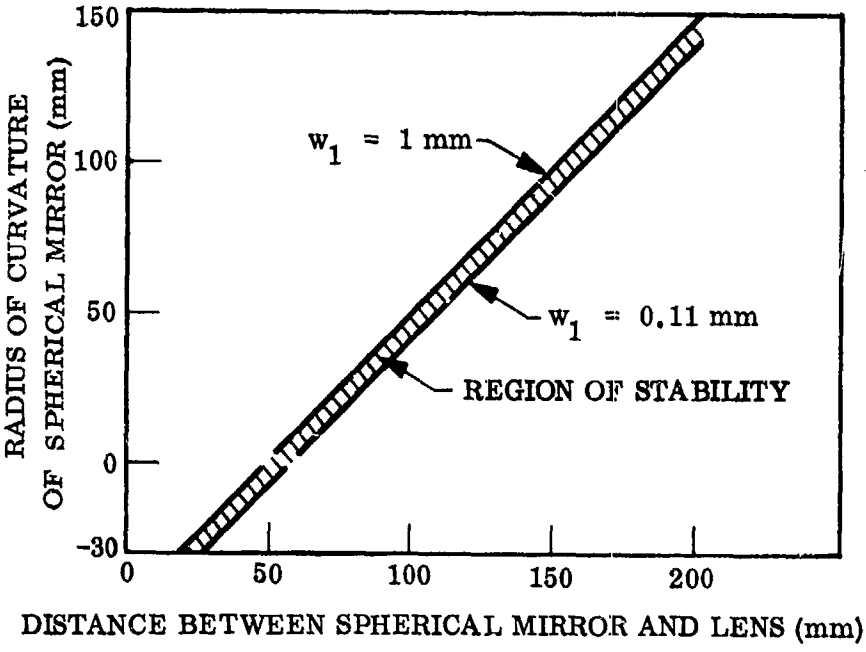

Figure 26 Stability Region for Cavity With Lens

uncertain at this time. Some material seems to come from the anode frit of the lamp, and there is also some question about the integrity of the lamp envelope, a question that is still being investigated.

In the course of aligning the laser and attempting to obtain lasing, the beam tubes (0.25-in.-OD straight stainless types with 0.012-in. walls) proved difficult to align and were a potential interference in the path of the beam. The beam tubes were replaced with thin-wall tapered beam type turned on a mandrel and supported at both ends in the laser frame. These tubes are expected to shield the beam from argon turbulence and lamp vapors, while not interfering with the laser beam.

4. OPERATION WITH A Kr PUMP LAMP

Krypton lamps were purchased from ILC, Inc., and from EG&G, Inc. The lamps are 2-in. arc-length, 4-mm-bore lamps developed for Nd:YAG pumping. An 11-mm-OD water jacket was fabricated for use with the lamps. A starting supply was constructed for a 150-V 15-A constant current power supply. The design of the starting supply, which simply augments the 150-V supply with a small capacitor-charging supply to furnish additional current in starting the lamp, is shown in Figure 27.

The initial test with the Airtron No. 956 5-mm × 50-mm rod indicated that the Kr lamp requires approximately 900 W to produce the same distortion and approximately the same excitation of the Nd:YAG rod as the K-Rb lamp does at 300 W. This comparison was based on the number of fringes produced in the Fizeau pattern. Lasing tests using this lamp and an intracavity lens will be conducted under a subsequent contract.

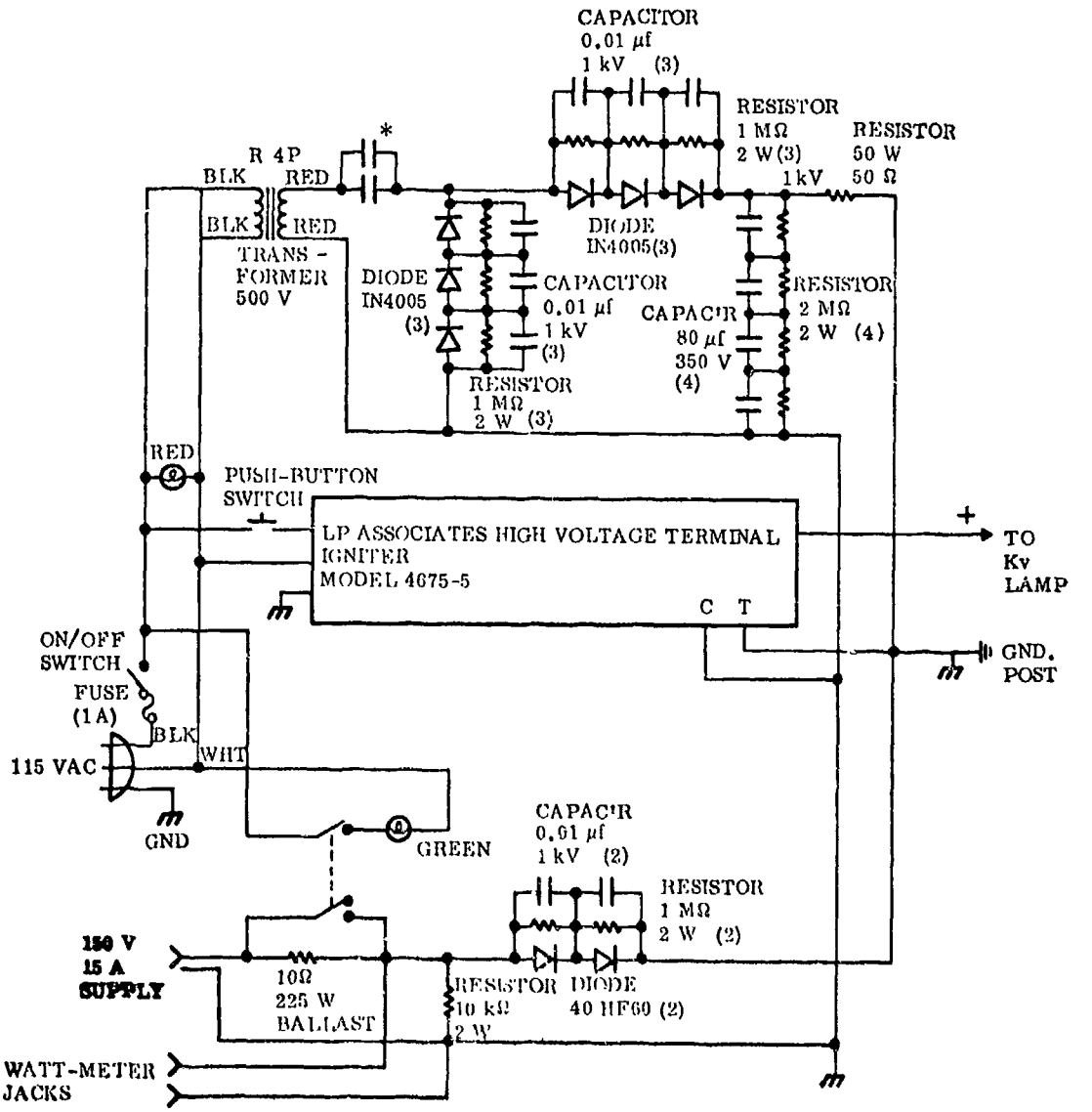

*0.01 μf AT 1/V DISK CAPACITORS ADDED IN PARALLEL TO ADJUST OUTPUT VOLTAGE TO 1 kV

Figure 27 Krypton Lamp Starting Supply

SECTION VII

CONCLUSIONS AND RECOMMENDATIONS

1. GENERAL

The spherical pump cavity is still a candidate for the space laser for the Air Force 405B Program. It has shown relatively good performance in producing 700 mW of multimode power with 300 W into a K-Rb lamp, using a flat-end rod and without compensation for thermally induced astigmatism. The unavailability of K-Rb lamps during the last 2 mo of the program did not permit a thorough evaluation for TEM_{00} power output using compensation. This evaluation will be continued on a following program.

2. CONDUCTION COOLING

The small number of fringes produced in the rod mounting process (i.e., three) indicates that the method employed for rod mounting is satisfactory. Further, lasing tests are necessary to confirm fully this conclusion.

It is not known whether or not the niobium tip on the slotted copper mount is necessary. It therefore would be desirable to try a slotted copper mount without the Nb tip, and such a mount has been fabricated, but not tested.

Probably the best way to correct the rod astigmatism would be to grind a compensating cylindrical lens on one end of the rod. This has not yet been attempted. The curvature required should be determined by Twyman-Green rather than by Fizeau interferometry. Another approach is to examine the curvature of the end faces from the displacements calculated by the SAAS II structural analysis program used for the stress calculations, and thus determine whether or not lensing due to end-face bowing is significant compared to the lensing caused by thermal refractive index changes. It is recommended that a rod be ground with a compensating cylindrical curvature, once the appropriate radius has been established.

3. SPHERICAL PUMPING CAVITY

The spherical pumping geometry permits very effective cold mirror design, because all light is at or near normal incidence on the sphere. From the standpoint of imaging the pump lamp onto the laser rod, perfect imaging takes place only when both source and absorber coincide at the center. The aberrations increase with increasing distance from the center of the sphere, so that longitudinal nonuniformity results when the ends of the laser rod are significantly farther from the sphere center than the middle of the laser rod is. Ray tracing in the spherical cavity indicates that loss of pump intensity due to aberrations becomes severe when source/image points are more than 1/10 the

sphere radius from the center. Thus, for 5-cm long lamps and laser rods, the sphere radius should be greater than 30-cm to satisfy this criterion, and the 10-cm radius used in the experiments reported here may suffer from significant loss due to aberrations. The 10-cm diameter was initially selected for use with 30-mm-long lamps and laser rods.

The good efficiency obtained with water-jacketed laser rods in the spherical pump reflector, and the relatively poor efficiency with bare, conductively cooled laser rods, indicate that a cylindrical high index imaging sleeve may be required to minimize the effects of aberrations in the spherical reflector. The question of whether the large volume required for optically efficient spherical pump reflectors is justified by their somewhat better infrared rejection, relative to an elliptical reflector, must be answered by using criteria extrinsic to the present contract requirements.

For purposes of longitudinal mode control, it is desirable to keep the resonant cavity short. This resonant cavity can be made as short, using a spherical pump cavity, as with an elliptical pump cavity by increasing the size of the beam exit ports to allow mounting of components close to the laser rod. Efficiency measurements have shown that the diameter of these ports can be increased to as much as 5-in. with only 10 percent loss in pumping efficiency.

Present reductions in cavity length are limited mainly by the length of the K-Rb lamp and the focal length of focusing elements in the cavity. As the focal length of the focusing element is reduced, the radius of the intracavity waist thus formed is reduced, and the power density at the waist is increased. The limit on reduction of cavity length may therefore be set by the power density tolerance of the frequency-doubling crystal. At present, sufficient information is not available regarding the damage thresholds for intracavity doubling of single-frequency 1.06 radiation to determine the appropriate power density limit.

The heat removal caps are presently rather heavy but can be reduced in weight by accepting a somewhat higher temperature drop between hemisphere edge and center than the present temperature value (calculated) of 13° C or less. Use of aluminum rather than copper would increase the value to 26° C and cut the weight by a factor of 3.3. Furthermore, the thickness could be judiciously reduced for additonal weight reduction. An edge-to-center temperature difference of at least 50° C should be acceptable.

4. K-Rb LAMPS

Considerable development work is evidently still needed on the K-Rb lamp to provide reasonable lifetimes. Also, development work is needed on the protected end-seal version of this lamp since that version has many advantages for use in development work on the laser and in a final product.

In conclusion, it is believed that the LMSC Space Laser Design holds certain advantages and may be the best design for the 405B program. LMSC also believes that development work should be continued on this laser in order to evaluate its full potential.

APPENDIX

THERMAL STRESS ANALYSIS OF LASER ASSEMBLY

1. INTRODUCTION AND SUMMARY

Reported below are the results of a thermal stress analysis to assess the magnitude and distribution of stresses in a cylindrical YAG laser rod heated in the pumping process and conductively cooled from one side through a niobium and copper support. Supporting the rod on one side gives rise to two types of stresses. The first is a bending stress associated with forcing the laser rod to remain straight when the nonsymmetric heat flow field would cause it to bend if free. The second is a residual tensile stress resulting from the inability of the laser rod to contract freely along its length because it is attached to a support.

The results of the analysis indicate that the bending stresses developed by straightening the rod are small compared to the axial stresses that might result if the rod were rigidly attached (soldered) to the support at a temperature of 200° C, and cooled to the operating temperature of 0° C.

The axial stress can be greatly alleviated by providing narrow slots in the support structure which allow the rod to contract to a nearly free condition but do not significantly degrade the heat conduction path from the rod.

2. DESCRIPTION OF PROBLEM

The temperature field for a typical cross section of the YAG rod is shown in Figure A-1. This field is based on 10 W absorbed uniformly in the YAG volume, a value which may be somewhat low to represent pumping a 5- x 50-mm rod at 300 W input to a potassium lamp. For the cases studied in this report, the temperature in the Nb was assumed to vary linearly from 0 to -2.5° C. It has been assumed that the distribution does not vary along the length of the rod. The temperature distribution shown will lead to both longitudinal and transverse stresses. Stresses will exist in the rod even if it is completely free. The larger gradient through the rod thickness from top to bottom would be expected to lead to much larger stresses than the small gradient from side to side; if the rod is restrained, additional stresses will be induced both in the longitudinal and transverse directions. Since the laser rod is long, but not wide, compared to its thickness, and since some stress relief occurs near the edges, the stresses associated with constraining the rod to lie flat should be greater in the longitudinal (axial) direction than in the transverse direction.

The problem, as posed, is three-dimensional, requiring a three-dimensional analysis. Since the stresses in the axial direction should be much larger than those in the transverse direction, however, the laser can be reasonably modeled to a two-dimensional body in which transverse gradient effects are neglected. Such a model, a vertical slab subjected to a one-dimensional thermal gradient, can be analyzed

economically, using existing computer programs. The program used in this analysis is an LMSC version of the SAAS II Program (Ref. A-1). This Program is a two-dimensional, finite-element, elastic/plastic program which is used extensively for structural analysis and thermal stress problems.

3. ANALYSIS AND RESULTS

In order to consider the interaction effects of YAG bonded to Nb, the finite element model consisted of two slabs of equal height (5 mm) rigidly attached together. The length was 5 cm. The finite element mesh is shown in Figure A-2. As noted, YAG is the material to the right of the midline; Nb is the material to the left. The temperature gradient used in the analysis is shown in the contour plot (Figure A-3). A plane stress boundary condition was used in all of the analyses. When using a plane stress boundary condition, one assumes that the slab faces parallel to the plane of the paper are stress free; that is a good approximation for thin bodies.

To obtain an estimate of the stress level induced by the thermal gradient only, the first case considered was that of an unrestrained YAG rod. The mesh for the two materials was used, but the properties of the Nb were reduced to negligibly small values so that it did not affect the response of the YAG. The material properties for the YAG were obtained from Ref. A-2 and are the modulus of elasticity (47.8×10^6 psi), thermal expansion coefficient (Figure A-4), and Poisson's ratio (0.33). A plot of the axial (Z) stress is shown in Figure A-5. The "I" designations refer to lines in the finite element mesh. Line I=20 is the top row of elements in the YAG (rightmost in Figure A-2); I=11 is the bottom row of elements in the YAG; and I=10 is the top row of elements in the Nb. The vertical and shear stresses were both small compared to the axial stress. Due to the thermal gradient, a self-equilibrating axial stress distribution results with an outer fiber tensile (positive) stress of 400 psi and a central compressive (negative) stress of 250 psi (not shown). The stresses represent an approximate lower bound on the stresses expected in the assembled laser. Any restraint of the free movement of the rod should lead to higher stresses.

To obtain an upper bound on the stresses, the case of a fully restrained YAG rod was considered. The same model was used as before except that the nodal points along the lower edge of the YAG (i.e., along the midline of the finite element mesh) were restrained against vertical, R direction displacement. They were still free to move horizontally (Z direction), however, so that the rod was free to expand axially.

The axial and vertical stresses are shown in Figures A-6 and A-7. The stress distribution differs appreciably from that for the free rod. The top surface now has a compressive stress of 950 psi, and the lower surface has a tensile stress of 1,650 psi, with the stress in the central portion varying between these two values. This distribution results from the restraint of the curvature which the rod would assume if free. The curvature caused by the thermal gradient is eliminated by a bending moment through the restraints, leading to a bending stress distribution – tension on one side, compression on the other. The bending moment required to do this is applied to the rod ends by the combination of vertical R tensile compressive stresses as shown on the ends in Figure A-7. These two cases provide bounds on the axial tensile stress expected in the YAG of no less than 400 psi and no greater than 1,650 psi.

Two cases were then run in which a slab of Nb was rigidly attached to the YAG. Bounds were obtained by again considering free-free and restrained beams. For the restrained case, the finite element nodal points on the far left of the model (Figure A-2) were restrained against R displacement but free to move in the Z direction. The material properties for the Nb were obtained from Ref. A-3 and are modulus of elasticity (17.5×10^6 psi), thermal expansion coefficient (Figure A-4), and Poisson's ratio (0.33).

As expected, peak stress values are between the bounds for the YAG only. The axial Z stress for the free-free case is shown in Figure A-8. The peak tensile stress in the YAG is 615 psi along the interface between the YAG and Nb. There is a small vertical R stress (Figure A-9) near the ends to account for the curvature mismatch between the two materials as well as a small shear stress along the interface as shown in Figure A-10. However, the largest stress occurs in the axial (Z) direction.

The peak axial tension stress values for the restrained YAG/Nb composite beam are larger than for the free-free beam but still below those of the restricted YAG only. The peak axial tension at the interface is 1,070 psi (Figure A-11). A compressive stress of 1,630 psi is developed in the top of the YAG. This stress is higher than for the YAG only. The increased compressive stress is attributed to the YAG, with a slightly higher coefficient of thermal expansion and bulk temperature than the Nb, trying to expand more than the Nb will permit. This is further evidenced by the compensating tensile stress in the Nb (I=10 in Figure A-11). The contour plots in Figures A-12 through A-14 provide an overall picture of the stress distributions in the YAG and Nb. The results of the preceding four cases are summarized in Figures A-15 and A-16. In Figure A-15, the axial stress through the thickness is plotted for each model, indicating the change in both the stress distribution and magnitude with varying degrees of restraint. The plots are presented in increasing order of restraint from the top to the bottom of the page. Corresponding plots of the vertical R displacement along the lower edge of the YAG are shown in Figure A-16, again in increasing order of restraint. As the amount of curvature in the YAG is reduced to zero, the YAG peak tensile stress increases.

A final finite element model was analyzed, representing a complete laser assembly including the copper support. The finite element model is shown in Figure A-17. The model, as before, consists of a unit slab through the center of the assembly. The change in coordinate directions should be noted as the rod now runs parallel to the R direction. Taking advantage of symmetry, only half the assembly was considered; the symmetry line is along the Z axis. The YAG is at the top of the figure as indicated. The YAG and Nb were both 5 mm wide; the copper was 10 cm wide; the length was 5 cm. The temperature gradient is shown in Figure A-18. The gradient in the YAG and Nb is the same as before. The gradient in the copper is nearly linear and is -4.0° C at the base. The axial stress R is shown in Figure A-19 at four locations: the upper edge of the YAG (I = 28), the lower edge of the YAG (I = 24), the upper edge of the Nb (I = 23), and the upper edge of the copper (I = 18). The peak tensile stress in the YAG is 330 psi at the Nb interface; the peak compressive stress is 1,400 psi on the top surface. Due to the axial restraint of a large mass of cooler copper, the tensile stress is reduced to a value below the previous lower bound of the free-free beam.

It can be concluded from the foregoing analyses that the tensile stress in the YAG will be not more than 1,700 psi (restrained YAG/Nb). There is some doubt as to whether the compressive stress in the YAG may not be larger, depending on the effective bulk temperature of the copper.

During assembly of the YAG to the Nb, the two parts will be subjected to a temperature of about 200° C. Although the coefficients of thermal expansion of the two materials are similar near the operating temperature, this is not true at higher temperatures. (See Figure A-4.) There is the possibility that the residual stresses resulting from assembly might be much higher than those due to the operational gradient. Since the SAAS II computer program does not take into account time history effects, a simplified two-material model was used to obtain an estimate of residual stress.

It was assumed that the two beams were stress-free and of equal length at 200° C. Each beam was assumed to have no temperature gradient during cooldown; in addition, both beams were at the same temperature. A Tymshare computer program was written to compute the total residual stress by integrating differential contraction over small temperature steps. The coefficient of thermal expansion of YAG is larger than for Nb in the temperature range of interest. During cooldown the YAG will attempt to contract more than the Nb, leading to tensile stresses in the YAG and compressive stresses in the Nb. The tensile stress induced in the YAG by cooling to any temperature from 200° C is shown in Figure A-20. At 0° C, the tensile stress would be 7,000 psi, considerably larger than any of the stresses determined earlier. The model used here assumes a rigid connection between the YAG and Nb. Any "softness" in the body will tend to alleviate the stresses to some degree.

In view of the possible high stresses that might be produced due to differential contraction, the possibility of supporting the YAG rod on slotted Nb was considered. An estimate of the axial and shear stress that might be applied to the YAG rod was obtained by considering the following simple model. It was assumed that all of the axial expansion of the YAG with respect to the Nb would be taken by bending a thin Nb beam or fin. A beam length (i.e., slot depth) of 1 in. was chosen, with a beam thickness of 0.090 in. and an effective width of 0.35 in. The load required to bend the Nb beam by an amount equal to the differential displacement between the Nb and YAG was computed. The conservative assumption was employed that the difference in the coefficients of thermal expansion is constant (actually it decreases to 0 at -8° C). The load, so computed at 0.59 lb, would induce a shear stress of 66 psi to the YAG or an equivalent axial tensile stress of 19 psi which is negligible compared to the earlier stresses.

Although the earlier residual stress calculations are conservative to the extent that they neglect the effects of a soft bond, it is recommended that the support structure be slotted to avoid any possibility of high residual stresses due to assembly.

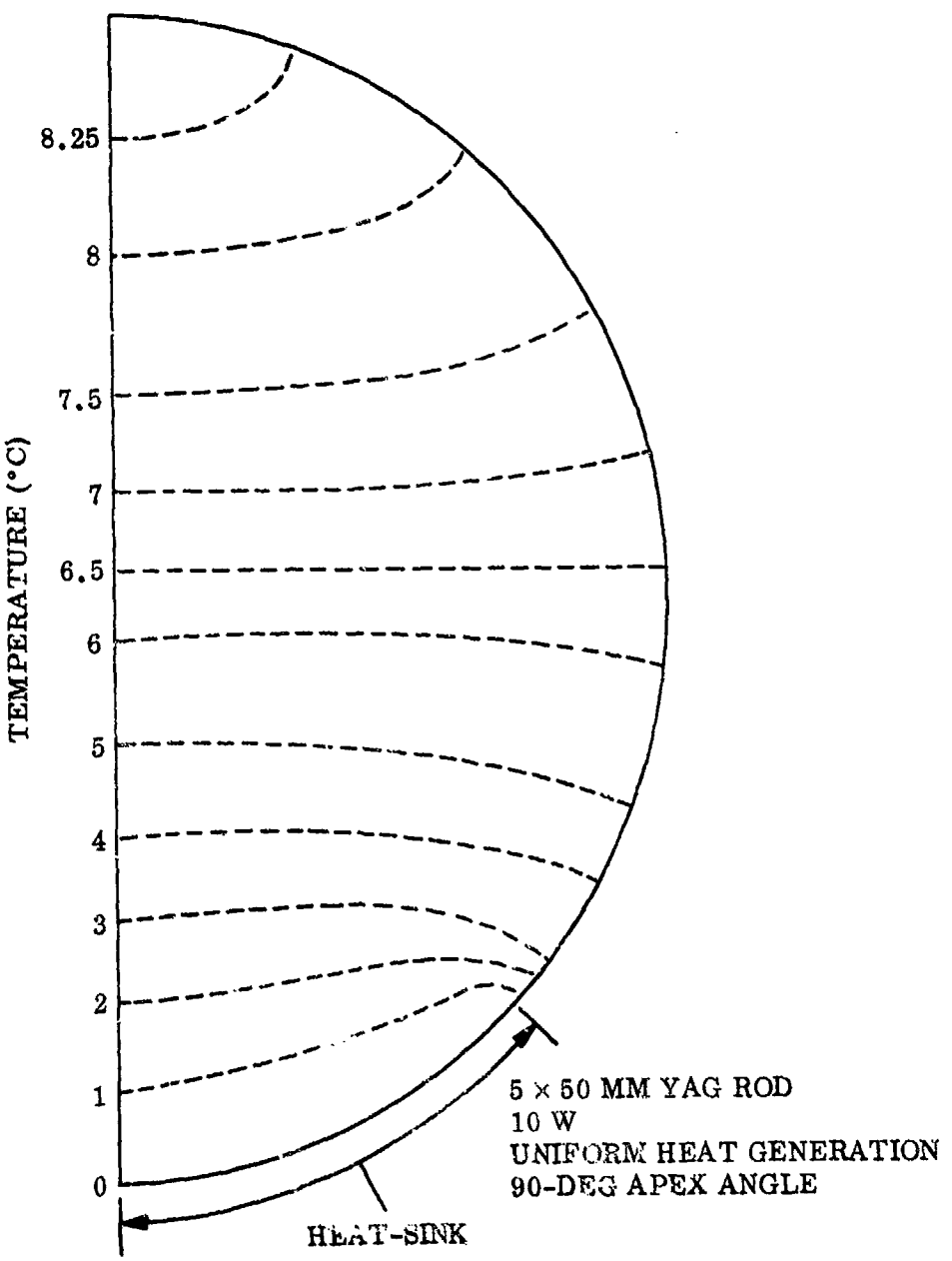

Figure A-1 Temperature Field in YAG Rod

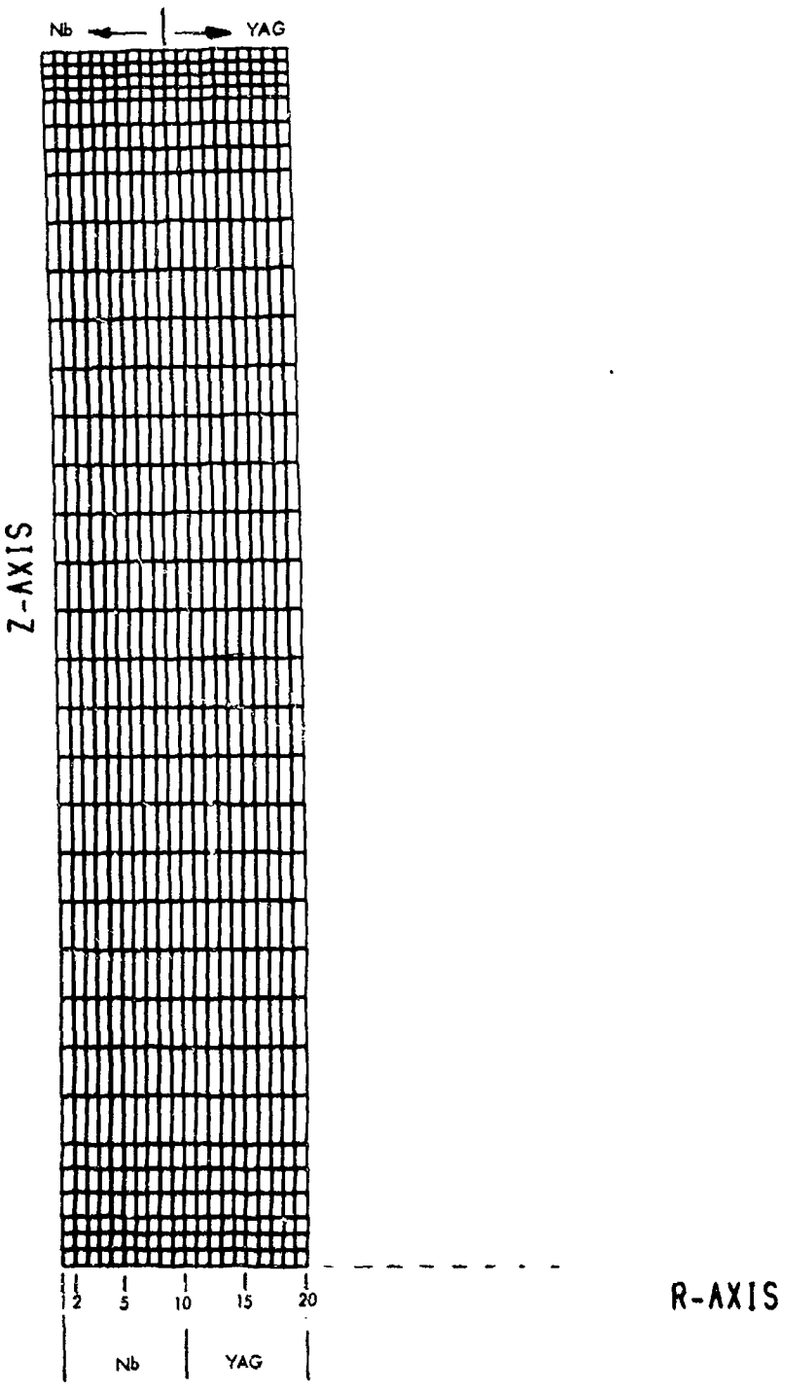

Figure A-2 Finite Element Mesh

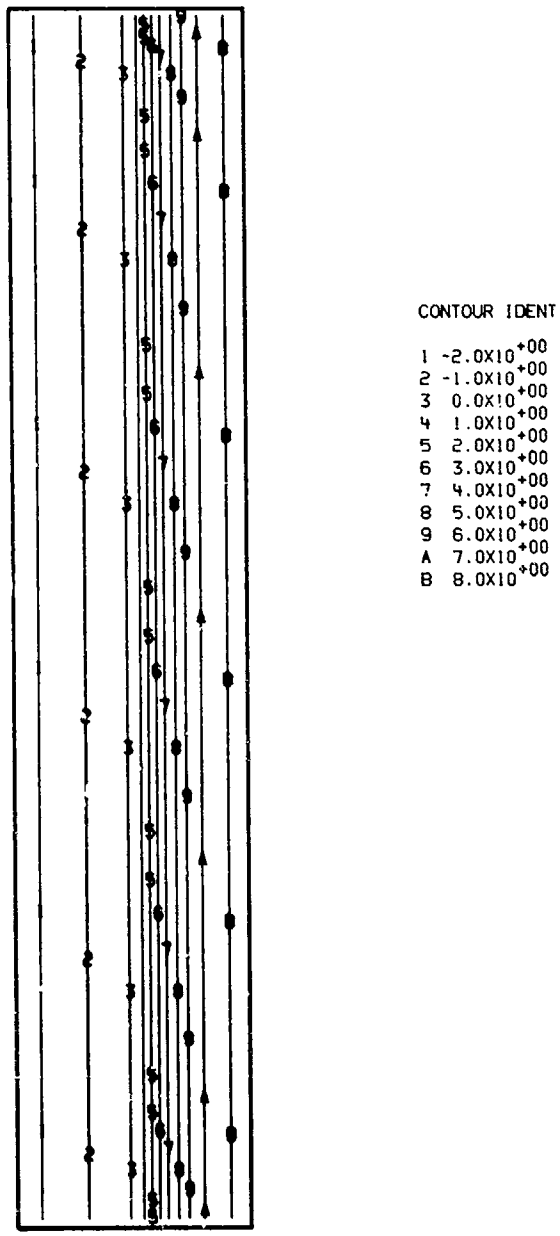

Figure A-3 Contour Map of Temperature

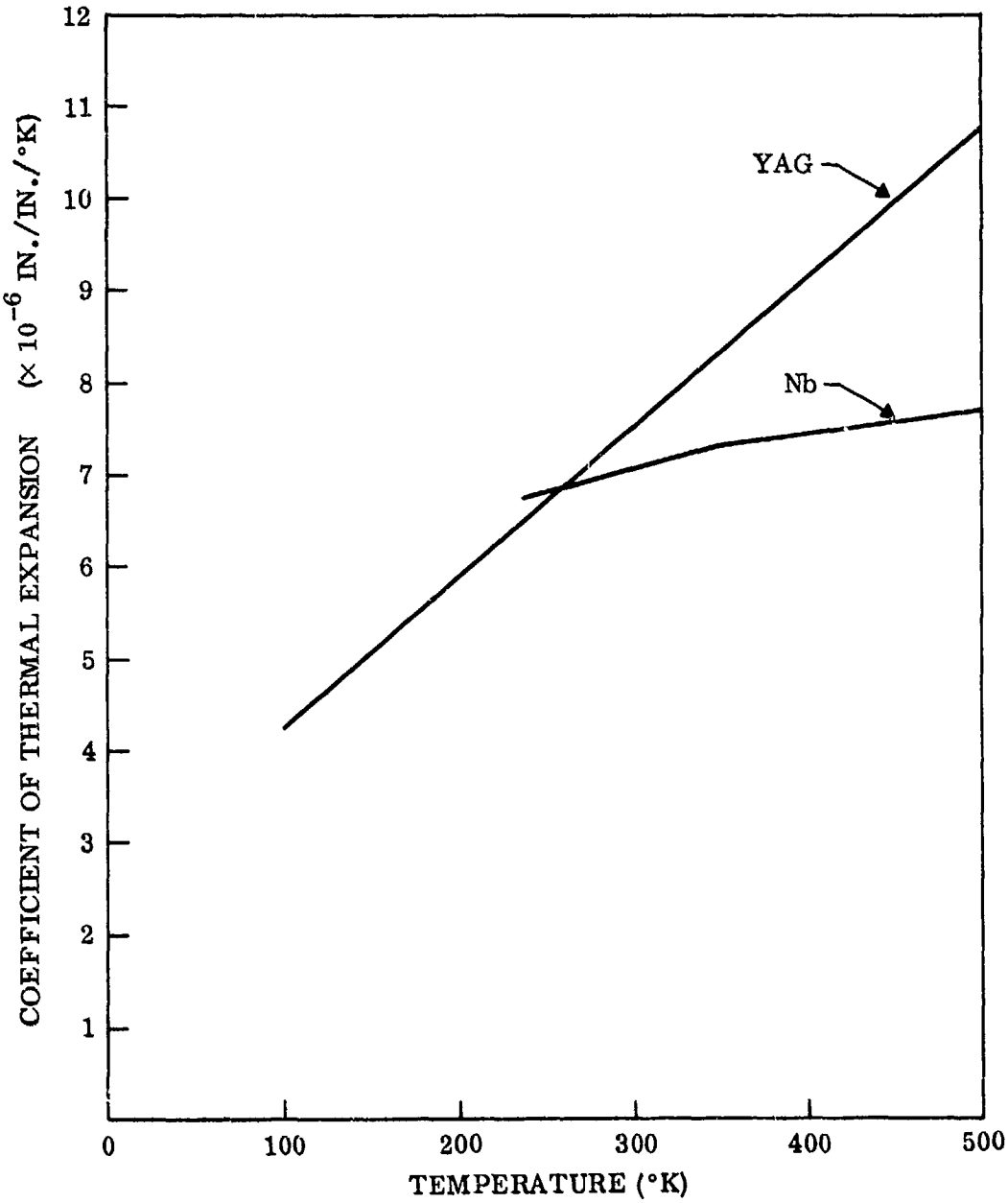

Figure A-4 Coefficients of Thermal Expansion for YAG and Nb

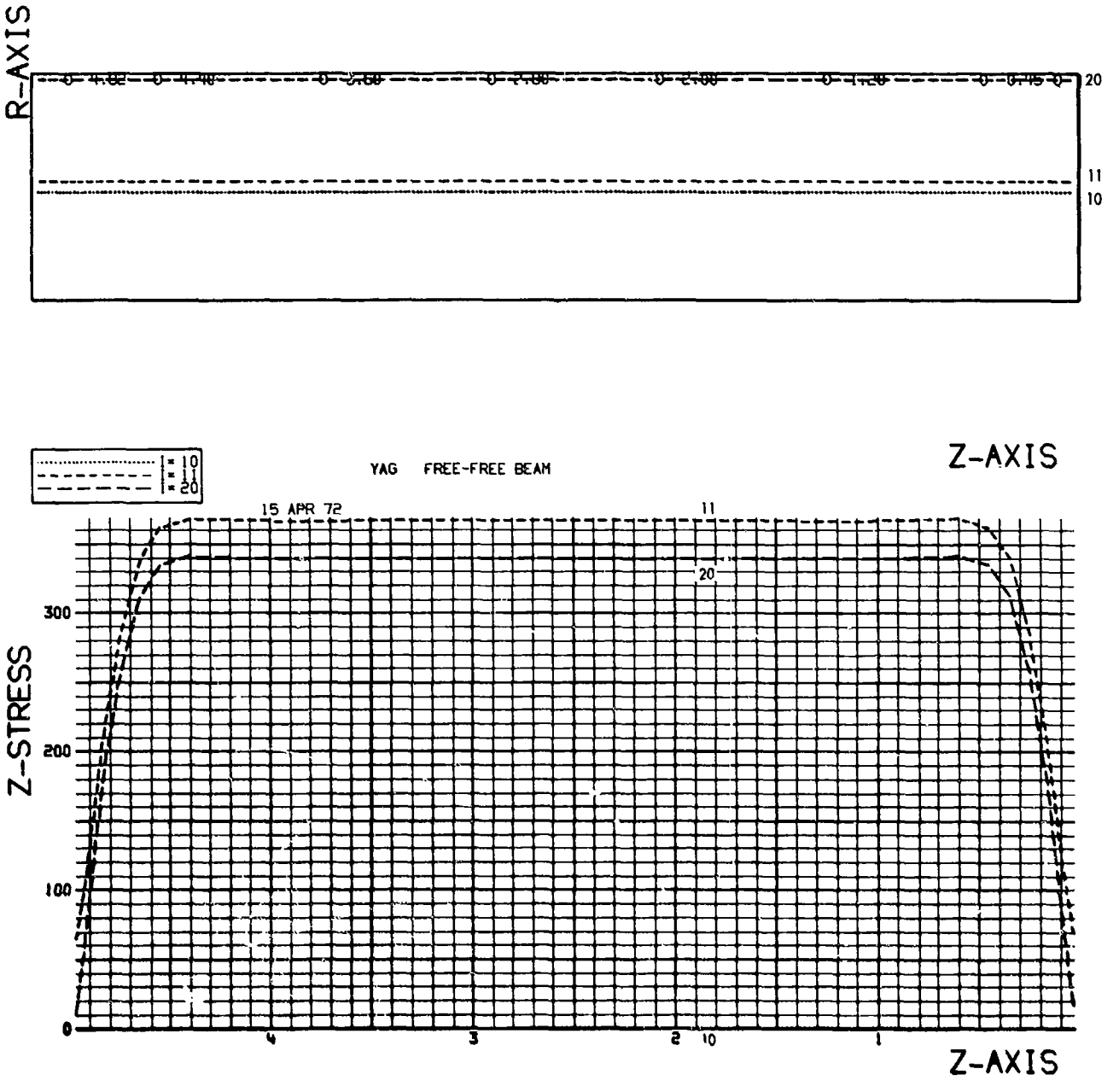

Figure A-5 Axial Stress Along Upper and Lower Edge of Unrestrained YAG Rod

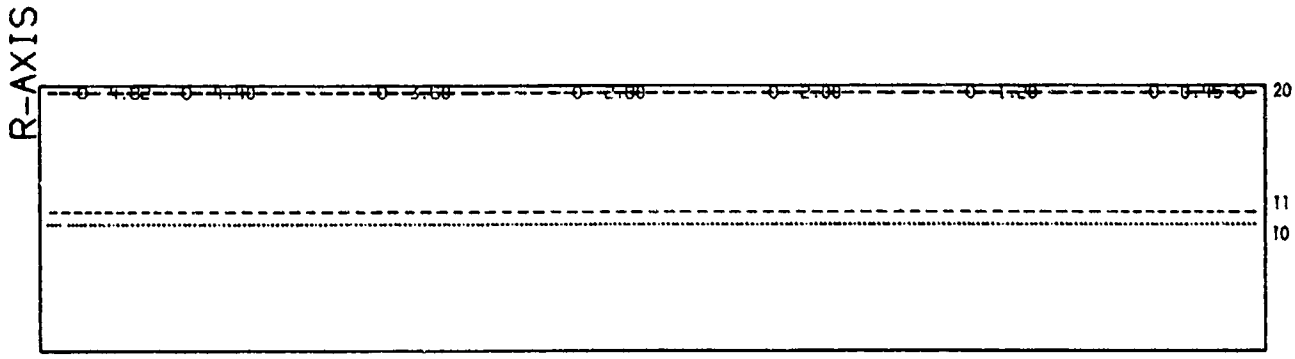

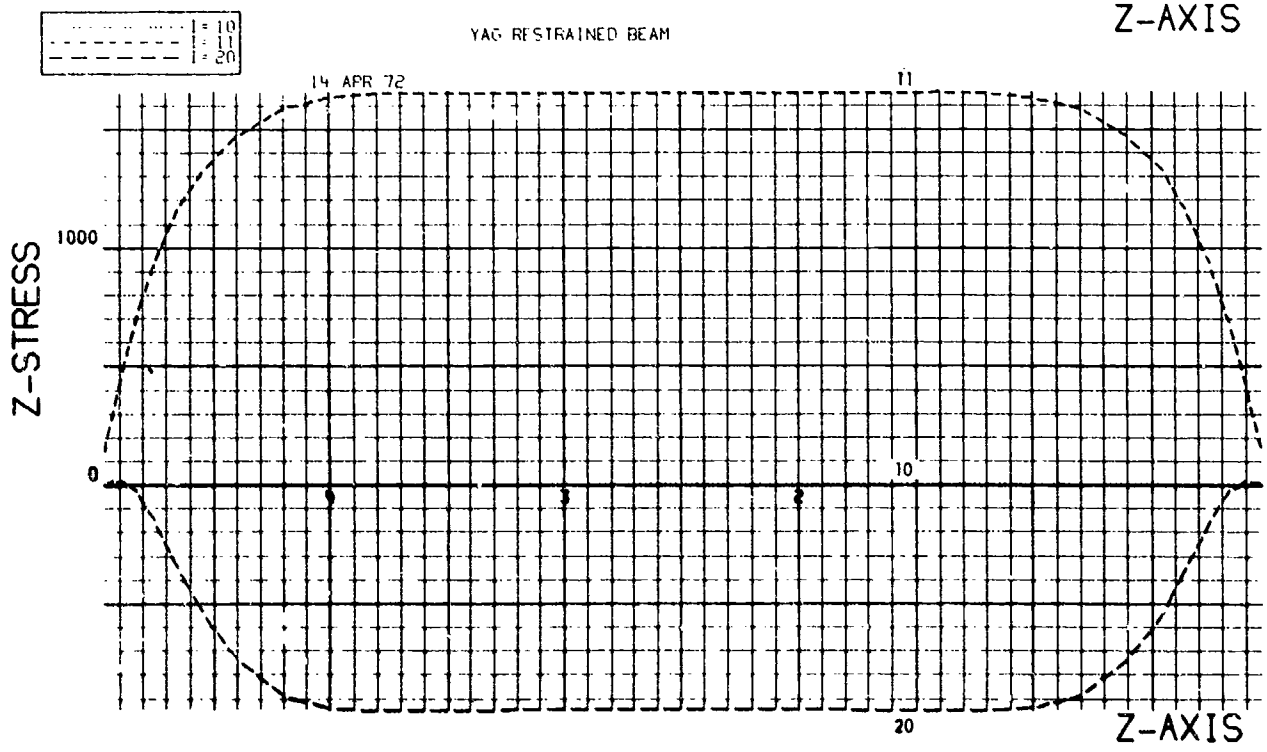

Figure A-6 Axial Stress Along Upper and Lower Edge of Restrained YAG Rod

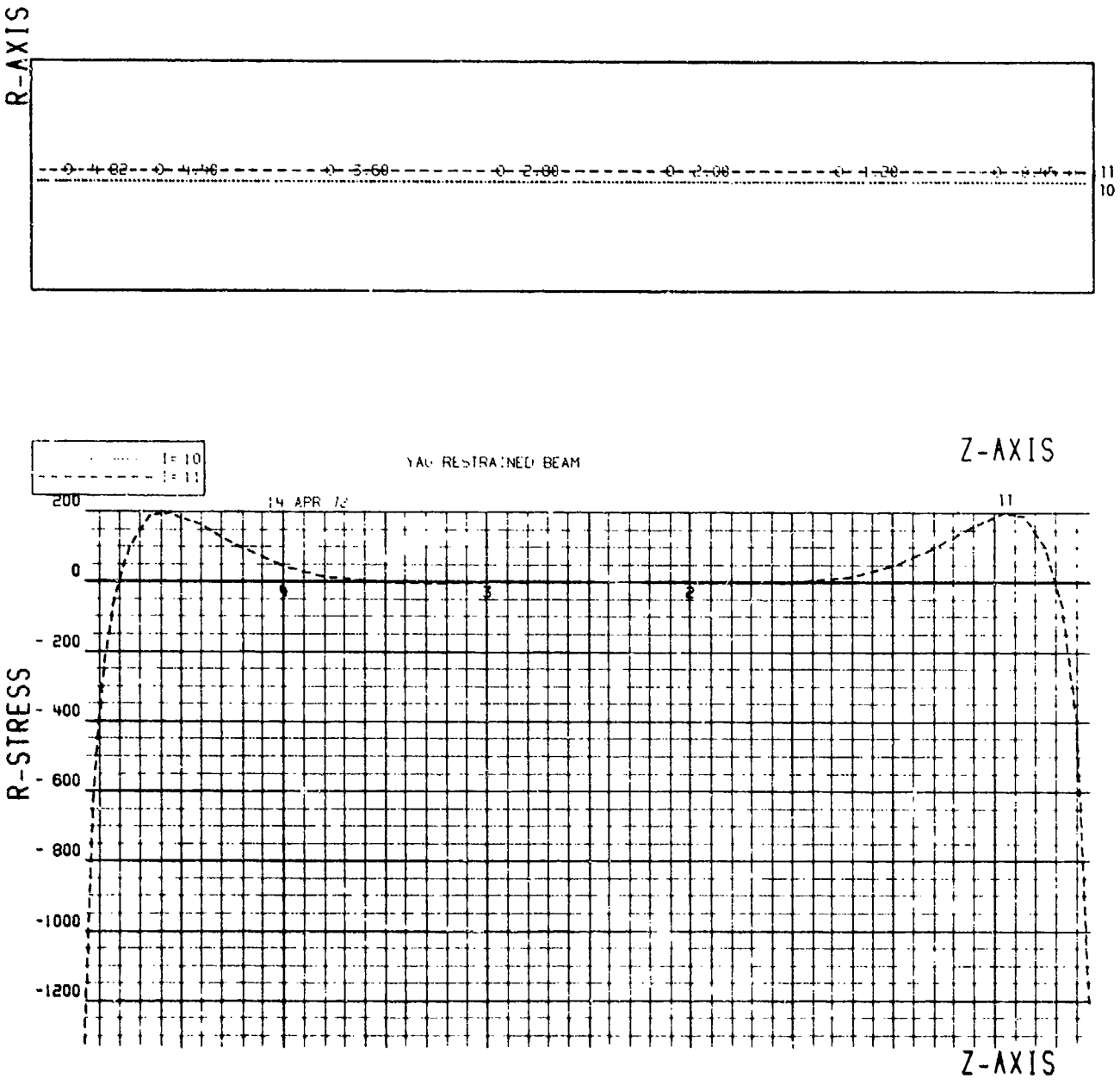

Figure A-7 Vertical Stress Along Lower Edge of Restrained YAG Rod

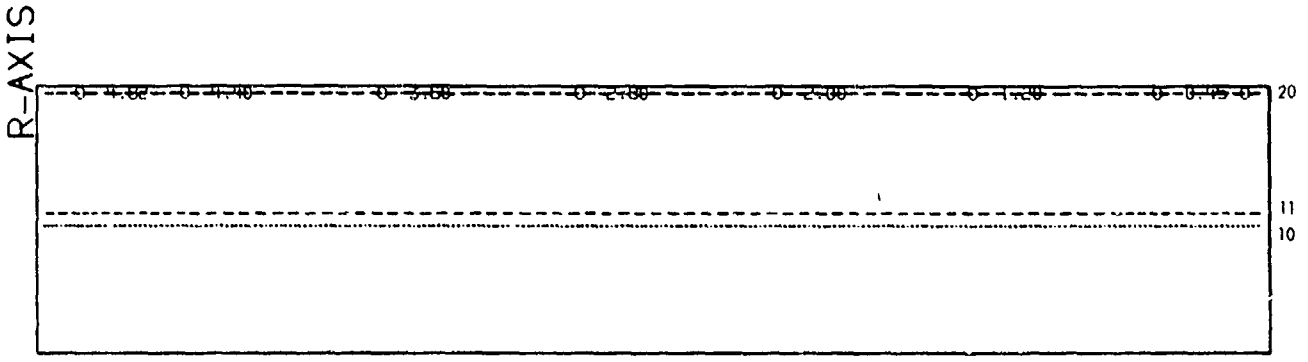

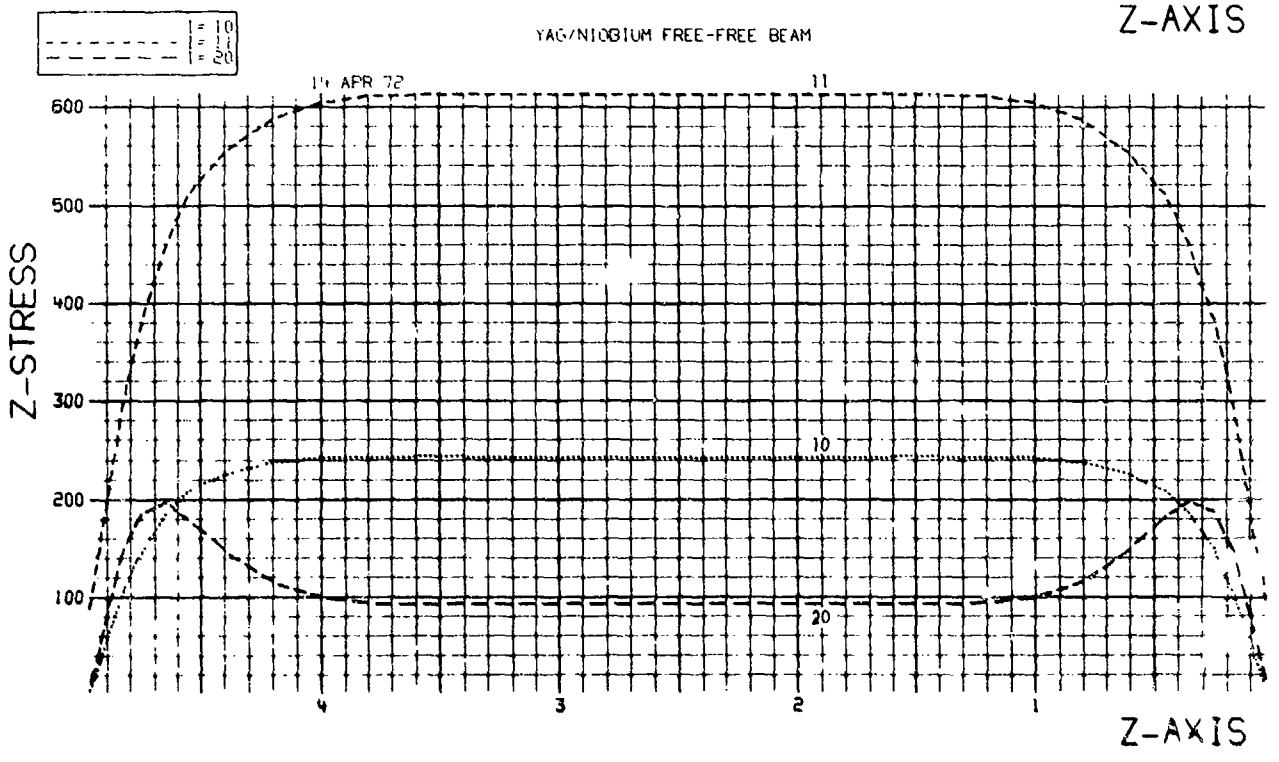

Figure A-8 Axial Stress in Unrestrained YAG/Nb Composite Beam

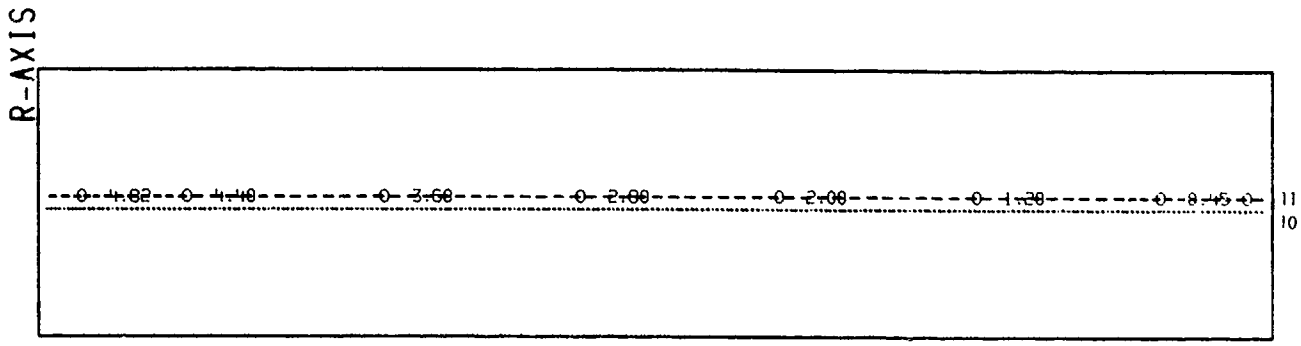

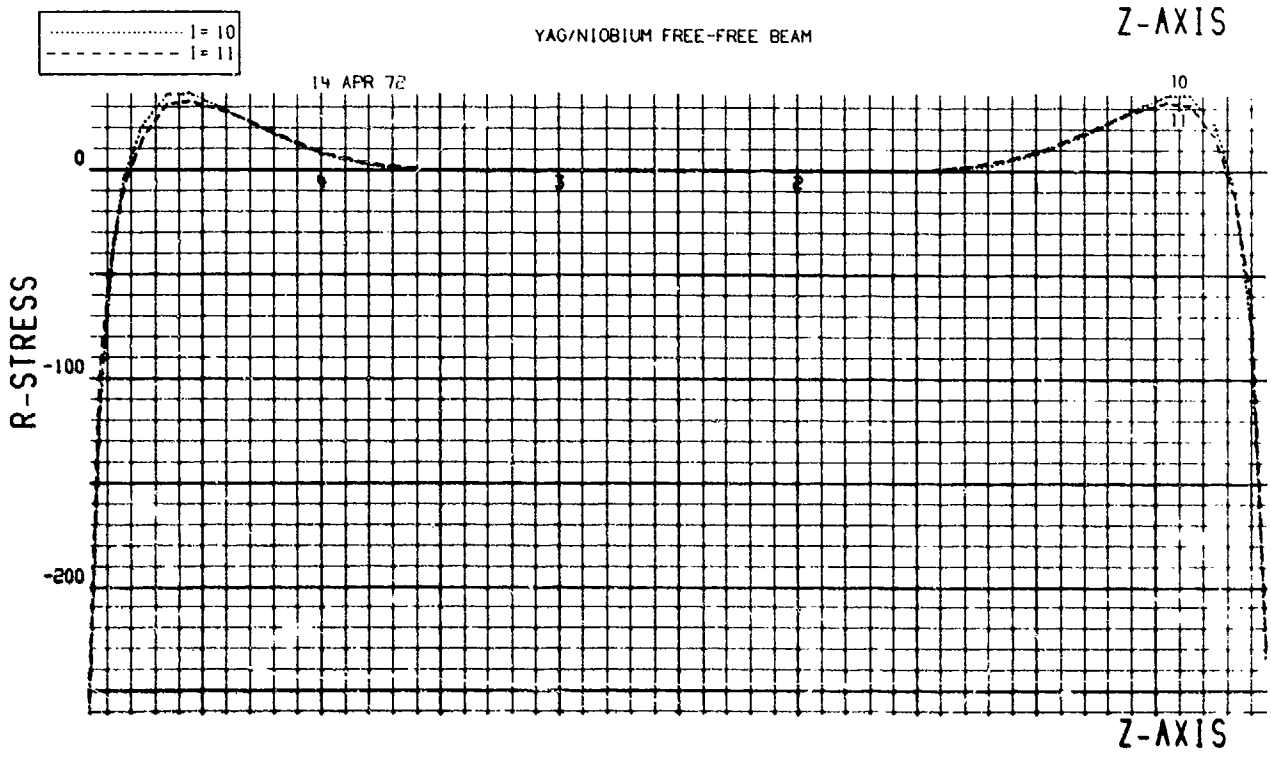

Figure A-9 Vertical Stress in Unrestrained YAG/Nb Composite Beam

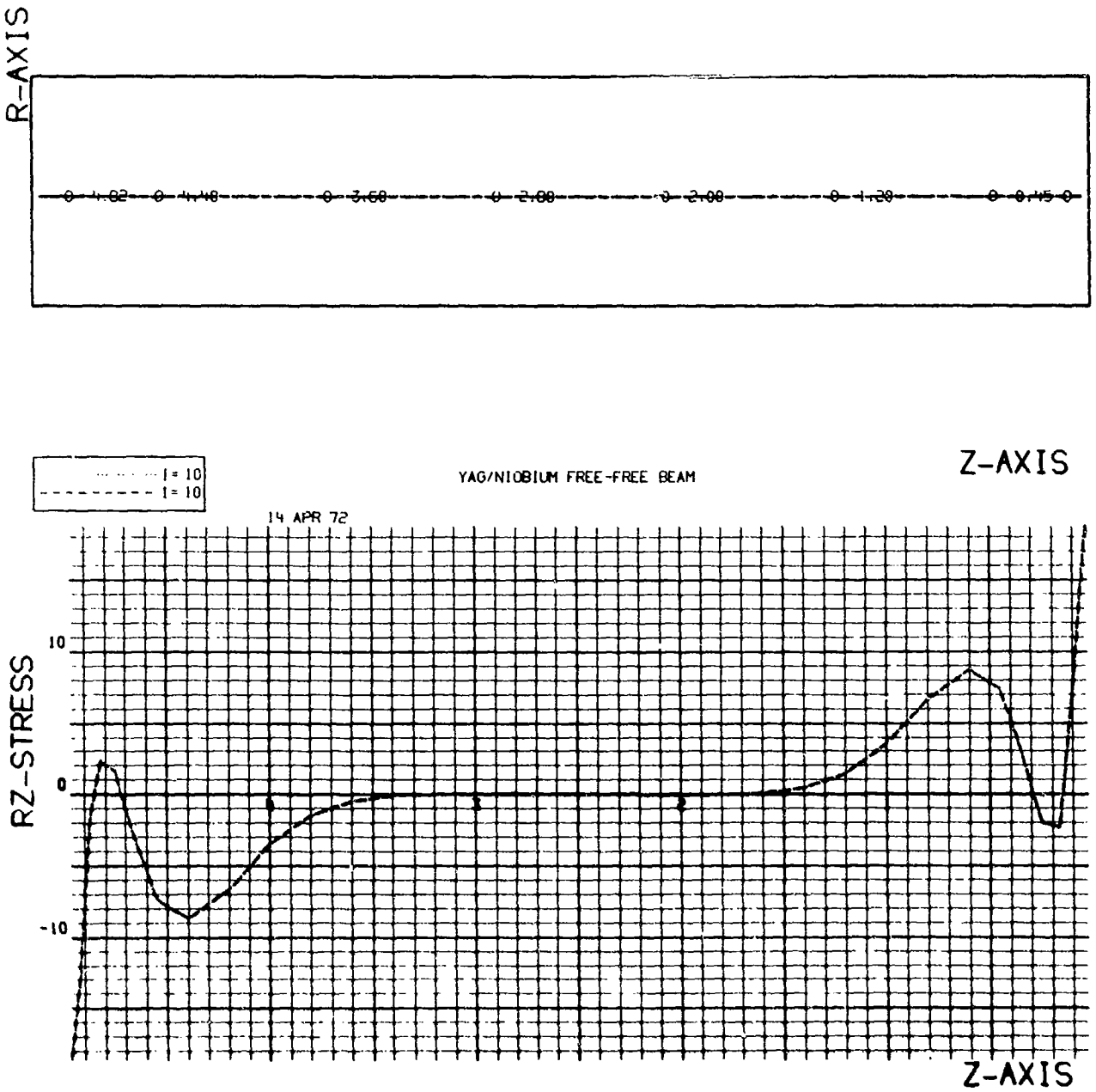

Figure A-10 Interface Shear Stress in Unrestrained YAG/Nb Composite Beam

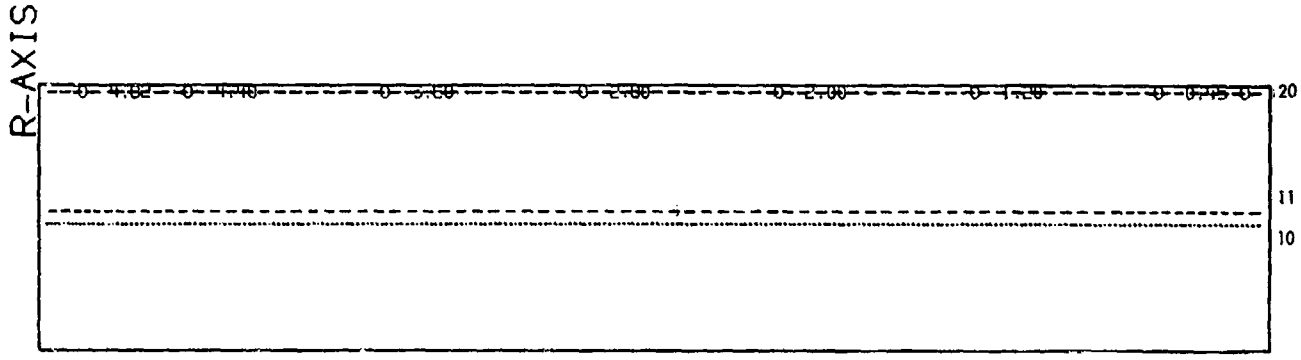

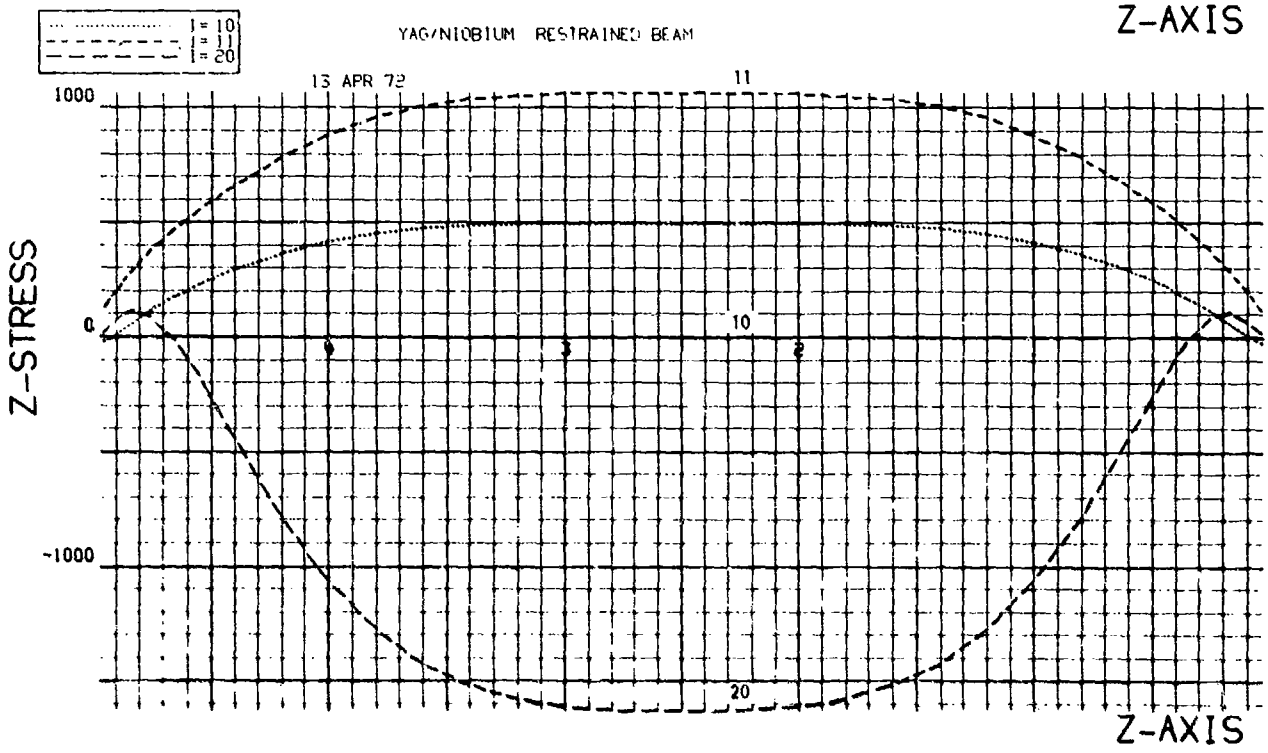

Figure A-11 Axial Stress in Restrained YAG/Nb Composite Beam

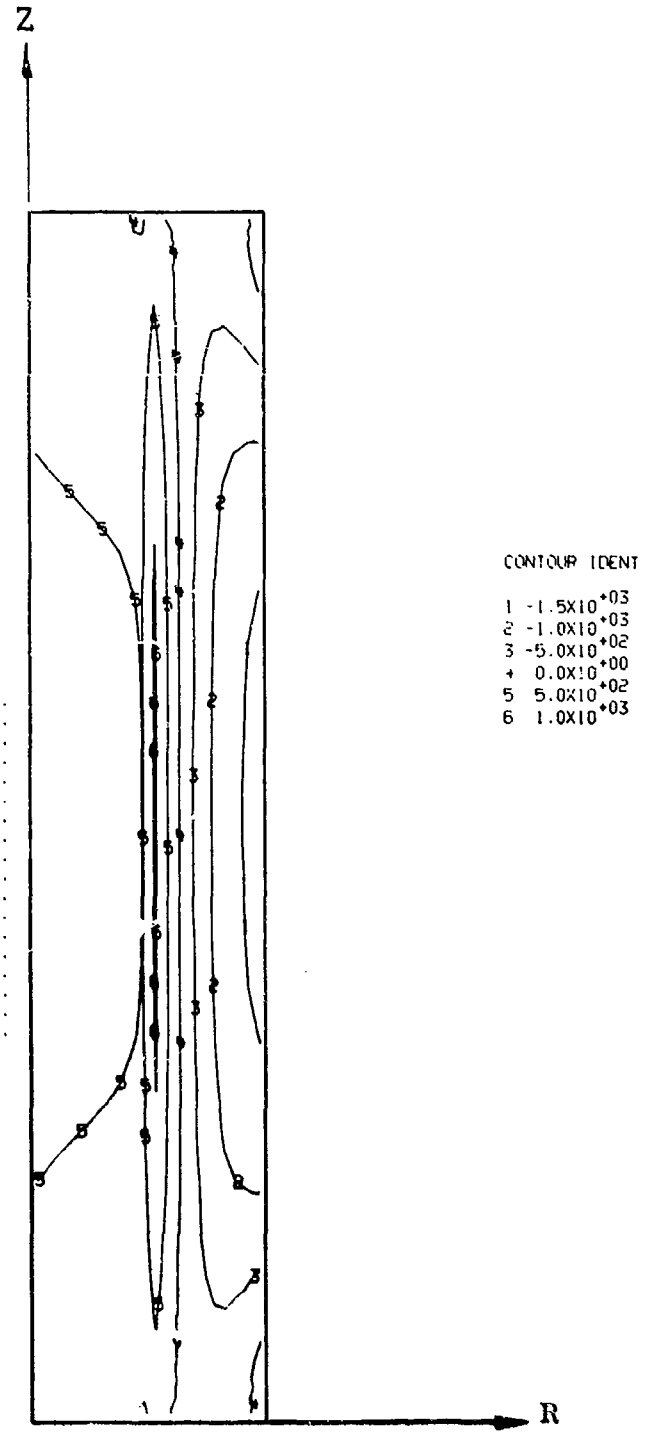

Figure A-12 Contour Map of Axial Stress in Restrained YAG/Nb Rod

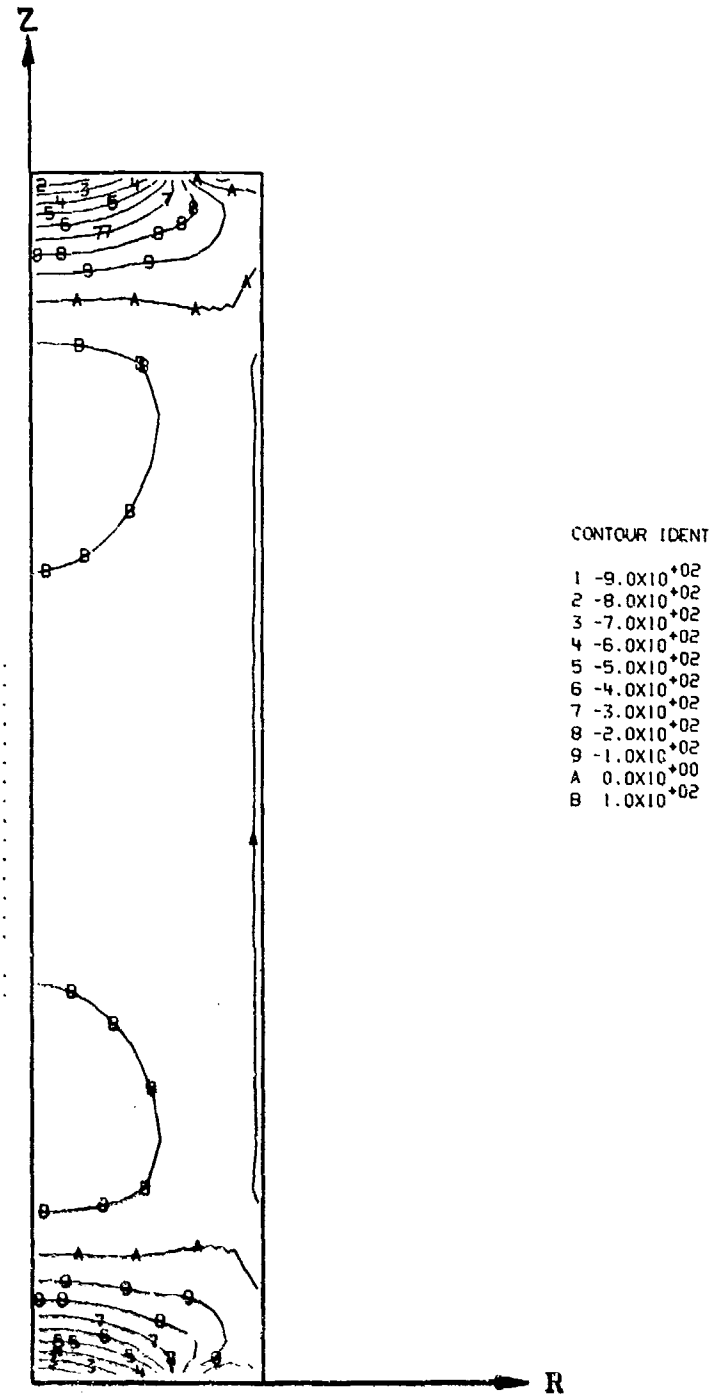

Figure A-13 Contour Map of Vertical Stress in Restrained YAG/Nb Rod

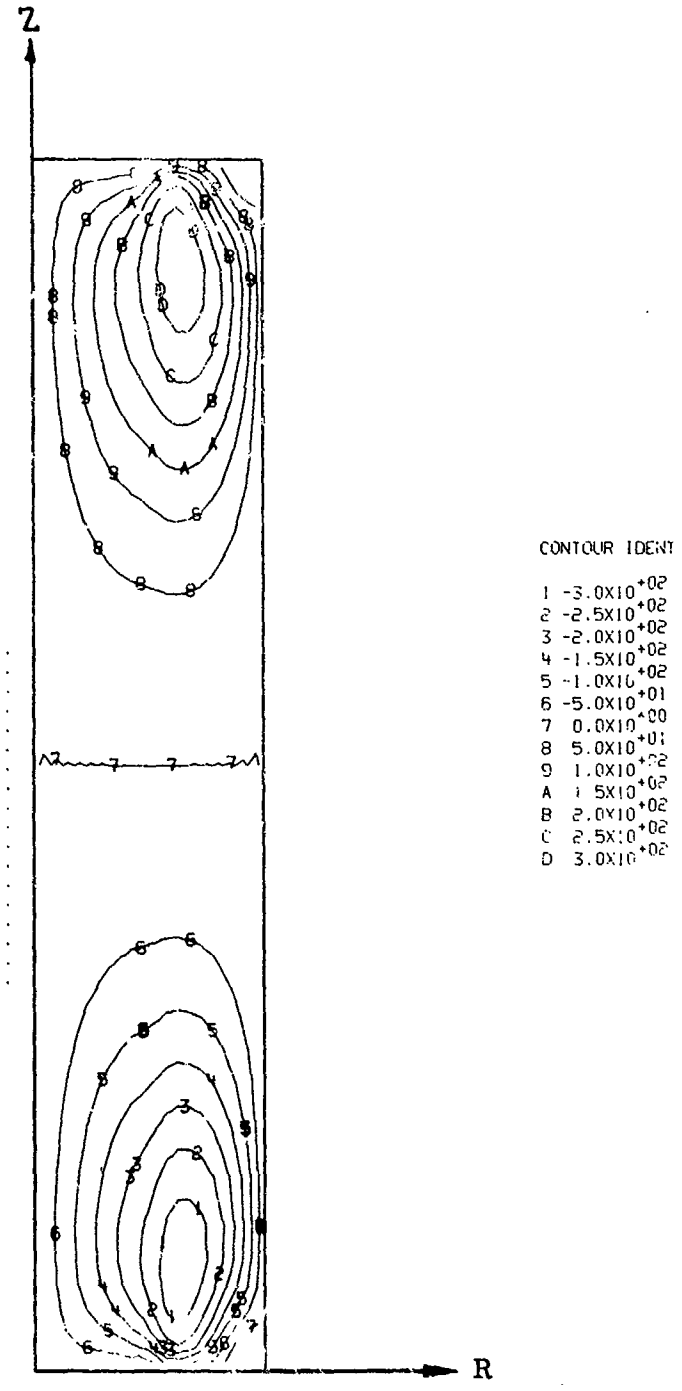

Figure A-14 Contour Map of Shear Stress in Retained YAG/Nb Rod

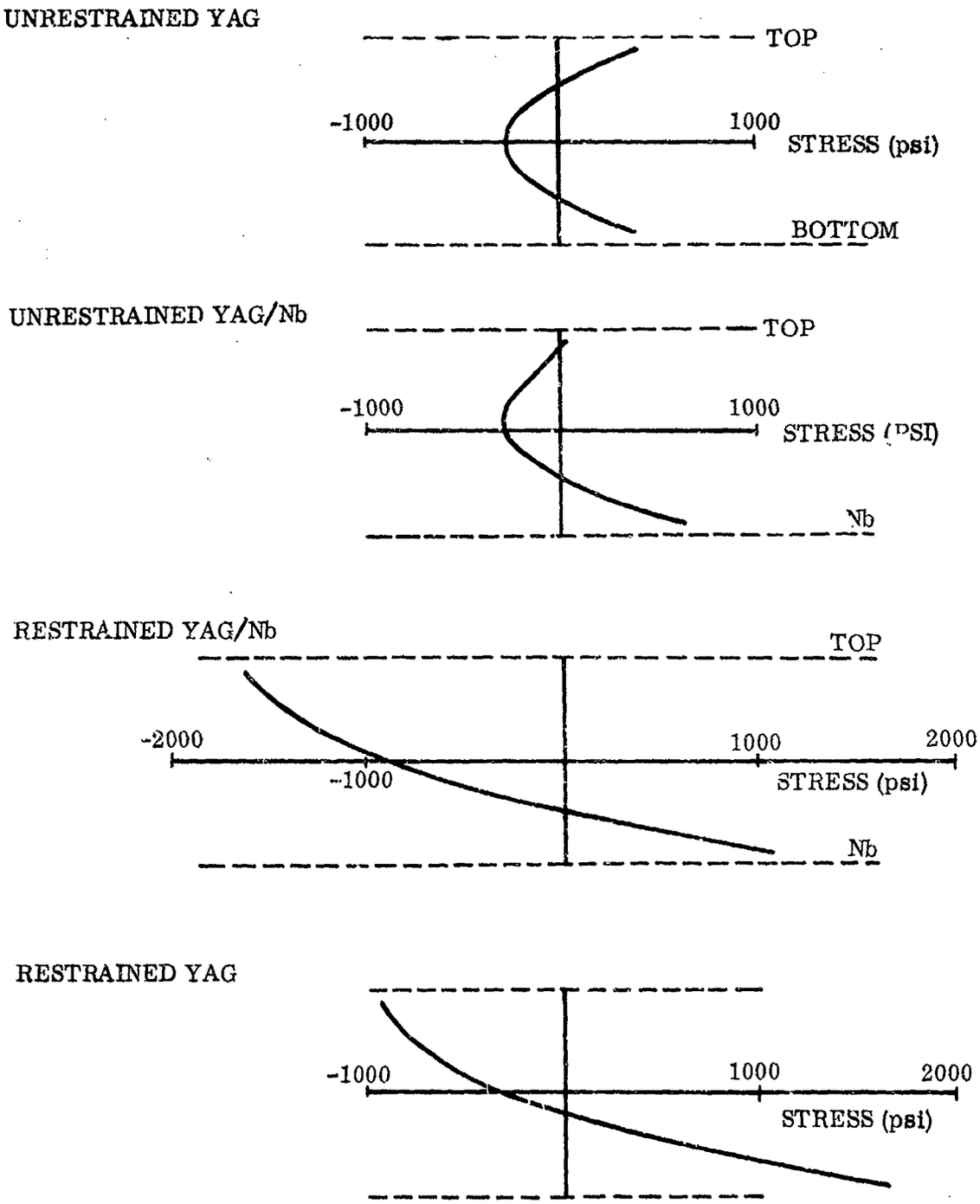

Figure A-15 Axial Stress in Central Region of the YAG Rod

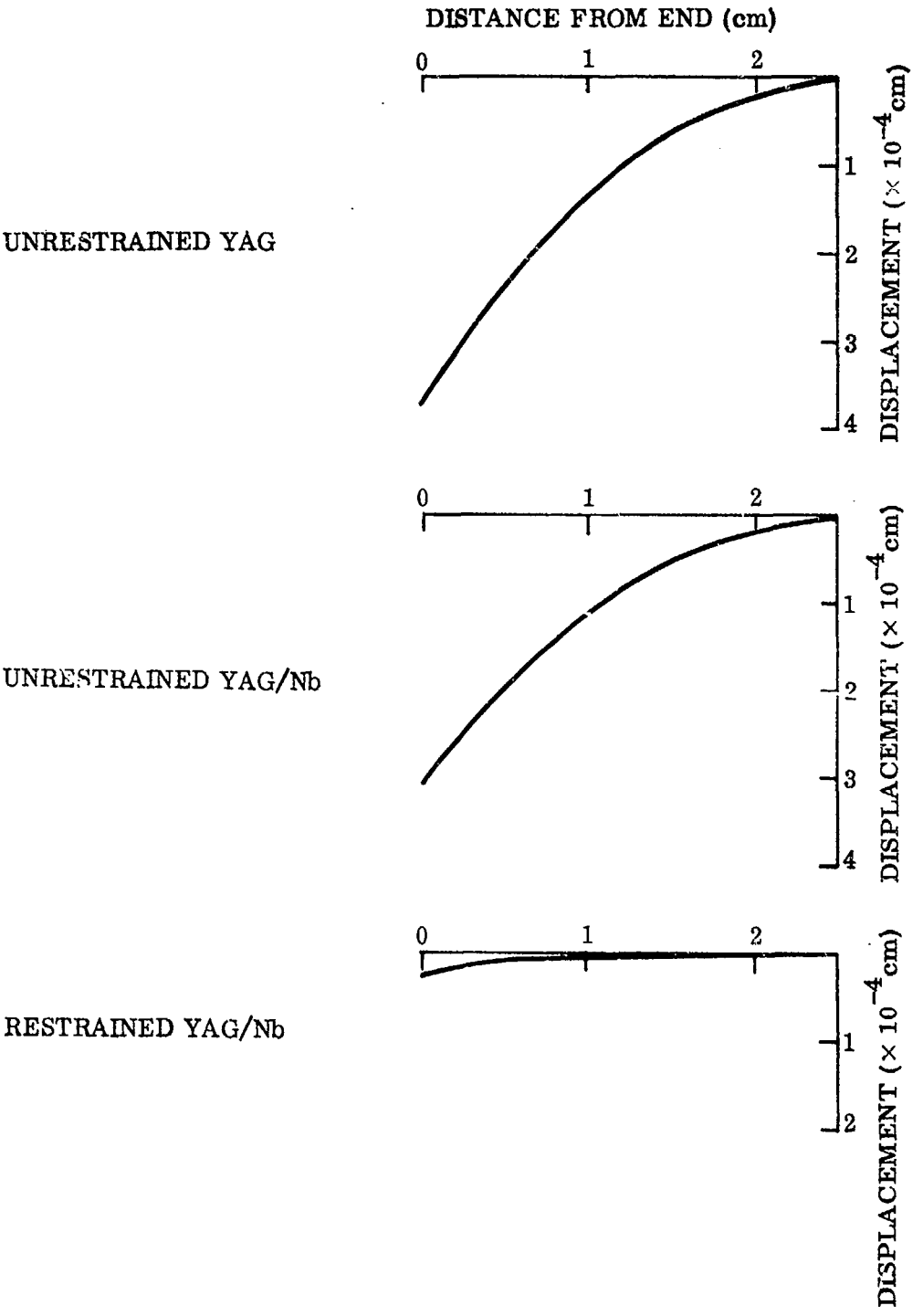

Figure A-16 Normal Displacement Along Lower Edge of the YAG Rod

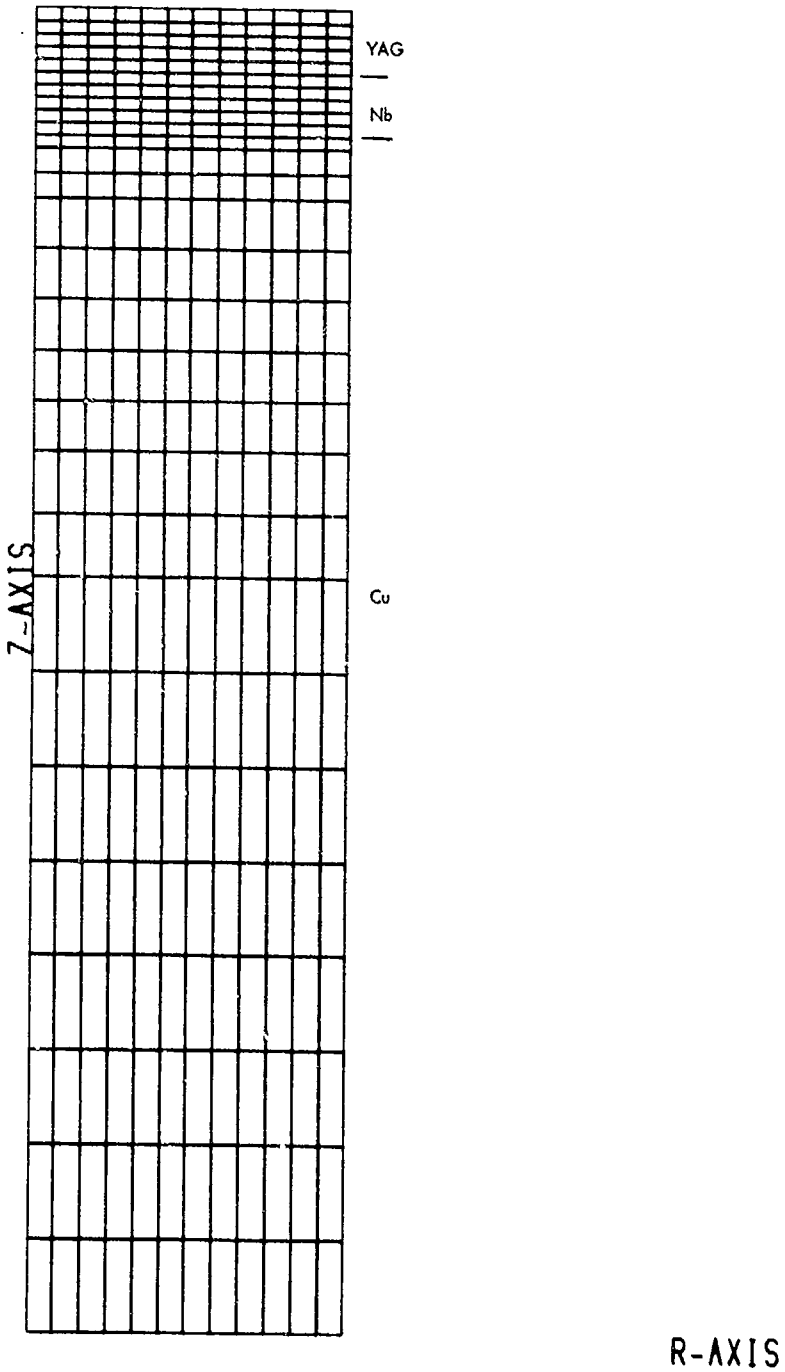

Figure A-17 Finite Element Mesh for YAG/Nb/Copper Assembly

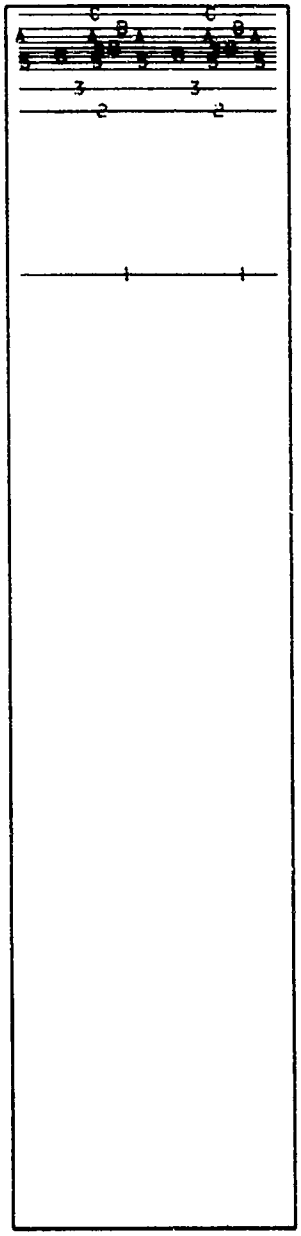

CONTOUR IDENT

1 $-3.0X10^{+00}$
2 $-2.0X10^{+00}$
3 $-1.0X10^{+00}$
4 $0.0X10^{+00}$
5 $1.0X10^{+00}$
6 $2.0X10^{+00}$
7 $3.0X10^{+00}$
8 $4.0X10^{+00}$
9 $5.0X10^{+00}$
A $6.0X10^{+00}$
B $7.0X10^{+00}$
C $8.0X10^{+00}$

Figure A-18 Contour Map of Temperature for YAG/Nb/Copper Assembly

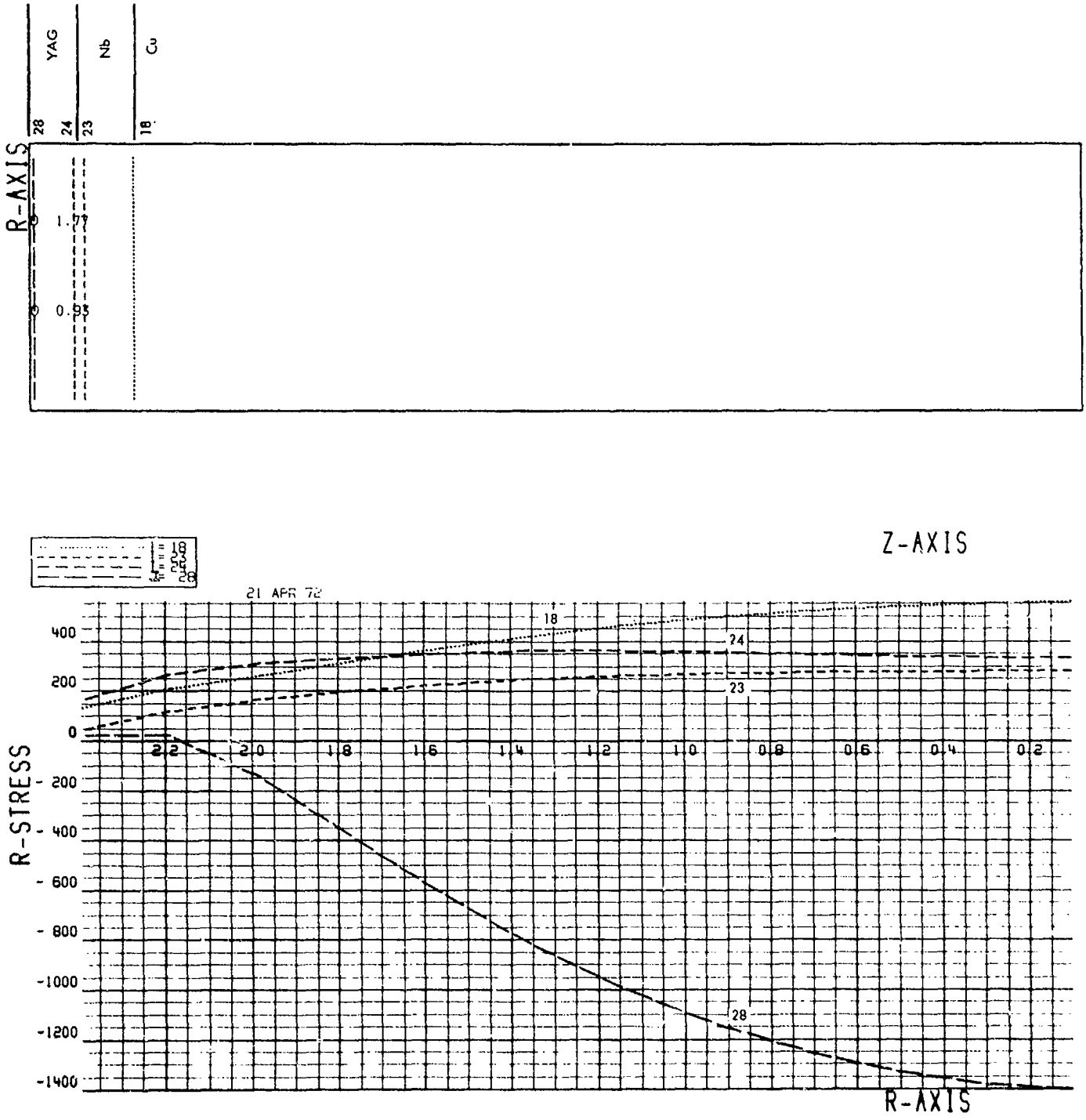

Figure A-19 Axial Stress in YAG/Nb/Copper Assembly

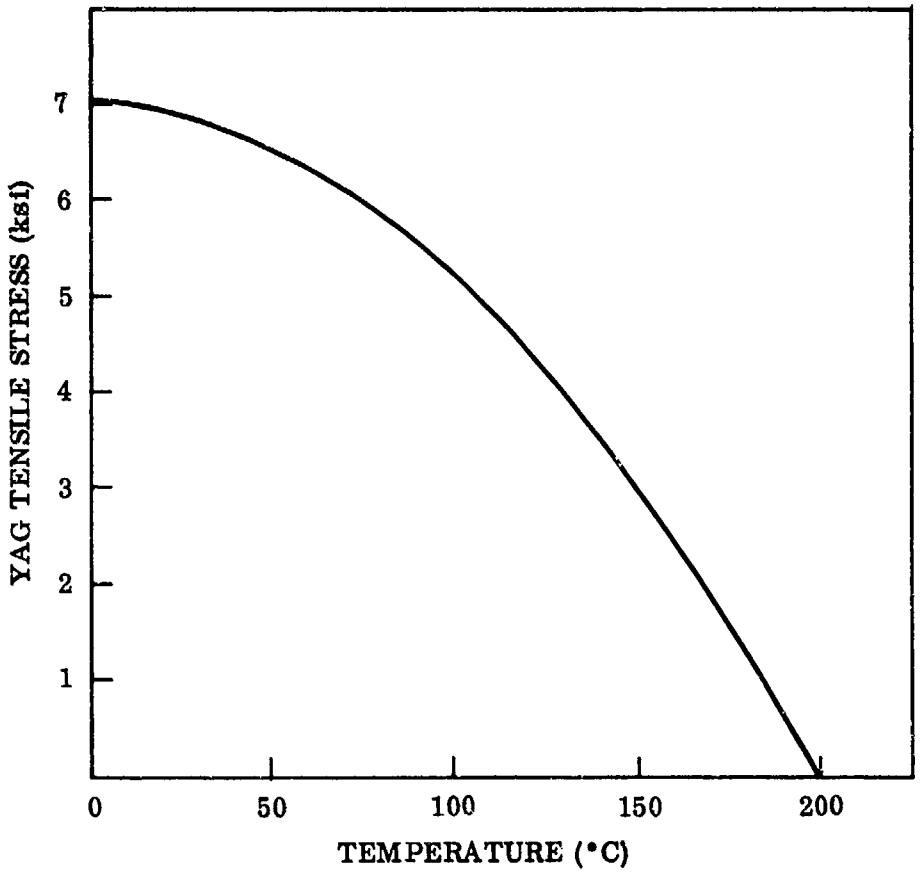

Figure A-20 Residual Tensile Stress in YAG for YAG/Nb Composite Beam Stress Free Temperature 200°C

REFERENCES

1. C. H. Church and I. Liberman, "The Spherical Reflector for Use in the Optical Pumping of Lasers," Appl. Opt., 6, Nov 1967, pp. 1966 - 1968

2. H. W. Koechner and D. K. Rice, "Effect of Birefringence on the Performance of Linearly Polarized YAG:Nd Lasers," IEEE Jour. of Quantum Electronics, Vol. QE-6, Sep 1970

3. J. D. Foster and L. M. Osterink, "Thermal Effects in a Nd:YAG Laser," J. App. Phys., 41, Aug 1970

4. L. Noble, Pump Lamps for Nd:YAG Lasers, AFAL TR-72-50, Air Force Avionics Laboratory, Wright-Patterson AFB, O., Feb 1972

5. A. D. Kraus, Cooling Electronic Equipment, Prentice-Hall, New York, 1965

6. Hansen, M., Constitution of Binary Alloys, McGraw-Hill, New York, 1958, pp. 199, 1019

7. Ibid, p. 643

8. Ibid, pp. 33, 58, 137, 937, 954

9. Private communication from R. S. Reynolds, Sylvania Electronic Systems, Western Division, Mountain View, Calif.

A-1. R. M. Jones and J. G. Crose, SAAS II Finite Element Stress Analysis of Axisymmetric Solids with Orthotropic, Temperature-Dependent Material Properties, Aerospace Report No. TR-0200(S4980)-1, Air Force Report No. SAMSO TR-68-455, Sep 1968

A-2. R. F. Belt, "YAG: A Versatile Host," Laser Focus 6, Apr 1970, pp. 44-47

A-3. American Institute of Physics Handbook, McGraw-Hill, New York, 2nd ed., 1963

DOCUMENT CONTROL DATA - R & D

(Security classification of title, body of abstract and indexing annotation must be entered when the overall report is classified)

1. ORIGINATING ACTIVITY *(Corporate author)*
Lockheed Palo Alto Research Laboratory
Lockheed Missiles & Space Company, Inc.
Palo Alto, Calif. 94304

2a. REPORT SECURITY CLASSIFICATION
Unclassified

2b. GROUP
N/A

3. REPORT TITLE
SPACE LASER DESIGN

4. DESCRIPTIVE NOTES *(Type of report and inclusive dates)*
Final Technical Report, 24 May to 30 Nov 1972

5. AUTHOR(S) *(First name, middle initial, last name)*
J. E. Peterson, E. C. Yates

6. REPORT DATE	7a. TOTAL NO. OF PAGES	7b. NO. OF REFS
December 1972	94	12

8a. CONTRACT OR GRANT NO.
F33615-72-C-1960

b. PROJECT NO.
405B/01/64

c.

d.

9a. ORIGINATOR'S REPORT NUMBER(S)
LMSC-D315647

9b. OTHER REPORT NO(S) *(Any other numbers that may be assigned this report)*
AFAL-TR-73-28

10. DISTRIBUTION STATEMENT
Distribution is limited to U.S. Government agencies only, by reason of inclusion of test and evaluation data; applied Mar 1972. Other requests for this document must be referred to AFAL/TEL, Wright-Patterson AFB, Ohio 45433.

11. SUPPLEMENTARY NOTES

12. SPONSORING MILITARY ACTIVITY
Air Force Avionics Laboratory
Air Force Systems Command
Wright-Patterson Air Force Base, Ohio

13. ABSTRACT This report describes the results of a program to design and develop a high-efficiency CW Nd:YAG laser which has space-applicable thermal properties. The laser is being developed for use in the 405B Laser Communications System. Since liquid cooling in the laser was not allowed, other means were found for efficiently cooling the laser rod and pump lamp and for removing the lamp envelope infrared radiation from the pump cavity. A laser was constructed that incorporated radiation cooling of the CW potassium-rubidium-arc pump lamp and direct-conduction cooling of the laser rod. The rod was soldered to a slotted composite metal wedge heat sink for minimum residual stress and greatest uniformity of thermal gradients in the rod. An optical pumping cavity was developed, using a Pyrex sphere coated with a multilayer dielectric cold mirror which transmits or absorbs unwanted lamp radiation while efficiently imaging pump band radiation in the laser rod. To date, the laser has produced 0.7 W of multimode output at 1.06 μm without correction of the astigmatism thermally induced in the rod.

14. KEY WORDS	LINK A		LINK B		LINK C	
	ROLE	WT	ROLE	WT	ROLE	WT
Laser						
Nd:YAG						
High Efficiency						
Conduction Cooling						
Potassium-Rubidium Pumping						
Space Communications						